공학박사 학위논문

Performance Improvement of a GNSS Receiver Using MEMS Oscillator for Space Launch Vehicle

MEMS Oscillator를 탑재한

우주발사체용 위성항법수신기 성능 향상

2021년 8월

서울대학교 대학원

기계항공공학부

신 용 설

Performance Improvement of a GNSS Receiver Using MEMS Oscillator for Space Launch Vehicle

MEMS Oscillator 를 탑재한 우주발사체용 위성항법수신기 성능 향상

지도교수 박 찬 국

이 논문을 공학박사 학위논문으로 제출함

2021 년 6 월

서울대학교 대학원
기계항공공학부
신 용 설

신용설의 공학박사 학위논문을 인준함

2021 년 6 월

위 원 장 : _____

부위원장 : _____

위   원 : _____

위   원 : _____

위   원 : _____

Performance Improvement of a GNSS Receiver Using MEMS Oscillator for Space Launch Vehicle

A Dissertation
by
Yong Sul Shin

Submitted to the Department of Mechanical and Aerospace Engineering in partial
fulfillment of the requirements for the degree of

DOCTOR OF PHILOSOPHY

In Aerospace Engineering at the

SEOUL NATIONAL UNIVERSITY

June 2021

Approved as to style and content by:

_____
Prof. Youdan Kim
Dept. of Aerospace Engineering, Chairman of Committee

_____
Prof. Chan Gook Park
Dept. of Aerospace Engineering, Principal Advisor

_____
Prof. Changdon Kee
Dept. of Aerospace Engineering

_____
Ph. D. Moon Beom Heo
Korea Aerospace Research Institute

_____
Ph. D. Young Bum Park
Agency for Defense Development

Abstract

A Performance Improvement of a GNSS Receiver Using MEMS Oscillator for Space Launch Vehicle
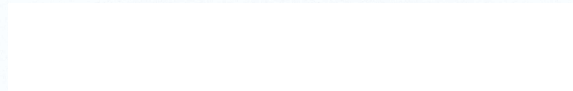
Yong Sul Shin

Department of Mechanical and Aerospace Engineering

The Graduate School

Seoul National University

In this dissertation, the environmental and performance results of TCXO (temperature-controlled crystal oscillator) and MEMS (micro-electro mechanical system) oscillator are presented. The test results for each oscillator are compared, and based on the test results for the GNSS receiver to which each oscillator is applied, the replaceability of TCXO with MEMS oscillator is discussed.

TCXO is a component that supplies a fixed and stable reference frequency by using a quartz crystal with a piezo-electric effect, and it has low phase noise, high Q-factor fitted for a resonator. The TCXO is widely used in precise clock and timing equipment as well as GNSS receivers. Through many temperature tests during development, the high level of frequency stability over temperature can be achieved by the surrounding compensation circuit.

MEMS oscillator drastically reduced its size and weight by introducing micro-scale manufacturing and packaging technology and uses silicon as a resonator. This

reduction in size and weight makes MEMS oscillator robust under physical stress such as vibration and shock. However, silicon, which is used as a resonator of MEMS oscillator, has lower frequency stability over temperature compared to a quartz crystal, and relatively high phase noise occurs as the complex compensation circuit is required. Despite its advantages, the MEMS oscillator has not been widely used so far due to the tendency to use existing TCXOs.

Electronic devices in space launch vehicles experience significant vibration, acceleration, and shock at the flight events such as lift-off, engine shutdown, stage, and pairing separation. And the performance tests under these physical stresses to verify operability should be conducted. In the pyrotechnic shock test, the GNSS receiver equipped with TCXO as a reference oscillator cannot maintain signal tracking, making the position fix fail. This phenomenon was caused by a sudden change in frequency output of TCXO due to the shock, and to address this issue, a MEMS oscillator, which is known to be robust in harsh environmental and stress conditions, was chosen to be utilized as a reference frequency oscillator instead of TCXO.

To use the MEMS oscillator as a reference frequency of a GNSS receiver, the pyrotechnic shock, vibration, and temperature test for the MEMS oscillator itself were performed before assemble the GNSS receiver. In order to check the behavior of the GNSS receiver under the reference frequency change, the test using a signal generator, which simulates the reference frequency change without physical shock, was performed.

After the test for the MEMS oscillator itself, the test of the GNSS receiver with the MEMS oscillator was conducted. The GNSS receiver can maintain signal tracking and calculate position normally under the pyrotechnic shock test, and the

vibration and temperature tests are done without any issues. In environmental and performance tests, there are no problems due to the high phase noise of the MEMS oscillator, and the navigation accuracy was not much different from the existing GNSS receiver with TCXO.

Contents

List of Figures

vii

List of Tables

Abbreviations

C/N0	Carrier to Noise Ratio
dBc	Decibels relative to the Carrier
ECEF	Earth Centered Earth Fixed
FLL	Frequency Locked Loop
GLONASS	GLObal Navigation Satellite System
GNSS	Global Navigation Satellite System
GPS	Global Positioning System
INS	Inertial Navigation System
KSLV	Korea Space Launch Vehicle
MEMS	Micro Electro Mechanical System
MTBF	Mean Time Between Failure
NCO	Numerically Controlled Oscillator
PIT	Pre-Integration Time
PPB	Part Per Billion
PPM	Part Per Million
PRN	Pseudo Random Number
PSD	Power Spectral Density
RF	Radio Frequency
RMS	Root Mean Squared
SDOF	Single Degree of Freedom
SRS	Shock Response Spectrum
TCXO	Temperature Compensated crystal Oscillator
TCF	Temperature Coefficient of Frequency

Chapter 1

Introduction

1.1   Motivation and Background

The GNSS receiver for KSLV-II receives navigation signals from multiple patch-type GNSS antennas installed on the surface of the vehicle and processes three navigation signals, GPS, GLONASS, and Galileo, in two frequency bands denoted as L1 and L5 [1]. As the attitude of the vehicle changes every moment during flight, the GNSS receiver receives satellite signals from two or more antennas to increase the availability and thus provides navigation information to the ground station for improved flight safety. Thus far, a GNSS receiver that utilizes external signals is only a secondary device used for flight safety, as such components must be highly reliable and should not be affected by factors in the external environment, such as vibration, temperature changes, vacuum conditions, or RFI (Radio frequency interference) [1-3]. Nevertheless, the ability to compensate for the diverging errors of an INS (inertial navigation system) during the long mission times of a launch vehicle has been highlighted, and the use of GNSS receivers for launch vehicles has gradually increased. In addition, the GNSS receiver for Atlas V functions as a primary sensor for flight safety as part of the trend of reducing the maintenance and operating costs of ground stations for the

tracking of the vehicle [4].

GNSS receivers, which should operate normally during the flight mission, undergo environmental testing during the manufacturing process for performance verification purposes [5,6]. Environmental testing should simulate the extreme conditions experienced in actual space circumstances on the ground, and these environmental test procedures refer to specifications used or published in Europe or the United States [7-9]. In order to establish the procedures for the environmental tests, application-specific tailoring is essential, especially for space launch vehicles, as vibration and shock stress occurs during events such as the lift-off, fairing separation, and engine shutdown. The environmental tests required for the manufacture of GNSS receivers of space launch vehicles should be configured to satisfy the dynamics of the space launch vehicles as outlined in Table 1.1, and typical commercial GNSS receivers cannot meet these environmental conditions. Product design and manufacturing considering these environmental conditions along with related tests significantly increase the prices of the devices used in space systems [5].

Table 1.1 Commercial GNSS receiver and space launch vehicle dynamics

	Commercial GNSS Receiver	Space Launch Vehicle Dynamics	
Altitude	< 18 km	> 300 km	Export Licensing Restrictions
Velocity	< 514 m/s	> 7 km/s	
Acceleration	10 - 16 g, When operating*	> 8 g	
Shock	40 g, Non-operating*	> 50 g	Environmental Tests are required
Vibration	7.7 g (random) 5 g (sinusoidal) When operating*	20 g (random) Varies with location	
*AsteRx3 from Septentrio, ProPak6 from NovAtel			

2

In order to perform normally for a GNSS receiver, the frequency output by the oscillator must remain constant in any environment. Temperature is a major factor, having the greatest effect on the frequency output, and TCXOs, which are designed to be robust against temperature changes, are already in use in most commercial GNSS receivers. In addition to the temperature, applying a strong physical load to an oscillator, such as vibration or a pyrotechnic shock, can cause temporary or permanent changes in the output frequency and can even lead to failure. In such a case, the GNSS receiver briefly cannot track the navigation signal [4]. For example, under a vibration load, the navigation performance can be reduced by increasing the phase noise and lowering the C/N0 (carrier-to-noise ratio), while during pyrotechnic shock stress, the oscillator output frequency varies abruptly, causing the tracking signals to be missed. To prevent such phenomena, vibration and shock stress conditions were considered when selecting the TCXO of the GNSS receiver for KSLV-II [10].

The TCXO has long been used, and its performance has improved such that it is becoming an essential aspect of GNSS receiver technology as the stability and accuracy of the output frequency increase [11]. However, considering the difficulty associated with the creation of resonant crystal and its susceptibility to the vibration of the TCXO, the MEMS oscillator has attracted attention recently [12,13]. MEMS technology has enabled the size of the oscillator to be reduced profoundly, raising expectations that it can replace the TCXO by improving the high phase noise shortcoming. MEMS oscillators are known to be strong against electromagnetic interference, shocks, vibration, and acceleration compared to the TCXO types [14-17].

1.2   Objectives and Contributions

In this study, the effect of changes in reference oscillator output on GNSS receivers is analysed when pyrotechnic shock is applied. In addition, performance and environmental tests of the MEMS oscillator were conducted to confirm the replaceability of TCXO, which is widely used as the reference oscillator for GNSS receivers. The contributions of this study are as follows.

- **Use of frequency data obtained from real test** : In the tracking loop analysis of the GNSS receiver, the measured frequency data in the pyrotechnic shock test is utilized. The simulation results were consistent with those of the tests conducted in practice.

- **Adoption of MEMS oscillator** : Verification tests of MEMS oscillator has been done to replace TCXO, which is used as the reference oscillator for GNSS receiver.

1.3   Organization of the Dissertation

This dissertation is organized as follows. Chapter 1 provides the motivation and background of this dissertation as well as the objective and contributions. In chapter 2, the criterion for the general oscillator is introduced, and fundamentals of the TCXO and the MEMS oscillator as reference frequency sources are reviewed. Chapter 3 provides the effects of environmental conditions of oscillators are examined from existing article and papers and analyzes the variation of the output frequency of oscillators by applying temperature changes, vibrations, and pyrotechnic shock test, and chapter 4 presents a tracking loop of a GNSS receiver and the behavior of the GNSS receiver under the change of reference frequency. Chapter 5 presents the results of environmental and performance tests with each oscillator assembled on the GNSS receiver, and in chapter 6, the summary and the factors associated with the possible replacement of TCXOs in the field of GNSS receiver technology are presented.

Chapter 2

Oscillators for Timing Source

An oscillator, which provides the accurate and precise reference frequency, is a key component in a GNSS receiver, which determines the user's position by measuring the exact time delay of a satellite signal. The oscillator vibrates a resonator with a high Q-factor (quality factor) and amplifies its signal to output a constant frequency corresponding to its natural frequency. The oscillator can be classified according to the resonator used, and this chapter introduces both the MEMS oscillator and the TCXO and examines their working principles with simple models.

2.1   Barkhausen Criterion

In order for a resonator to produce the stable frequency output without attenuation, the Barkhausen criterion must be satisfied. Consider the closed-loop feedback network as shown below.
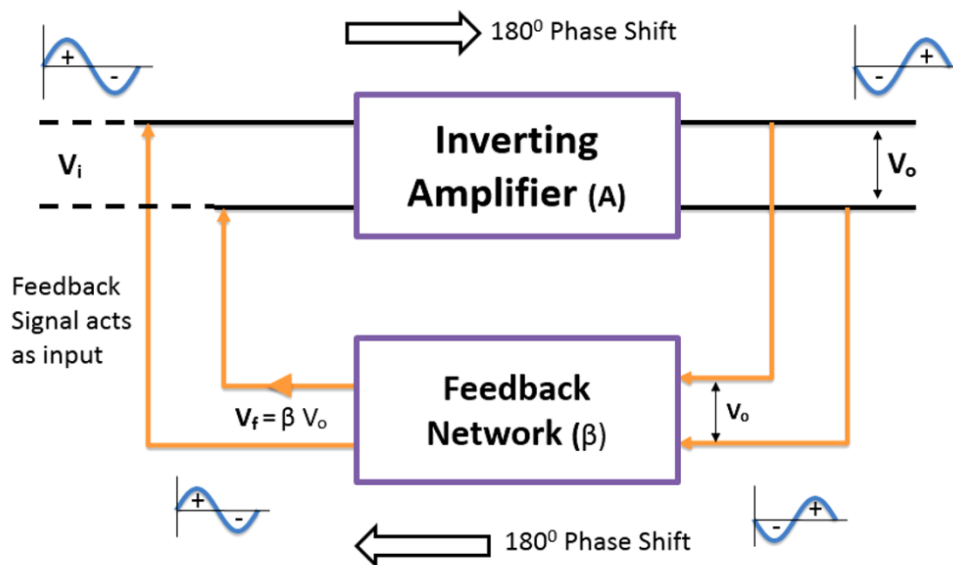
Figure 2.1 Oscillator closed-loop circuit

Consider a voltage V_i is applied at the input of the inverting amplifier,

$$V_o = A * V_i \qquad (2.1)$$

The feedback gain β determined the feedback voltage to be given to the input

$$V_f = \beta * V_o = A * \beta * V_i \qquad (2.2)$$

The two conditions required to work the circuit as an oscillator are called the Barkhausen criterion for oscillation below.

1. The total phase shift around the loop must be $0°$ or any integer multiple of 2π $(360°)$.

2. The magnitude of the product of the amplifier gain (A) and the feedback gain (β) is 1, $|A\beta| = 1$

If these conditions are met, the circuit works as an oscillator producing self-sustained oscillations of constant frequency and amplitude.

2.2 TCXO

Currently, the most widely used oscillator is the TCXO, which uses quartz crystal as a resonator. Quartz is a piezoelectric element that outputs a constant frequency through an exchange between physical vibration and electrical energy. The electrical interface is clear, and the Q-factor is fairly high, making this material suitable as a reference frequency source. Because it has a temperature-frequency relationship characterized by a cubic polynomial curve with an inflection point near room temperature, it provides relatively accurate frequencies over a wide temperature range even in the absence of a compensation process. TCXOs, which improve the frequency stability by adding temperature-compensation circuits, are widespread in areas such as wireless communication devices, which require high accuracy levels.

2.2.1   TCXO Fundamentals

TCXO, which uses quartz crystal as a resonator, has a lot of fundamental properties and characteristics such as piezoelectricity, crystal structure, crystal cuts, vibration mode, and crystal mounting. The output frequency of TCXO depends on these characteristics, and a closer look at these elements can help make a TCXO robust and stable.

- Piezoelectricity

Piezoelectricity is the important property of a crystal which makes it a resonator. Piezoelectricity is defined as electric polarization produced by mechanical strain in crystals belonging to certain classes, the polarization being proportional to the strain and changing sign with it. This electric polarization can be produced by deformations such as bending, shear, torsion, tension, and compression for quartz pieces. The electrical polarization provides an electric force. And the inverse piezoelectric effect can be made; a voltage applied across the crystal produces mechanical displacement.

- Crystal structure

The quartz crystal consists of silicon and oxygen (SiO_2). Its characteristics stem from the unit cells, which are identical and consist of atoms arranged in a repetitive geometric pattern. Quartz crystals have a three-dimensional geometric body, and most physical properties of a crystal are anisotropic; therefore, changes as it grows, affecting anisotropy, resulting in crystal imperfection. A change in the

piezoelectric coefficient creates a boundary in which the sign of the charge is different when strain is applied. This twin boundary is not suitable for a reference oscillator unit as it prevents the crystal piece from resonating. Since various works and efforts are required in making a good crystal oscillator, these defects and flaws should be found earlier stage of manufacturing.

- Crystal cuts and vibration mode

Quartz material is obtained by cutting the lump crystal at specific angles to the various axes. The choice of axis and angles determine the physical and electrical parameters and characteristics of the resonator. For example, an X plate crystal, cut in normal to the X axis, produces a relatively large voltage when compressed and decreases in frequency with temperature increases. The Y cut, however, exhibits a positive temperature coefficient with a similar voltage. Numerous other cuts can be made just by changing the angle and the axis of reference.

When a quartz crystal is subjected to a voltage, a force is produced. As the voltage alternates at the proper rate, the crystal begins to vibrate and produce a stable electrical signal. The mode of vibration depends on how the crystal was cut. That is, X cut exhibits an extensional vibration mode, whereas the AT cut, which is cut at 35 degrees off the Y axis, vibrates in the thickness shear mode. The various vibration modes are shown in Figure 2.2.

• Frequency Determination

The vibration frequency is determined by the crystal cuts, size, and shape of the resonator. The primary frequency determinant for the AT and BT cut is thickness because they oscillate in the thickness shear mode. The precision with which the thickness is controlled determines the change from correction to modification at the nominal center frequency. The adjustment of the center frequency is accomplished by plating a small amount of gold on the quartz. Circular crystals of the thickness shear vibrating mode, when designed with the proper radius of curvature at the center, will produce frequencies with no spurious. For this reason, high performance crystal oscillators will typically utilize highly polished and properly shaped quartz resonators. In fact, these crystals are polished with a surface finish that is 10 times finer than those used for eyeglasses.
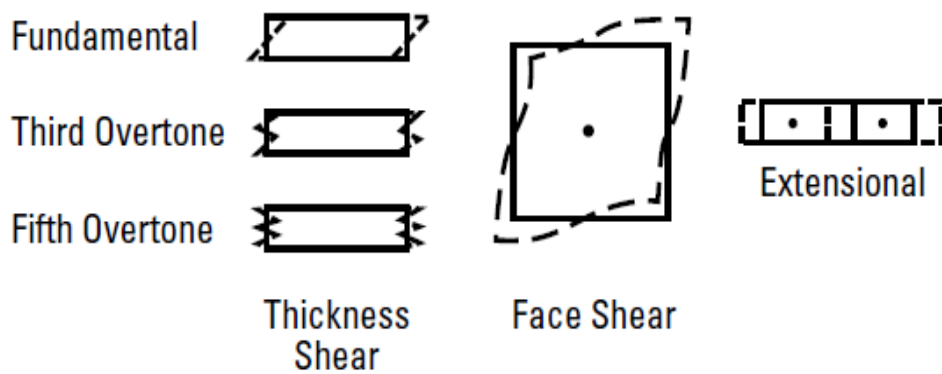
Figure 2.2 Vibration modes of various crystal cuts and the thickness shear overtone [11]

12

- Crystal Mounting

The supporting structure and methods used to obtain the electrical contacts are determined by the vibrating mode. Care must be taken in mounting to avoid placing a strain on the crystal. The support should not be a part of the resonator as it can absorb energy and cause an activity degradation, lowering Q value. A thickness shear mode crystal is supported by the edges at approximate null or zero nodes to avoid interfering with the vibration. A typical 1 MHz crystal, due to its size, maybe secured with tension wires at several points around the surface edge. A smaller 10 MHz crystal could be supported at two points on a ceramic header. Various support types are shown in Figure 2.3.

Once the crystal is mounted, a suitable encasement is selected. The cases reduce the effects of contamination, humidity, pressure, and atmospheric changes. Glass has been used for many years because it is easy to work when evacuation and inert gas replenishment are required. A newer technique is a cold-welded copper lid on a ceramic header. This method provides a cleaner environment and allows for uniform heat distribution, which is critical to compensate for the frequency change due to temperature.

Cemented Lead Type   Pressure Mounting   Solder Lead Type   Strap Type
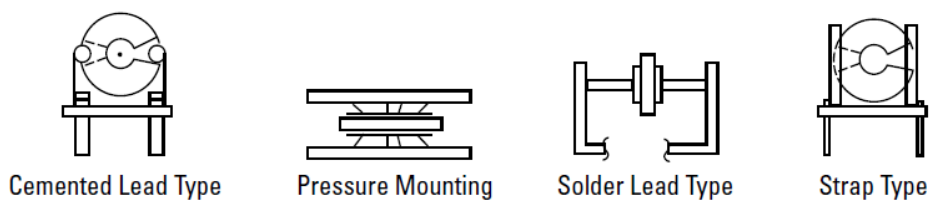
Figure 2.3 Methods of mounting crystals [11]

13

2.2.2　　TCXO Oscillator model

The TCXO, which uses quartz crystal as a resonator, can be modeled electrically as a series of RLC circuits with a shunt capacitance. The following Figure 2.4 shows the Pierce oscillator diagram, which is widely used in TCXOs today because of its simple circuit making, stable resonance frequency. A Pierce oscillator circuit has the following components like inverting amplifier(U_1), resistors(R_i), capacitors(C_i) and quartz crystal(modeled by R_1, L_1, C_1 and C_0).
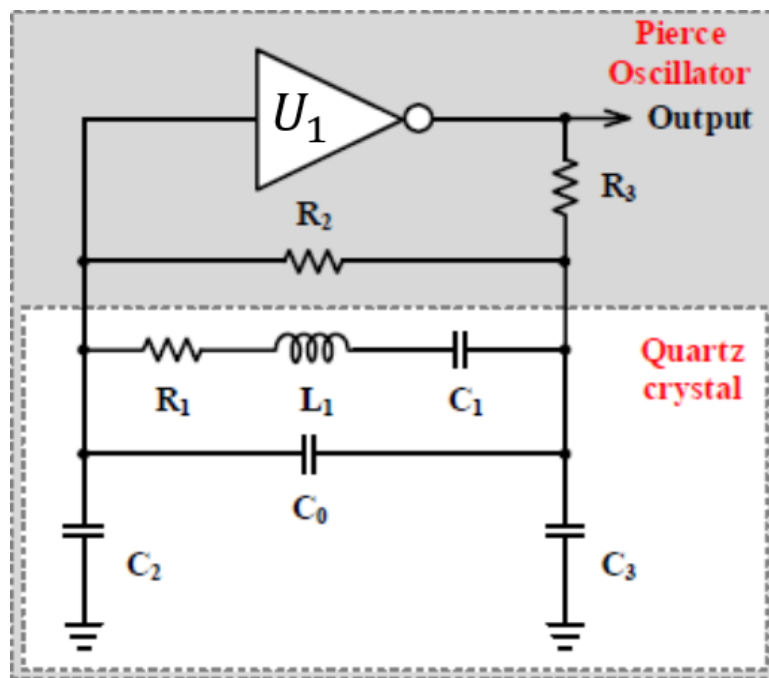
Figure 2.4 Pierce oscillator diagram [18]

The feedback resistor(R_2) is to linearize the inverting amplifier output by charging the inverting amplifier's input capacitance from the output of the

inverting amplifier. If the inverting amplifier is ideal, the input impedance is infinite, and the output impedance is zero.

The resistor in series with the output of the inverting amplifier, R_3, has two functions :

1. Isolation of the output driver of the inverting amplifier from the load impedance (C_2, C_3) and the crystal.
2. In conjunction with C_3, R_3 forms a lag network to add additional phase shift necessary at low frequencies, 8 MHz or below. This additional phase shift is needed to reduce the jitter in the time domain or phase noise in the frequency domain. R_3 is sometimes not needed since the output resistance of the inverting amplifier with C_3 will provide enough phase lag, it may still be needed to reduce the drive level on the crystal.

The inverting amplifier(U_1) provides the necessary loop gain to sustain oscillation as well as -180° phase shift. In general, the inverting amplifier is included in the microprocessor or ASIC. If it is not, the inverting amplifier must be selected with the proper gain/phase characteristics for the targeted frequency.

The quartz crystal, which is modeled by R_1, L_1, C_1 and C_0 together with C_2, C_3 and R_3, provide an additional -180° phase lag to satisfy the Barkhausen phase shift criteria for sustaining oscillation. Usually, load capacitance(C_2) is set equal to load capacitance(C_3). However, C_3 can be larger than C_2 by a small amount and set the center frequency and/or increase the loop gain. The shunt capacitance(C_0) represents the capacitance of the quartz crystal electrodes plus the capacitance of the leads. R_1, L_1, C_1 compose the motional arm of the quartz crystal and are

15

denoted as the motional parameters. The motional inductance represents the vibrating mass of the quartz crystal unit, and the motional capacitance represents the elasticity of the quartz, the resistance represents bulk losses occurring within a quartz crystal.

In the Pierce oscillator, the quartz crystal works in the inductive region of its reactance curve shown in the following Figure. A crystal that needs to operate in its inductive region is called a "Parallel Crystal".

A quartz crystal has two frequencies of zero phase, as illustrated in Figure 2.5. The lower of the two, is the series resonant frequency, denoted as F_s. At this frequency ($\frac{1}{2\pi\sqrt{L_1 C_1}}$), the quartz crystal acts like a resistor in the circuit, impedance is at a minimum, and current flow is maximum. As the frequency is increased beyond this series resonant frequency, the quartz crystal appears inductive in the circuit. When the reactances of the motional inductance and shunt capacitance cancel, the quartz crystal is at the anti-resonant frequency denoted as $F_a = (F_s + F_s * \frac{C_1}{2(C_0 + C_L)})$. At this frequency, impedance is maximized, and current flow is minimized. The quartz crystal oscillates at a frequency ranged from F_s to F_a.
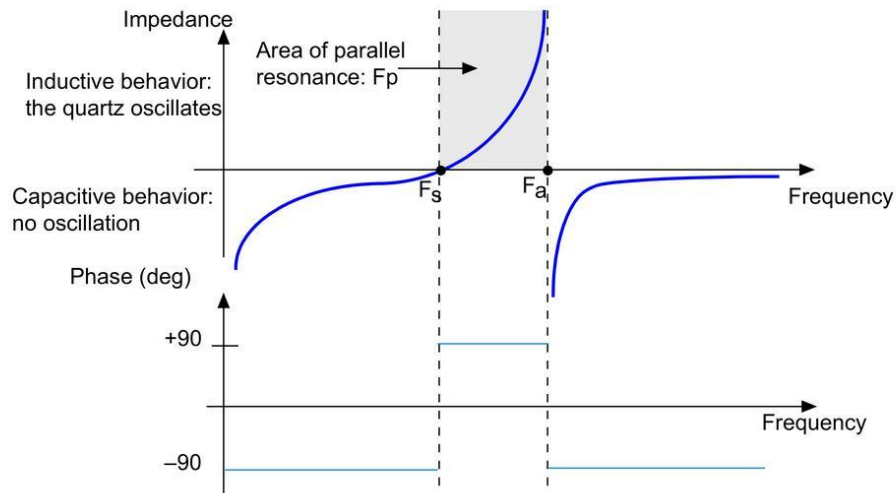
Figure 2.5 Reactance curve of parallel crystal and operating frequency region [18]

The pullability refers to the change in frequency of a crystal from natural frequency or series resonant frequency to load frequency or anti-resonant frequency. The amount of pullability exhibited by a given quartz crystal at a given load capacitance is a function of the shunt capacitance(C_0) and the motional capacitance(C_1). An approximation of the pulling limits for standard quartz crystals can be obtained from the following

$$\Delta\text{f} = F_S \frac{C_1}{2(C_0 + C_L)} \tag{2.3}$$

The exact pullability limits also depend upon the Q of the quartz crystal as well as associated stray capacitances. If the shunt capacitance and the motional capacitance are known, the trim sensitivity in ppm can be obtained using the following formula

17

$$\frac{\Delta f}{f} \ (\text{in PPM}) = \frac{C_1}{2(C_0 + C_L)^2} * 10^6 \tag{2.4}$$

When the shunt capacitance is 4.5 pF, and the motional capacitance is 0.02 pF, and the load capacitance is 30 pF, the pulling in ppm can be calculated as

$$\frac{\Delta f}{f} = \frac{0.02}{2(4.5 + 30)^2} * 10^6 = 8.40 \ \text{PPM} \tag{2.5}$$

This equation is useful since it gives values about how far off frequency the oscillator will be at room temperature every 1 pF under the 20 pF load capacitance due to component variation and tolerance. The problem here is that the equation requires the motional and shunt capacitances, which is not known.

2.2.3　Pierce Oscillator Design Example

Based on the following values of the Pierce oscillator circuit, an oscillator with the following requirements can be designed.

- Frequency : 10 MHz

- Temperature Stability over -20℃ to 70℃ : ±50 ppm

- Calibration/Tolerance at 25℃ : ±50 ppm

And the given conditions are

- Capacitances of Amp. Input(C_{in}) : 4 pF
- Capacitances of Amp. Output(C_{out}) : 9 pF

First, feedback resistor is not critical for designing Pierce oscillator and can be within 470k ~ 5MΩ at 10 MHz. The feedback resistor value can be chosen 1MΩ. The value of C_2, C_3, C_{in} and C_{out} will determine the load capacitance requirement on the quartz crystal. For a clock design, the load capacitance specification of the quartz crystal is the standard values of 20 pF. These are the two most common load capacitance values in the crystal industry. The load capacitance presented to the crystal in a Pierce oscillator is

$$C_{Load} = \frac{[(C_2 + C_{in})(C_3 + C_{out})]}{(C_2 + C_3 + C_{in} + C_{out})} + PCB\ strays\ (2\sim3\ pF) \qquad (2.6)$$

Assume that C_2 equals to C_3 and 3 pF for PCB strays, the C_2 can be obtained by solving the following equation

$$\frac{C_2^2 + 13C_2 + 36}{13 + 2C_2} = 17 \tag{2.7}$$

$C_2 = C_3 = 27\ pF$ are obtained from the above equation, and the load capacitance is set to 19.6 pF, which is close to the standard value of 20 pF.

The calibration/tolerance at 25℃ is ±50 ppm, and in order to meet this requirement in the crystal without trimming, the trim sensitivity equation is used. The typical commercial quartz crystal has a trim sensitivity range of -15 to -30 ppm/pF. If we set the trim sensitivity to ±30 ppm as calibration spec. with ±50 ppm tolerance requirement, the quartz crystal calibration specification is ±20 ppm.

Recently, a commercial quartz crystal is calibrated in the range of ±25 ppm to ±50 ppm at room temperature(25℃). The tighter the quartz crystal calibration specification, the higher the price. The load capacitance directly affects the calibration specification, as shown above. As the load capacitance is made smaller, the trim sensitivity becomes larger. Hence a quartz crystal with 10 pF load capacitance is much harder to calibrate than a quartz crystal with 20 pF load capacitance given the same design. It is harder to calibrate when a 3 pF load capacitance than with a 10 pF load capacitance under the same calibration/tolerance requirement.

The R_3 can be determined under the value of C_2=27 pF

$$R_3 = \frac{1}{2\pi f C_2} = \frac{1}{(2\pi)(10MHz)(27pF)} = 590 \ \Omega \qquad (2.8)$$

The quartz crystal type needs to be an AT-cut since a BT-cut cannot meet the ±40 ppm frequency stability over the temperature range of -20℃ to 70℃.

The oscillator circuit design parameters discussed above are as follows.

- Feedback resistor R_f : 1 MΩ

- Series resistor R_3 : 590 Ω

- Load capacitor $C_2 = C_3$: 27 pF

The quartz crystal specifications to meet the above oscillator requirements.

- Output frequency : 10 MHz
- Crystal type : AT Cut
- Load capacitance : 20 pF
- Calibration : ±20 ppm at 25℃

Even if the initial design is completed with validation, the higher the volumes of the product, the more attention should be paid to mass production and to reliability. Validation involves

- Measure gain margin

- Perform frequency Vs. Temperature tests over operation range

- Measure drive level of the crystal

- Specify the environmental test specification

2.2.4 TCXO in GNSS receivers

The TCXOs applied to GNSS receivers that operate under harsh environments must reliably generate accurate and stable frequencies in hot, cold, vibration, and pyrotechnic shock conditions and should use parts that have been proven to operate in such environments. The TCXO currently applied to the GNSS receiver for KSLV-II is the E7386 model by RAKON. This TCXO has been tested in multiple environmental conditions and is specialized in low acceleration sensitivity. Its temperature and physical stress specifications are correspondingly shown in Table 2.1 and Table 2.2 [21].

Table 2.1 TCXO E7386 temperature specifications [21]

Parameter	Min.	Max.	Unit	Test Description
Frequency Stability over Temperature		±1	ppm	Reference to (Fmax+Fmin)/2
Operating Temperature Range	-40	85	°C	Operating temperature range over which temperature stability is measured
Slope		±100	ppb/°C	Temperature ramp 1°C/min

Table 2.2 TCXO E7386 physical stress specifications [21]

Parameter	Test Description
Acceleration steady state	IEC 60068-2-7, test Ga duration: 1 minute peak acceleration: X1 & X2 axes 10,000g, Y1 & Y2 axes 20,000g, Z1 & Z2 axes 10,000g
Vibration	IEC 60068-2-6, test Fc Duration: 1.5 hours 20gn acceleration, 10Hz to 2000Hz, in each of three mutually perpendicular axes at 1 octave per minute.
Mechanical Shock	IEC 60068-2-27, test Ea duration 1ms, 3 shocks half-sine pulse in each of three mutually perpendicular axes (18 shocks total), X1 & X2 axes 10,000g, Y1 & Y2 axes 30,000g, Z1 & Z2 axes 5,000g.
Acceleration Sensitivity	0.2 ~ 0.5 ppb/g

Electronic devices, parts, including oscillators, will experience increased levels of thermal noise as the ambient temperature rises, while navigation errors tend to increase as the accuracy of the pseudo-range becomes degrades. Under considerable thermal noise, a sufficient integration time is required to cancel the thermal noise in order to acquire the navigation signal and/or improve the navigation accuracy, but in environments with highly dynamic characteristics, such as that of a space launch vehicle, long integration times are often not possible. The GNSS receiver for KSLV-II uses a FLL (Frequency Locked Loop) to track signals, and the tracking threshold of FLL is as follows [19]. The first term (σ_{tFLL}) is the frequency measurement noise caused by thermal noise, and f_e is the error induced by vibration, acceleration, or a shock. The sum of these two values should not exceed one-quarter of the pull-in range ($\frac{1}{T}$) of the FLL to enable accurate frequency tracking.

$$3\sigma_{FLL} = 3\sigma_{tFLL} + f_e \le \frac{1}{4T} \quad (Hz) \tag{2.9}$$

Once the signal has been acquired, the signal tracking is maintained unless the reference frequency from the oscillator undergoes a large discontinuity or jump for any reason. Even when external disturbances exist, the GNSS receiver can calculate its position and velocity accurately as long as signal tracking is maintained. However, phenomena such as 'activity dips', referring to abrupt frequency changes of TCXO within a certain temperature band, can interfere with signal tracking [20].

The specifications for acceleration, vibration, and shock are given in Table 2.2. However, there is no specific information regarding the test procedure, such as whether the reference frequency is measured during the stress interval or after the stress interval. Therefore, the operational capabilities under those loads should be verified by actual tests with the GNSS receiver.

The TCXO mounted on the GNSS receiver for KSLV-II is an oscillator specialized for specific types of physical stress, such as vibration, acceleration, and shock events, and its environmental conditions differ from those of the TCXOs used in commercial GNSS receivers and/or communication devices. The environmental specifications of TCXOs for commercial applications and for general GNSS receivers are shown in Table 2.3 [21-24]. The environmental test conditions for vibration and shock are often not specified in datasheets for commercial products, though it can be found that the E7386 specifications exceed those of the commercial products presented in Table 2.3. The vibration specification for Vectron's TCXO exceeds that of the E7386 model, but this is not true for the shock specification.

Table 2.3 Specifications of the commercial TCXO environment [21-24]

Manufacturer	Frequency Stability (-40 ~85℃)	Frequency Slope	Sine Vibration (Peak)	Shock
TXC	±2.0 ppm	0.5 ppm/℃	-	-
EPSON	±2.0 ppm	1 ppm/℃	-	-
IQD	±2.0 ppm	0.1 ppm/℃	10 g	3000 g, 0.3 ms
VECTRON	±1.0 ppm	-	50 g	5000 g, 0.3 ms

In order for the oscillator to function robustly under physical stress or loads such as vibration or shocks, an isolator can be installed. In a random vibration environment, isolators absorb high frequency vibration. However, when using an isolator, care must be taken as resonance can occur during low frequency vibration below 100 Hz, and shocks or vibration with large amplitudes may be transmitted, as can occur when the isolator is saturated [25].

When vibration is applied to an oscillator, the phase noise increases, changing the output waveform continuously. This phase noise causes clock errors in the random walk form and reduces C/N0, thereby degrading the navigation accuracy or increasing the time required for signal acquisition. After applying the acceleration sensitivity (0.5 ppb/g), phase noise values, and random vibration test specifications of E7386 to the below equation, the vibration simulation results are shown in Figure 2.6 and Table 2.4. It can be seen that the phase noise rises compared to that in the absence of vibration stress [26]. γ is the acceleration sensitivity, T is the transmissibility, PSD is the power spectral density of the random vibration, f_0 is the oscillator output frequency, and f is the offset frequency from the oscillator output frequency. As shown in below equation, the phase noise increases with greater acceleration sensitivity and higher transmissibility. Because the performed

simulation did not consider damping or the natural frequency, the actual phase noise is expected to be much greater compared to the values in Table 2.4.

$$L_{vib}(f) = L_{rest}(f) + (\frac{\gamma T(f)\sqrt{2PSD(f)}f_0}{2f})^2 \qquad (2.10)$$
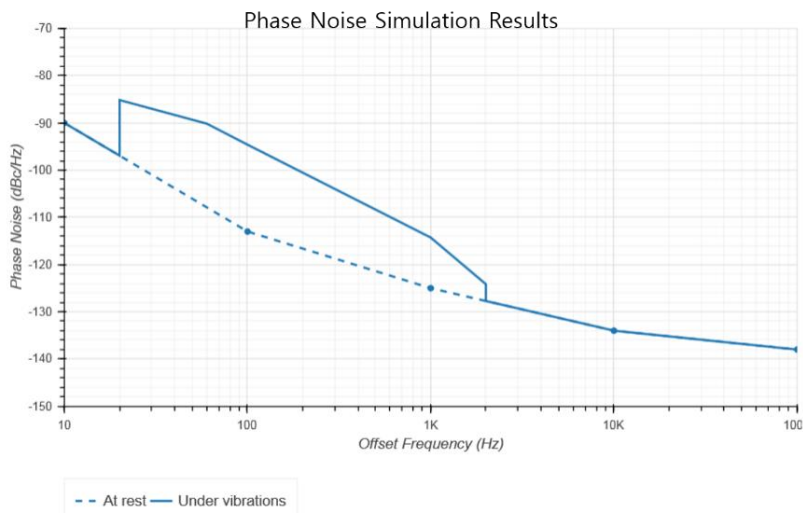
Figure 2.6 Phase noise simulation results in a random vibration environment (1/2)

Table 2.4 Phase noise simulation results in a random vibration environment (2/2)

Offset(Hz)	Phase Noise at Rest (dBc/Hz)	Phase Noise under Vibration (dBc/Hz)	Difference
10	-90	-90	0
100	-113	-94.6	+18.4
1000	-125	-114.3	+10.7
10k	-134	-134	0
100k	-138	.138	0

27

Normally, the output frequency or phase changes when an oscillator experiences an impact or shock. The output frequency of the oscillator changes permanently, as shown in Figure 2.7, when the amount of impact exceeds the elastic limit or when the capacitance of the oscillator circuit is varied [27]. Upon more severe impacts, the oscillator may be broken, and normal operation may not be possible, as shown in Figure 2.7. It should be noted that the surface treatment is very important because small scratches on the resonator surface seriously impair the resistance to impacts.
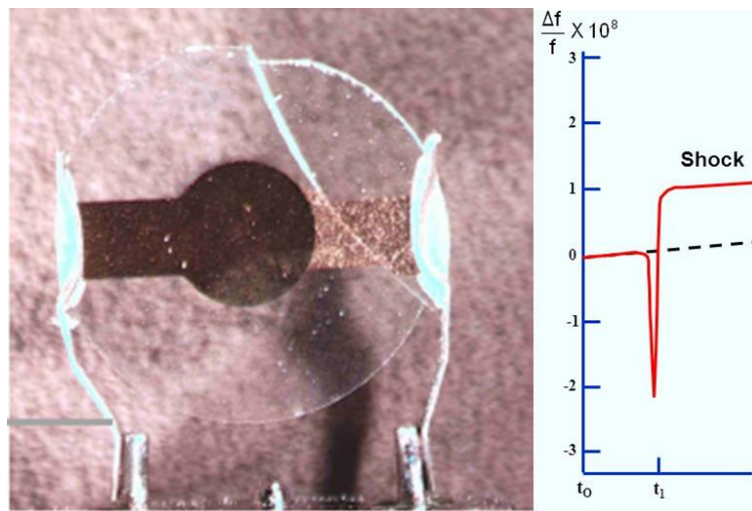
Figure 2.7 Broken resonator with the frequency output changed by a severe impact [27]

2.3   MEMS Oscillator

MEMS refers to ultra-fine structures such as highly integrated circuits, ultra-small gear, and finger-sized hard disks consisting of silicon, crystal, rings, and glass [28-31]. The operation of the MEMS oscillator, built on the basis of MEMS technology, is the process in which electrostatic(capacitive) and vibration motion are converted into each other with oscillation sustaining circuit, and it can also be fabricated with a surface treatment that adds piezoelectric materials to a small resonator as a thin film, reducing the physical size and weight over 1/10 times. The reduced size and weight of the MEMS Oscillator mean that the supporting structure of the internal resonator becomes relatively strong, making it more robust in physical stress or load environments such as vibration, shock, and acceleration [32].

Research on MEMS oscillators has been conducted since the 1990s, and companies from various areas, such as Discera, SiTime, Epson, and Avago, have jumped into manufacturing. Although robustness to harsh environments existed in the early days of MEMS oscillators, they were not widely used in commercial products due to the high phase noise they presented, whereas it has been announced more recently that the phase noise has improved to an extent comparable to the TCXO type [16]. This could be a good opportunity for MEMS oscillator makers to replace TCXOs, which thus far dominate most oscillator markets.

Depending on the direction and manner of the cutting of the quartz crystal, a plane with a TCF (Temperature Coefficient of Frequency) of nearly zero exists, and each TCXO's resonator is manufactured using this plane. However, MEMS oscillators, made of a thin film or silicon, require compensation for frequency changes due to temperature changes because the TCF of a MEMS oscillator can

greatly exceed that of a TCXO [33]. Commonly used methods are mechanical compensation to make the TCF close to zero through mixing with a material with an opposite TCF, or circuit compensation to adjust the output frequency according to temperature changes by adding a temperature sensor to the compensation circuit [17,29]. The stability of recently released MEMS oscillator's during temperature changes is much better than that of TCXOs, and manufacturers appear to have solved the problem of 'activity dips', previously unavoidable in TCXOs [34].

The results of random vibration and shock tests for oscillators performed by ILSI, which produces many types of oscillators, are shown in Figure 2.8 and Figure 2.9. Figure 2.8 shows that the phase noise of the MEMS oscillator is slightly higher than the phase noise of TCXOs during calm periods, whereas the phase noise of TCXOs increases significantly compared to that of the MEMS oscillator during random vibration, implying that this type is less affected by vibration stress. When the oscillators are subjected to shocks on the level of 500g, the frequency offsets of the TCXO and MEMS oscillator are shown in Figure 2.10, which indicates that the resistance to shocks of the MEMS oscillator is much higher than that of any other TCXO sample [35].
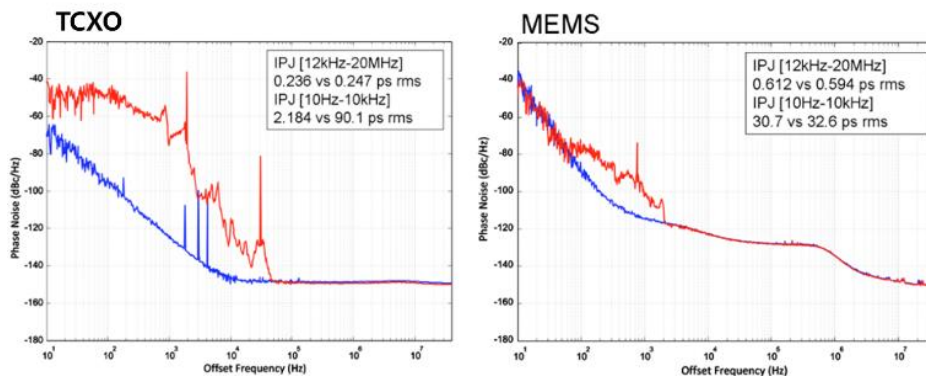
Figure 2.8 Phase noise comparison in a random vibration environment [35]
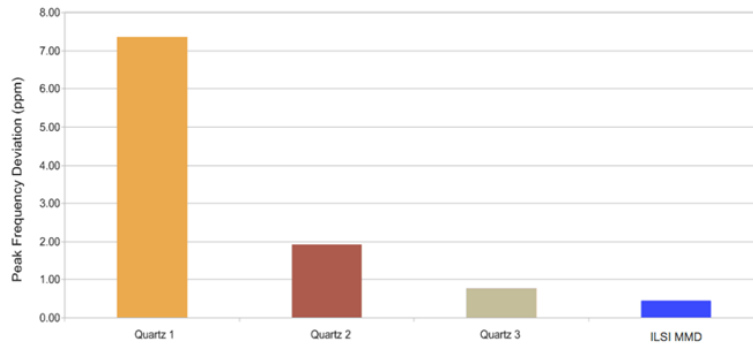
Figure 2.9 Frequency deviation comparison in a shock stress environment [35]

The MEMS oscillators also are less sensitive to EMI. An electromagnetic energy can be measured by exposed PCBs that connect the quartz crystal resonator to the oscillator circuit. This noise can be mixed into the oscillator circuit and passed to the output adding unwanted noise to the system. However, integrated oscillators have no exposed PCB connections between the resonator and oscillator circuit, and the wires and balls that connect the MEMS resonator to the IC are very short. This makes MEMS oscillators much less sensitive to EMI than TCXO.

And MEMS oscillators offer much better reliability. Quartz resonators, while a mature manufacturing technology, involve a complicated process in which each individual resonator is tuned to the targeted frequency. This step occurs before crystal is encapsulated and causes the resonator to be susceptible to contamination. In cantrast to the manufacturing processes of quartz crystals, MEMS oscillator is fabricated using standard semiconductor batch mode techniques. This includes wafer level production of resonators and oscillator and die bonding with plastic encapsulation. And ultra-clean hermetic vacuum seal ensures the resonator structure is protected and free of contamination eliminating aging mechnisms. The MTBF(Mean Time Between Failure) of MEMS oscillators (1140 million hrs.) are

31

about 30 times better than quartz (10 ~ 40 million hrs.), providing very reliable platform that endures severe environmental stresses and provides a high quality to the end user.

2.3.1   Electrostatic MEMS Oscillator model

In the MEMS oscillator, the vibrating elements are generated by micro-scale etching using silicon. A voltage is applied through the fine gap between a resonator and electrodes, and the mechanical vibration incurs the exchange of energy between the mechanical energy and electrical energy under the electrostatic force. An oscillator circuit maintains the vibration with amplifier energy under Barkhausen criteria. The resonator is a passive device that determines the resonant frequency according to its size, shape, and density. With the recent development of semi-conductor technology, a MEMS oscillator can be produced much smaller and lighter than TCXO, which uses piezo-electric elements. A small size MEMS oscillator has properties favorable to harsh environmental conditions compared to relatively large TCXO.
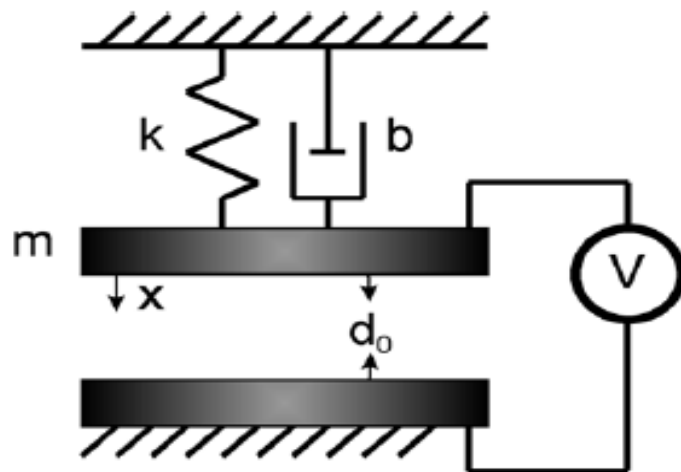
Figure 2.10 MEMS oscillator model for parallel plate [36]

Frequently used model of MEMS oscillator in the form of Parallel-Plate and anon-linear oscillation equation, Duffing equation are as follows [36].

$$m\ddot{x} + c\dot{x} + kx + \beta x^3 = F_e \qquad (2.11)$$

In the above equation, m represents mass, c is damping coefficient, k is elastic constant, and β is non-linear elastic constant. In Parallel-Plate case shown in Figure 2.10, F_e, electrostatic force can be written as follows.

Electrostatic force (F_e) is described as charge (Q) and electric field (E)

$$F_e = \frac{1}{2}QE \qquad (2.12)$$

Charge (Q) is the multiplication of C and V.

$$Q = CV \qquad (2.13)$$

The electric field is given as follows using V and $(d_0 - x)$.

$$E = \frac{V}{(d_0 - x)} \qquad (2.14)$$

Capacitance can be written as

$$C = \frac{\varepsilon_0 A}{(d_0 - x)} \qquad (2.15)$$

Electrostatic force can be rewritten as

$$F_e = \frac{\varepsilon_0 A V^2}{2(d_0 - x)^2} \qquad (2.16)$$

To simplify modeling, assume that a non-linear elastic constant is zero and a quasi-static situation in which the electrostatic force and the elastic force are the same. Then, the displacement is as follows.

$$kx = \frac{\varepsilon_0 A V^2}{2(d_0 - x)^2} \qquad (2.17)$$

Rearranging with respect to V^2 gives

$$V^2 = \frac{2kx(d_0 - x)^2}{\varepsilon_0 A} \qquad (2.18)$$

Taking derivative the right side to obtain the maximum value, V_{max} and x are as follows.

$$V_{max} = \sqrt{\frac{8kd_0^3}{27\varepsilon_0 A}}$$ (2.19)

$$x = \frac{d_0}{3}$$

Denote V', x' as normalized V and normalized x using V_{max}, d_0, above V' is expressed as follows.

$$V'^2 = \frac{27x'(1-x')^2}{4}$$ (2.20)
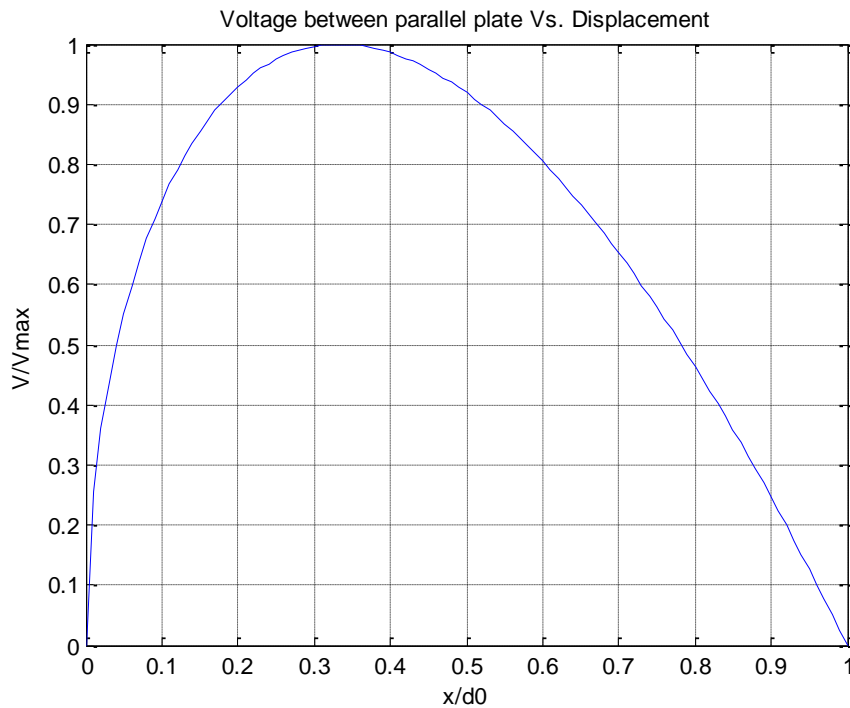
Figure 2.11 Voltage difference vs. separation between plates

The maximum point of V under $x < d_0$ is called 'pull-in' point and depends on the voltage applied to two electrodes. The resonator maintains its vibration within pull-in region. If the applied voltage is larger than V_{max}, the resonator moves outside the pull-in region and can stick to the electrode. This is called a bifurcation phenomenon.

This system potential energy is calculated by the sum of electrostatic and spring elastic potential energy when the displacement from one electrode is changed from 0 to x. It can be expressed as follows.

$$U = \int_0^x F_e dx + \frac{1}{2}kx^2 \tag{2.21}$$

$$U = \int_0^x \frac{1}{2}QE dx + \frac{1}{2}kx^2 \tag{2.22}$$

Substituting Q, E gives the following

$$U = \int_0^x \frac{1}{2}\frac{\varepsilon_0 AV^2}{(d_0-x)^2} dx + \frac{1}{2}kx^2 \tag{2.23}$$

Integrating the first term

$$U = \varepsilon_0 AV^2 \left(\frac{1}{2d_0} - \frac{1}{2(d_0-x)}\right) + \frac{1}{2}kx^2 \tag{2.24}$$

Rewriting the above equation with normalized variables

$$U' = \frac{4}{27}V'^2 \left(\frac{-x'}{(1-x')}\right) + \frac{1}{2}x'^2 \tag{2.25}$$

Figure 2.12 illustrates the potential energy in the case of $V' = 0.6, 0.8, 1.0, 1.2$ for x'. In Figure 2.13, there is no stable point when V' is larger than 1.0. The bifurcation occurs, and the resonator sticks to one electrode. If V' is less than 1.0, the stable point exists between two electrodes, which causes the resonator to vibrate by electrostatic force and spring elastic force.

This pull-in effect or pull-in instability is important for designing resonator or vibrating devices like MEMS sensors using electrostatic force and has been

observed for many applications[37-41]. When there is an electrical potential between the plate and substrate, the attractive force will attract the plate while the elastic force of the plate will restore the plate original displacement. In this case, the electrostatic force and the elastic restoring force are in an equilibrium state. The deformation of the plate would cause an electric charge distribution change. And the redistribution of the electric field achieves a new equilibrium state.

During beam resonator or plate resonator movement, the device could be affected by the air damping, drag. When the devices vibrate with greater amplitude, the effect of air damping force would be increased. Thus, it is critical to establish an air damping model of components under movement. A simplified electrostatic driven beam model under non-linear air damping is studied, and an analytical formula of the air damping force and the damping coefficient of the plate is developed using the Fourier series [42, 43].
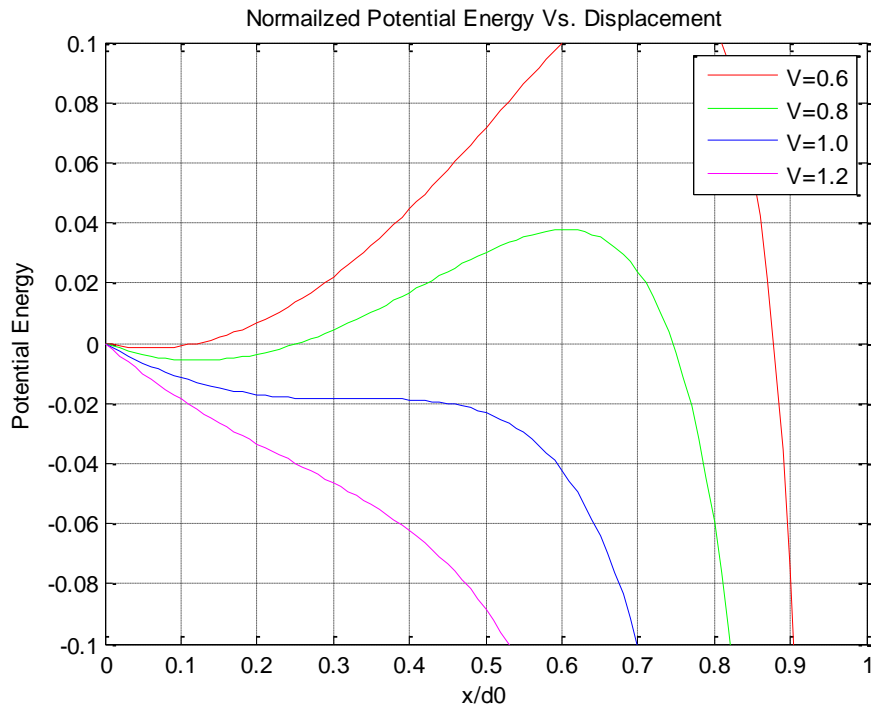
Figure 2.12 Energy vs. separation between plates for three values of voltage

2.3.2   MEMS Oscillator Design Example

Based on the previous modeling on MEMS oscillator, a clamped-clamped beam oscillator with the following design parameters is simulated. The diagram of a clamped-clamped beam resonator is shown in Fig. 2.13. A resonator is made of aluminum, and the electrode anchors, beams are developed using metal in the CMOS process [44].
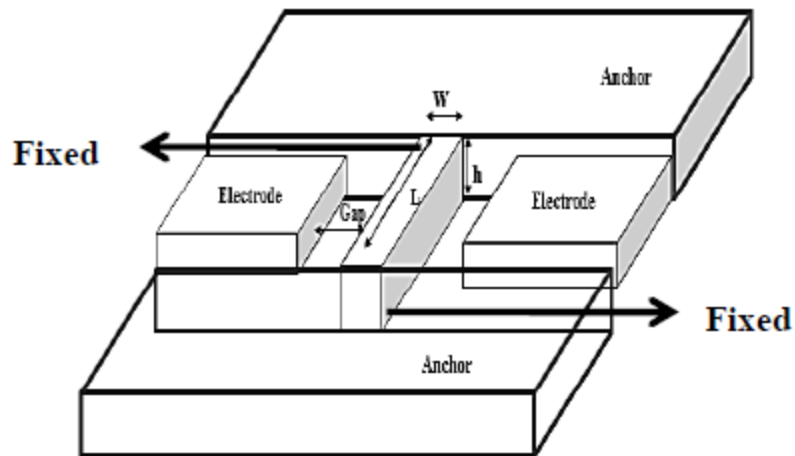
Figure 2.13 clamped-clamped beam resonator [44]

Table 2.5 MEMS oscillator with 10 MHz output design parameters

Input parameter	Value	Unit
Beam length, L	15	µm
Effective beam width, W	0.45	µm
Beam thickness, h	1	µm
Poisson ratio, ν	0.36	-
Young's Modulus, E	64	GPa
Density of beam, ρ	2700	Kg/m^3

The natural frequency of the above resonator depends on physical parameters such as length, width, thickness, and material properties. The frequency of a resonator is calculated according to the below equation [45].

$$f = 1.03 \sqrt{\frac{E}{\rho}} \frac{W}{L^2} \qquad (2.26)$$

Chapter 3

Environmental Test Results of Oscillators

Rakon's low acceleration sensitivity TCXO E7386 has already been used in the GNSS receiver for KSLV-II, and temperature tests, vibration tests, and pyrotechnic shock tests were completed during the manufacturing process. However, the GNSS receiver cannot track or will lose track of the navigation signal due to an abrupt change in the reference frequency of the TCXO during a pyrotechnic shock. Pyrotechnic shock tests were conducted with several TCXO samples as screening, and the oscillator that showed the least change in the output frequency was selected and applied to the GNSS receiver [10].

While searching for oscillators that are robust against physical stress and can be used in GNSS receivers, it was confirmed that the environmental specifications of the MEMS oscillator were superior to those of the TCXO. Environmental tests of MEMS oscillator samples were conducted to confirm the possibility of using the MEMS oscillator as a replacement in GNSS receiver applications. The conducted environmental tests used the specifications shown in Table 3.1 for the MEMS oscillator samples, and the results are described in this chapter.

Table 3.1 Environmental test specifications

Test		Test Description, Method		Measurement
Temperature		-15°C ~ 60°C (Chamber) Low: 5 Hours Soak @ -15°C High: 5 Hours Soak @ -60°C		Frequency Offset (ppm, ppb) From 10 MHz
Vibration	Sinusoidal	5 ~ 2000 Hz, 2 octave/min. 22 g @ 60 ~ 200 Hz		
	Random	20 gRMS*, 4 minutes		
Shock	Pyrotechnic shock	Freq. (Hz)	SRS (g) [Q = 10]	3 times/axis, along 3 axes
		100	40	
		100 ~ 2,000	+8.7 dB/oct	
		2,000 ~ 10,000	3,000	

3.1   Oscillator Behavior under Environmental Stress

The frequency and amplitude of the output signal of a reference oscillator are affected by various environmental conditions. The major causes of oscillator frequency instabilities are shown in Figure 3.1. This chapter examines the physical basis for the sensitivity of oscillators to time, temperature, humidity, pressure, vibration, electro-magnetic field, and radiation.
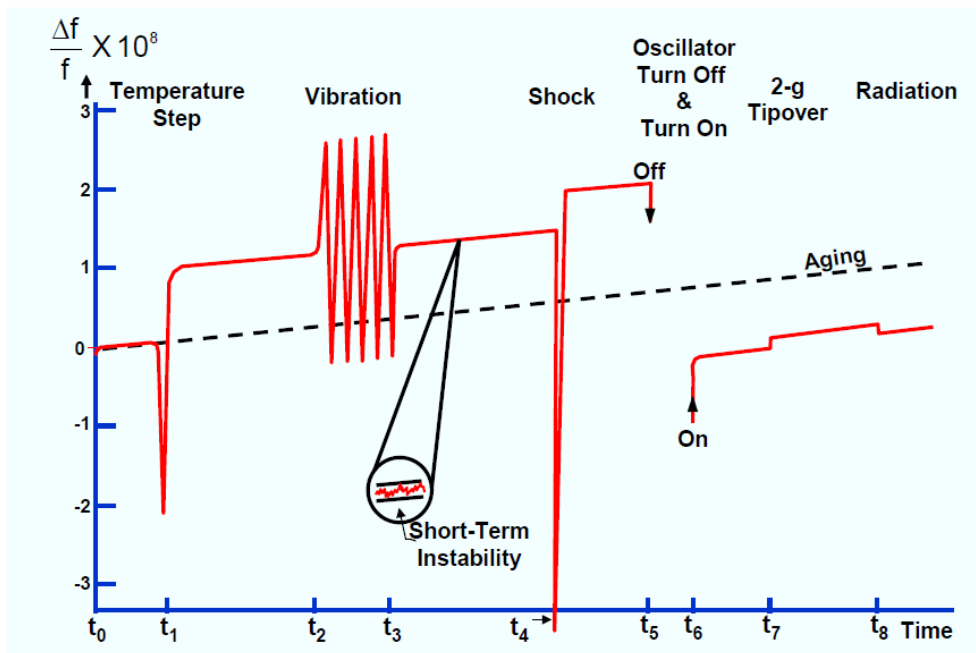
Figure 3.1 Various factors affecting oscillator's frequency [42]

3.1.1 Vibration and Acceleration Sensitivity

Every acceleration makes force, and force can cause a device to deform in some ways. The acceleration can affect resonant frequency, clock rates, optical properties, and even amplifier gain. Typical levels of acceleration that equipment may experience in various operating environments are shown in Table 3.2. Sources of vibration are anywhere from inside a moving vehicle or aircraft to handheld mobile devices. For example, the performance of aircraft radar is directly related to the oscillator phase noise in the system. Vibration induced phase noise translates to the blurring of targets and a decrease in the accuracy of detection. Medical imaging applications are also quite sensitive to vibration. In these systems, the oscillator phase noise limits the resolution, so the system must be resilient to vibration operate reliably.

Table 3.2 Typical acceleration levels in various environments [47]

Environment	Typical Acceleration (G's)
Building, quiescent	0.02 rms
Tractor-trailer	0.2 peak
Armored personnel carrier	0.5 ~ 3 rms
Ship-calm seas	0.01 ~ 0.1 peak
Ship-rough seas	0.8 peak
Railroads	0.1 ~ 1 peak
Propeller aircraft	0.3 ~ 5 rms
Helicopter	0.1 ~ 7 rms
Jet aircraft	0.02 ~ 2 rms
Missile – boost phase	15 peak

Although large shocks or vibrations can change the long-term frequency of the resonator, the main effect is typically a momentary change in the resonator frequency due to changes in the stress on the resonator through the mounting structure [49-54]. The frequency changes are linear up to approximately 50 g of acceleration or vibration depending on the direction. The maximum sensitivity is typical of the order $2 * 10^{-9}$/g.

Significant efforts in compensation [49,51], installation techniques [52], and resonator fabrication techniques [54] have been made to minimize the sensitivity. The net sensitivity for specially compensated or fabricated oscillators ranges from approximately $1 * 10^{-11}$/g to $3 * 10^{-10}$/g.

When a resonator experiences acceleration, a vibration frequency changes due to the stresses caused by acceleration. Under varying vibration frequency or amplitude circumstances, the resonator vibration frequency also changes according to the environmental condition. The relationship between frequency and acceleration can be nonlinear at higher acceleration due to deformation of mounting and supporting structure. The acceleration sensitivity can also be a function of temperature. The relationship between frequency change and acceleration is usually linear, with acceleration magnitude up to least 50 g's. How a varying vibration frequency changes the frequency of a resonator is shown in Figure 3.2 [48].
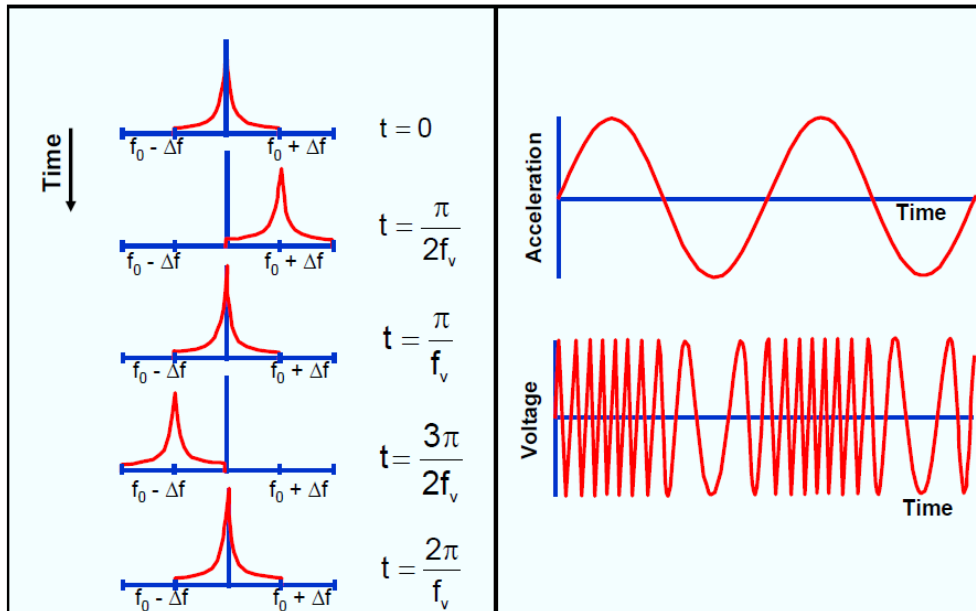
Figure 3.2 Sinusoidal vibration modulated resonator frequency [48]

Experience shows that the acceleration sensitivity of a quartz crystal oscillator is a vector. The frequency of the accelerated oscillator is maximum when the direction of acceleration is parallel to the acceleration sensitivity vectors. The frequency change due to acceleration with an acceleration sensitivity vector is $\Delta f = \Gamma \bullet A$. Therefore, the frequency shift is zero for acceleration in planes perpendicular to the acceleration sensitive vector and negative for opposite acceleration to the acceleration sensitive vector. Typical values of Γ for commercial crystal oscillators range from 10^{-9}/g to 10^{-10}/g. Γ is independent of applied acceleration amplitude up to 20 g. However, high acceleration levels can cause changes in the mounting structure, which can lead Γ being a function of acceleration or a function of temperature. The magnitude of the acceleration

46

sensitivity is the vector sum (square root of the sum of the squares) of the sensitivities of the three mutually perpendicular axes.

To prevent a vibration induced noise, an isolation system can be introduced. Even a simple vibration isolation system itself is a resonant structure. It can be effective at high frequencies (along one direction), but it amplifies the vibration below its resonant frequencies, as shown in Figure 3.3. In addition, the isolation system should accommodate large displacement at low frequency and high accelerations. For sinusoidal oscillation, the vibration displacement $d = d_0\sin(2\pi f t)$, and the acceleration $a = -d_0(2\pi f)^2\sin(2\pi f t)$, where d_0 is the peak displacement, and f is the vibration frequency. Therefore, $d_0 = \frac{a}{(2\pi f)^2}$, peak-to-peak. Therefore, the peak-to-peak displacement is inversely proportional to the square of the vibration frequency under the constant acceleration.
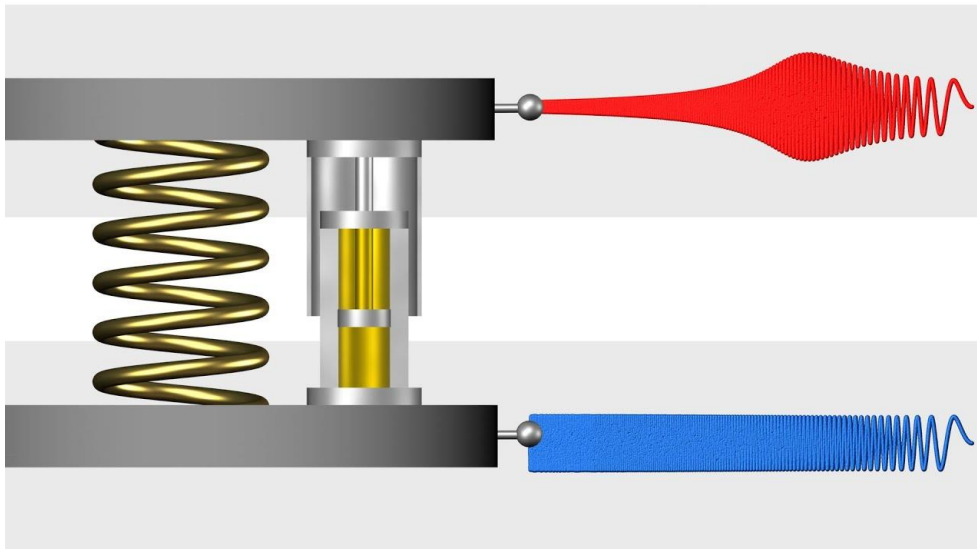
Figure 3.3 Response of passive vibration isolation system
to sinusoidal excitation (Blue) [11]

Acoustic noise can be particularly problematic in certain applications. For example, if an aircraft radar applications require extremely low noise oscillators, the isolation system was effective in isolating the oscillator from the vibration of aircraft induced vibration. The designer discovered that the expected phase noise could not be realized because it was failed to block the intense acoustic noise. The isolation system can isolate the oscillator from the vibration of the aircraft itself, but it was not able to manage sound waves, which are relatively low frequencies.

3.1.2   Temperature Sensitivity

A main influence on the crystal frequency is operation under the temperature changes. With a frequency change of 5 ppm/°C at a 25°C, the oscillator can experience a frequency offset of 25 ppm only with a temperature increase of 5°C. The amount of frequency variation depends on the crystal cuts because of the crystal temperature coefficient. A frequency-temperature graph for various cuts is shown in Figure 3.4.

The curves of some crystal cuts remain relatively flat over a limited temperature range. Others have both positive and negative frequency deviation that makes an "S" curve. A small change in the cutting angle can limit the deviation and make the slope less steep, as shown in Figure 3.5. Clearly, this frequency change cannot be compensated or avoided completely if the crystal is used over a wide range of temperatures. Therefore, other techniques must be utilized to reduce this effect.

Temperature variations change the value of the elastic constants and the dimensions of the resonator. The resulting change in resonator frequency with temperature depends largely on crystallographic cutting and orientation [57-60]. There are several cuts that compensate for frequency dependence on temperature. The actual values depend on the resonator cut, overtone, frequency, diameter, and mounting techniques. Temperature changes and temperature gradients often cause large frequency change compared to the slope of a static curve. Typical coefficients for frequency-temperature effect for 5-MHz resonators for 5th overtone AT cuts are
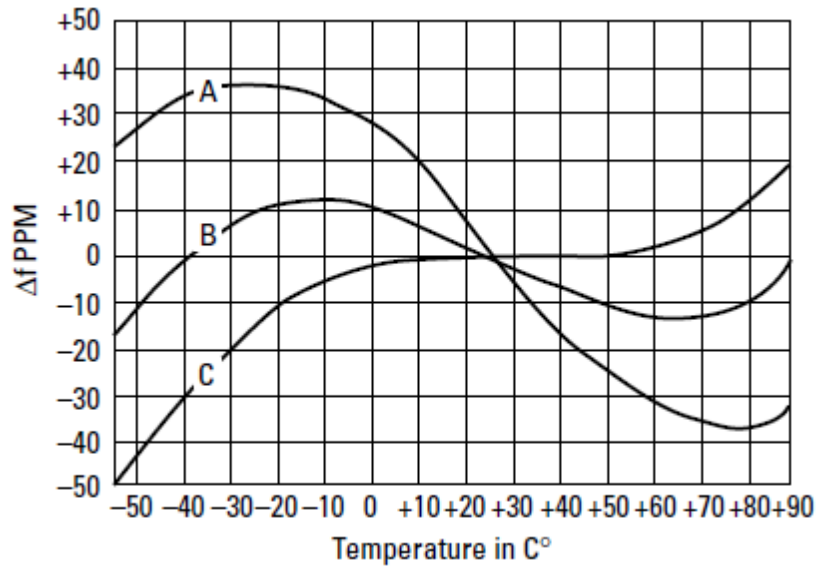
Figure 3.4 Frequency vs. Temperature relations for crystal cuts [57]
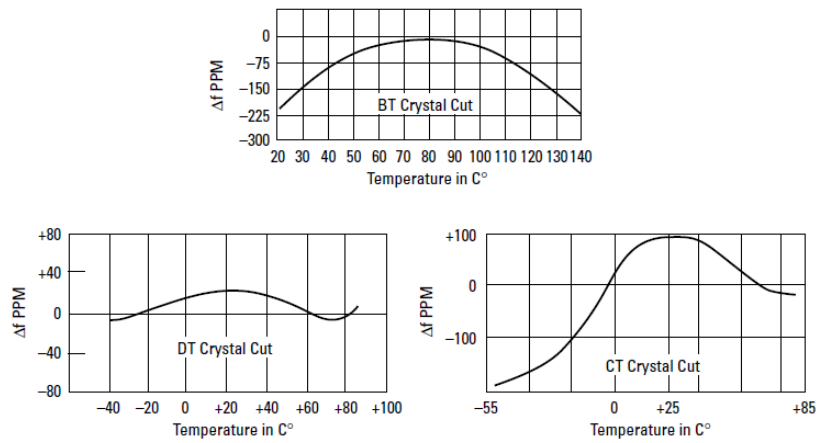
Figure 3.5 Frequency vs. Temperature plots of AT cuts with various cutting angle [57]

$$\frac{\Delta f}{f_0} = 10^{-9}\Delta T^2 - 10^{-5}dT/dt \tag{3.1}$$

For 3rd overtone SC cuts,

$$\frac{\Delta f}{f_0} = 10^{-9}\Delta T^2 + 10^{-7}dT/dt \tag{3.2}$$

The frequency-temperature characteristics of the crystal oscillator are not repeated exactly upon temperature cycling. The lack of repeatability in temperature-compensated crystal oscillators (TCXOs), called "thermal hysteresis," is depicted in Figure 3.6 [48]. They are showing that the frequency-temperature characteristics during temperature rise are different from those of temperature decrease. This effect makes it hard to find the exact inflection point.

Hysteresis is defined as the difference between the up-cycle and the down-cycle frequency-temperature characteristics and is quantified by the value of the difference at the temperature where the difference is maximum. Hysteresis is determined for one or more complete quasi-static temperature cycles between the specified temperature limits. Hysteresis is a major factor limiting stability that can be achieved with TCXOs. Typical hysteresis values for TCXO range from 1 ppm to 0.1 ppm with a temperature cycle ranges of 0°C to 60°C, and -55°C to +85°C. Some SC-cut resonators have observed hysteresis less than 10^{-9}, but some common resonator hysteresis is around some parts in 10^8.

As mentioned earlier, the vibration mode of the crystal depends on the crystal cuts, and there can be an accidental overlap with the main resonance mode over a narrow temperature range. This anomaly is called "activity dips," as illustrated in Figure 3.7. This unwanted coupling leads to increased resistance and a reduction in the oscillator amplitude. When the oscillator gain is insufficient, it can stop the oscillation. Near the activity dip region, the frequency-temperature coefficient

varies rapidly. This phenomenon is influenced by the crystal's drive level and load capacitance. The activity dip temperature is a function of C_L because the interfering mode frequency usually has a large temperature coefficient and a C_1 that is different from that of the desired mode. When the frequency of the interfering mode coincides with the frequency of the main resonance mode, the frequency cancels out, and an activity dip occurs.
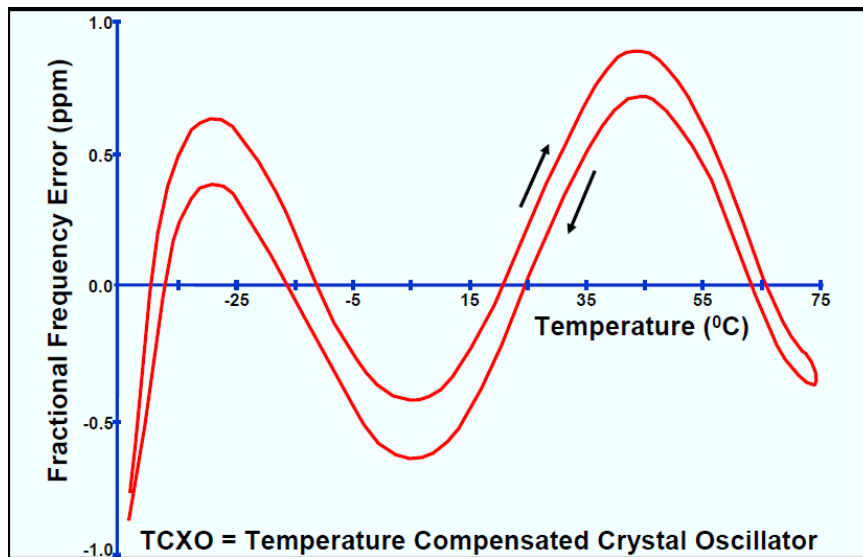
Figure 3.6 TCXO thermal hysteresis [48]

An important note in TCXOs is the interaction between the frequency adjustment during calibration and the frequency-temperature relation. This phenomenon is called the trim effect. In TCXOs, temperature-dependent reactance changes are used to compensate for the crystal's frequency-temperature coefficients. During calibration, the load reactance of the crystal is changed to compensate for the aging of TCXOs. Because the frequency-reactance relationship is nonlinear, the capacitance change during calibration changes the compensation process, such as the operating point on the frequency-reactance curve, to a point where the slope of the curve is different.
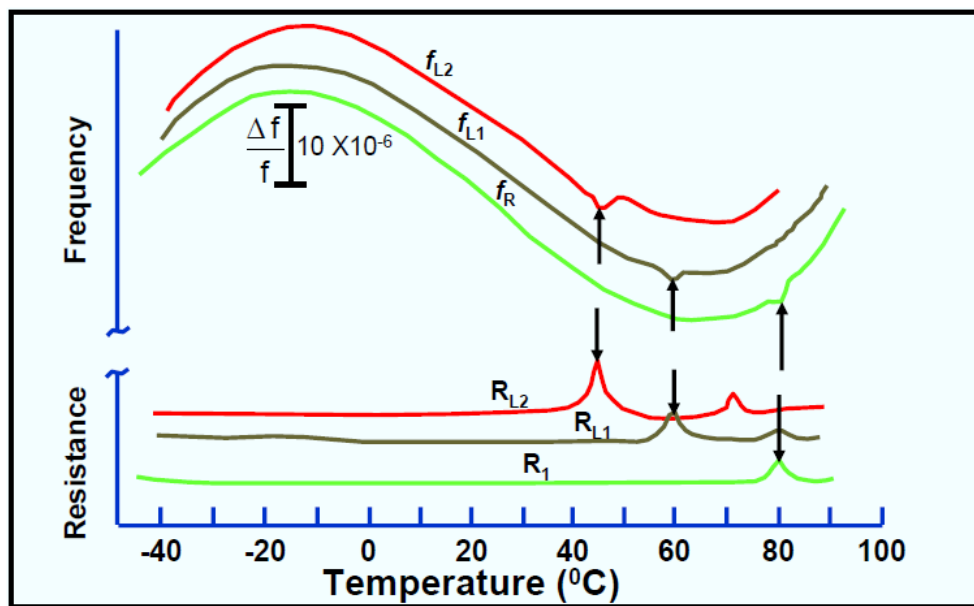
Figure 3.7 Activity dips in the Frequency vs. Temperature plot
with and without load capacitors [48]
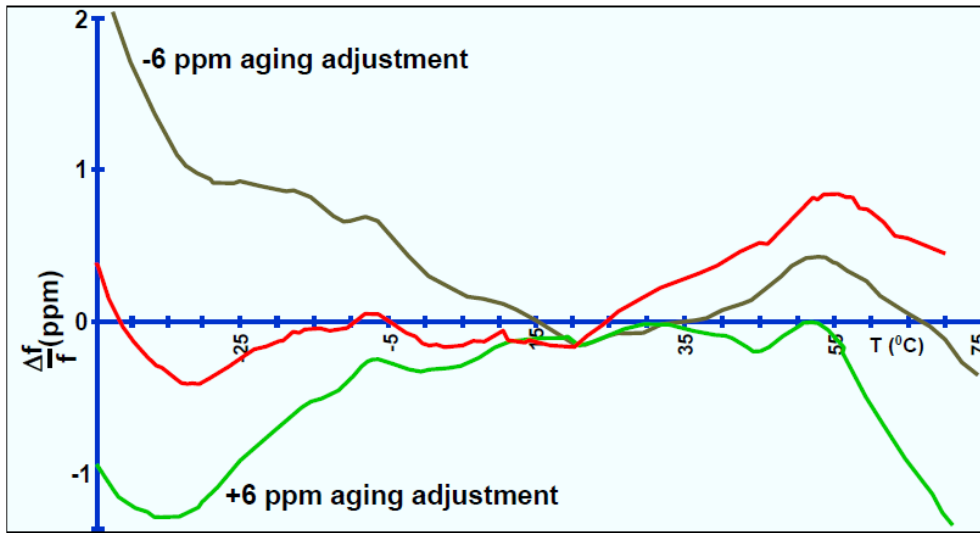
Figure 3.8 Frequency vs. Temperature stability curve of a 0.5 ppm TCXO

at zero trim and at ±6 ppm trim

How compensation frequency-temperature changes when the operating point is moved to a different C_L for the same compensation C_L-temperature is illustrated in Figure 3.9. Shown above are test results for a '0.5 ppm TCXO' that had a ±6 ppm frequency adjustment range (to allow for aging compensation for the life of the device). When delivered, this TCXO met its 0.5 ppm f vs. T specification. However, when the frequency was adjusted ±6 ppm during testing, the f vs. T performance degraded significantly. The 0.5 ppm TCXO was shown to be a 2 ppm TCXO. In specifying a TCXO, it is important to require that the f vs. T stability include the hysteresis and trim effects.
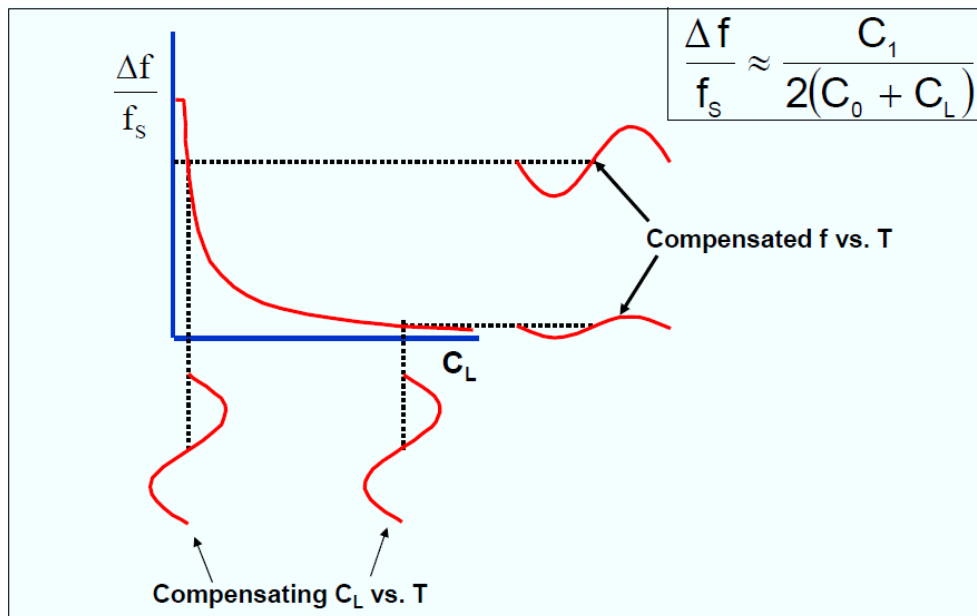
Figure 3.9 Trim effect [48]

$$\frac{\Delta f}{f_s} \approx \frac{C_1}{2(C_0 + C_L)}$$

3.1.3 Pyrotechnic Shock

A shocking test is intended to determine the suitability of the devices for use in electronic equipment which may be subjected to severe shocks as a result of suddenly applied forces or abrupt changes in motion produced by rough handling, transportation, or special operations. Current space vehicle and satellite design use numerous pyrotechnic shock devices during missions. These devices are typically used to separate structural sub-systems, accessories of structure and activate the on-board operating system with a high level of integrity.

The initial pyrotechnic shock peak acceleration can be as high as 200,000 g with high frequency content of 1 MHz. These values rely heavily on the method of measurement and recording as well as the subsequent digital data analysis. The pyrotechnic shock acceleration time history has a short duration of less than 20 ms and depends largely on source type and size, intermediate structural path characteristics, and distances from the source to the response point of interest. Due to high frequency content, many hardware elements and small components are vulnerable to pyrotechnic shock failures while resisting a variety of low frequency environments, including random vibrations. Those high frequency contents can make the analysis method and calculation procedure not applicable to system verification under the pyrotechnic shock. Therefore, the pyrotechnic shock test should be accomplished by qualification or flight acceptance test and is essential to mission success.

Frequency shift during shock impact is due to the stress sensitivity of the oscillator. The amount of frequency shift is a function of the oscillator design and the shock induced stress on the oscillator. The stress changes, resonator surfaces

deformation, and changes in the oscillator circuitry can change oscillator output frequency permanently. When there are imperfections on resonator surfaces, it is hard to survive under shock. The scratch-free resonator produced by chemical abrasives endured up to 36,000 g of shock in the air gun tests and up to 16,000 g of shock with 12 ms duration.

The pyrotechnic shock response in Figure 3.10 is a complex waveform. It tends to oscillate in a somewhat symmetric manner about the zero line. Its overall envelope has an exponential decay. Unlike the transportation shock pulse, this pyrotechnic shock response is too complicated to represent by a time domain mathematical function. Therefore, the SRS (Shock Response Spectrum) is a useful tool for estimating the damage potential of a shock pulse, as well as for test level specification. [61-70]
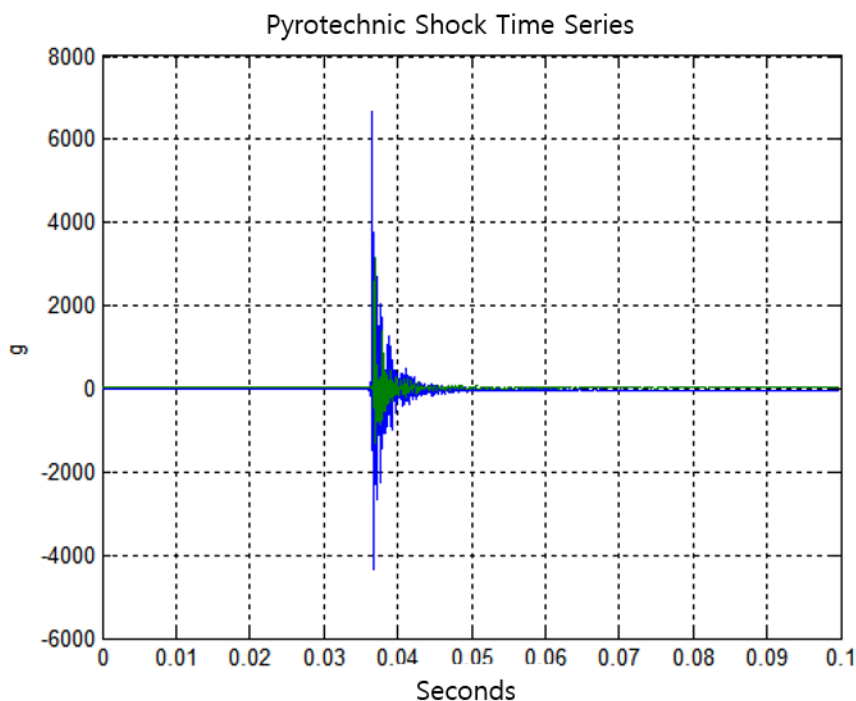
Figure 3.10 Time series of acceleration in pyrotechnic shock

The shock response spectrum is a calculated function based on the acceleration time history. It applies an acceleration time history as a base excitation to an array of single-degree-of-freedom (SDOF) systems, as shown in Figure 3.11. Note that each system is assumed to have no mass-loading effect on the base input. Y is the common base input for each system, X_n is the absolute response of each system to the input. The dot means derivative, M_n is the mass, C_n is the damping coefficient and K_n is the stiffness for each system. F_n is the natural frequency for n-th system. The SRS consists of each system's maximum acceleration values versus the resonance frequencies. The damping of each system is typically assumed as 5%, which is equivalent to Q = 10. The natural frequency is an independent variable. Thus, the calculation is performed for a number of independent SDOF systems, each with a unique natural frequency. The SRS plot is shown in Figure 3.12 converted from Figure 3.10. Unlike Figure 3.10, which is hard to measure or check the shock values, the SRS plot can show the amount of shock in terms of acceleration.
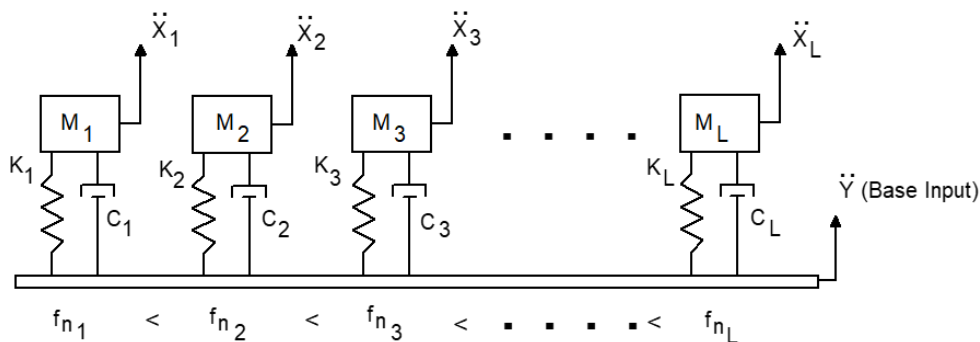
Figure 3.11 SDOF systems for SRS representation [67]
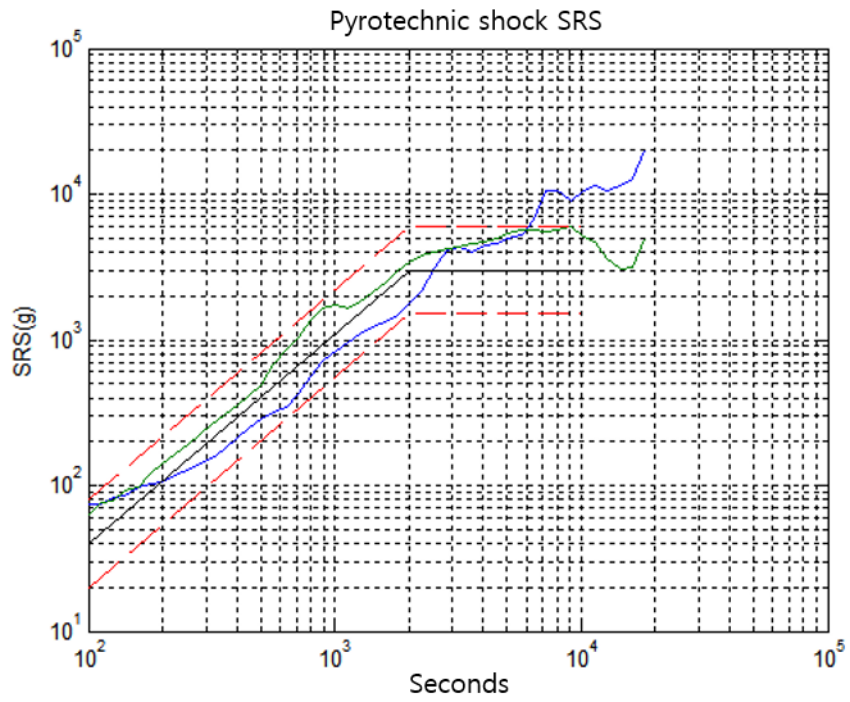
Figure 3.12 SRS plot in pyrotechnic shock

3.2   Frequency Stability during the Temperature Test

In accordance with the test specifications shown in Table 3.1, temperature tests were conducted, which indicated changes in the frequency output of the TCXOs and MEMS oscillators. The frequency stability and frequency slope of each TCXO and MEMS oscillator as measured during the temperature tests are shown in Tables 3.3 and Table 3.4, respectively. For the TCXO, the results were acceptable considering the specifications given in the data sheet, but accurate values could not be obtained because the tested temperature range is narrower than that in the specifications. Regarding the frequency slope, though the temperature change rates during the temperature tests were greater than the temperature change rates given in the data sheet (1°C/min), the performance exceeded the specified level. Moreover, these frequency changes do not present problems while performing the navigation process.

With the same temperature range for the MEMS oscillator in the temperature test, the frequency stability is one-fifth, and the frequency slope is one-third to one-half compared to the results for the TCXO, generating much more stable frequency output in environments with varying temperature. Figure 3.13 illustrates the change in the output frequency offset of the TCXO and MEMS oscillator, indicating that the change of the MEMS oscillator output frequency is much less than that of the TCXO. Note that the 20°C to 30°C section is connected by a solid blue line because the data of TCXO cannot be stored. Moreover, the temperature test is divided into low and high temperature tests, explaining that the data is not continuous near room temperature (25°C).

Table 3.3 Frequency stability and slope of the TCXO under low and high
temperature environments

Parameter	Specification in Datasheet	Test Results	Etc.
Frequency Stability	±1 PPM (–40°C ~ 85°C)	±0.13 PPM (–4°C ~ 76°C)	Referenced to (Fmax+Fmin)/2
Slope	100 PPB/°C	3.13 PPB/°C	Temperature ramp 1°C/min

Table 3.4 Frequency stability and slope of the MEMS oscillator under low and high
temperature environments

Parameter	Specification in Datasheet	Test Results	Etc.
Frequency Stability	±0.1 PPM (–40°C ~ 85°C)	±0.025 PPM (–4°C ~ 76°C)	Referenced to (Fmax+Fmin)/2
Slope	±2.5 PPB/°C	-1.0 PPB/°C ~ +1.67 PPB/°C	Temperature ramp 1°C/min
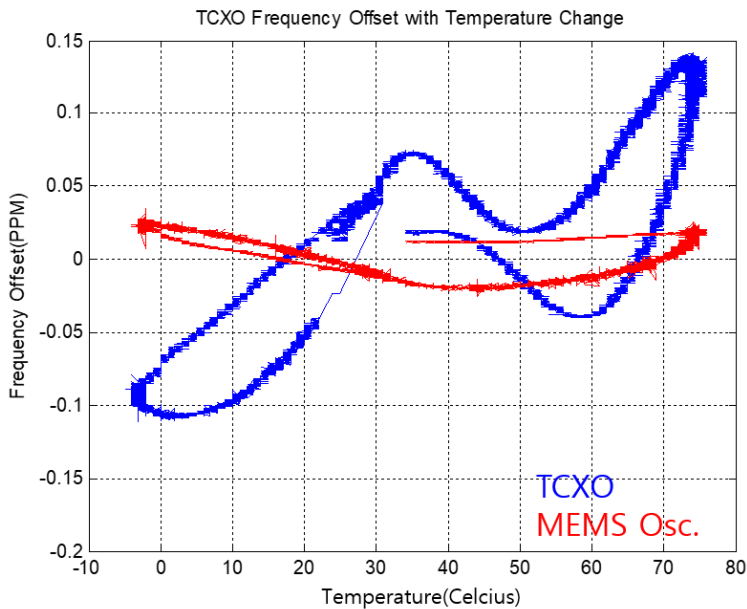
Figure 3.13 Frequency offset comparison under low and high
temperature environments
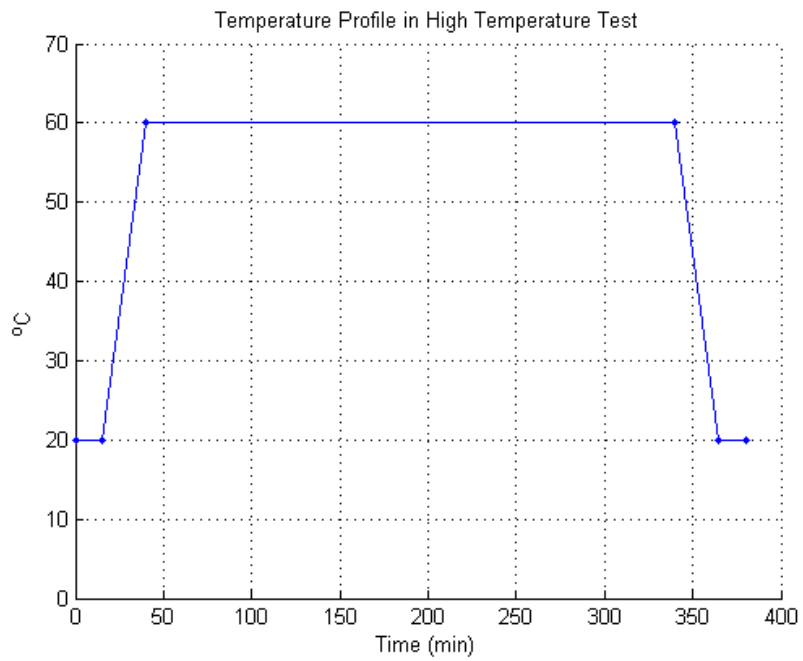
Figure 3.14 Temperature profile in high temperature environment test
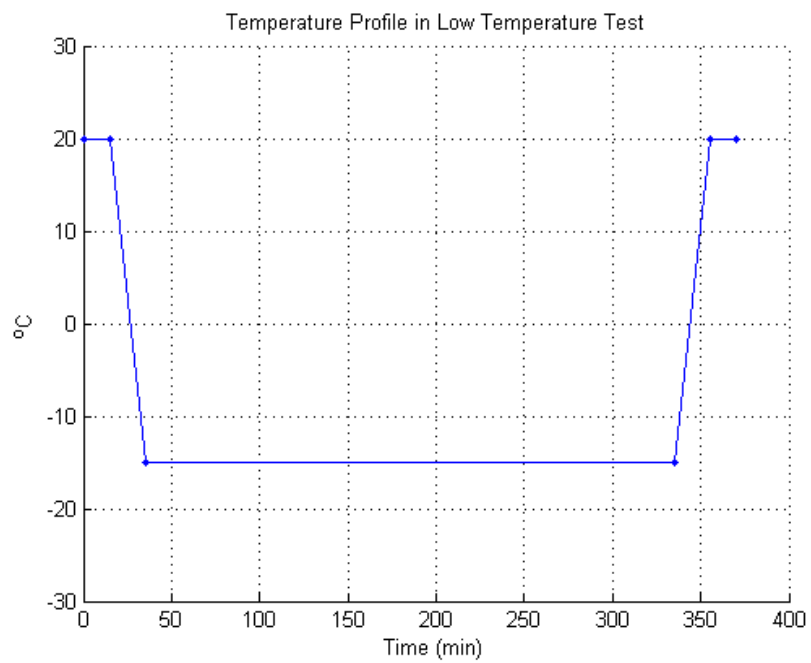
Figure 3.15 Temperature profile in low temperature environment test

The MEMS oscillator has better frequency stability than the TCXO in varying temperature environments because it can be manufactured in a very small size. The general TCXO consists of an oscillator circuit and a resonator, which are separate components, and the thermometer for temperature compensation is attached to the oscillator circuit, for which the measured temperature differs from that of the resonator. However, the MEMS oscillator, when manufactured in a very compact size, predicts the temperature at which the actual resonator operates very accurately because the thermometer and resonator are positioned in close proximity, compensating for the output frequency based on the measured temperature. For this reason, the frequency stability of the MEMS oscillator is better than that of the TCXO [13]. Although not listed on the datasheet, the hysteresis of the MEMS oscillator in the tested temperature range, as shown in Figure 3.13, is also significantly lower than that of the TCXO.

3.3　Frequency Stability during the Vibration Test

In accordance with the test specifications shown in Table 3.1 and Figure 3.16, the random vibration test and sinusoidal vibration test were conducted, and the variations in the output frequency of the TCXO and the MEMS oscillator during the vibration period denoted by the red lines were investigated. During the vibration test, which directly measured the output frequency of the oscillator instead, the variation of the output frequency is estimated based on the calculated clock drift from the GNSS receiver. The random vibration specifications are not given in the datasheet, and the frequency variations of each oscillator are shown in Table 3.5. In addition, Figure 3.17 illustrates the estimated frequency variations during the random vibration interval.
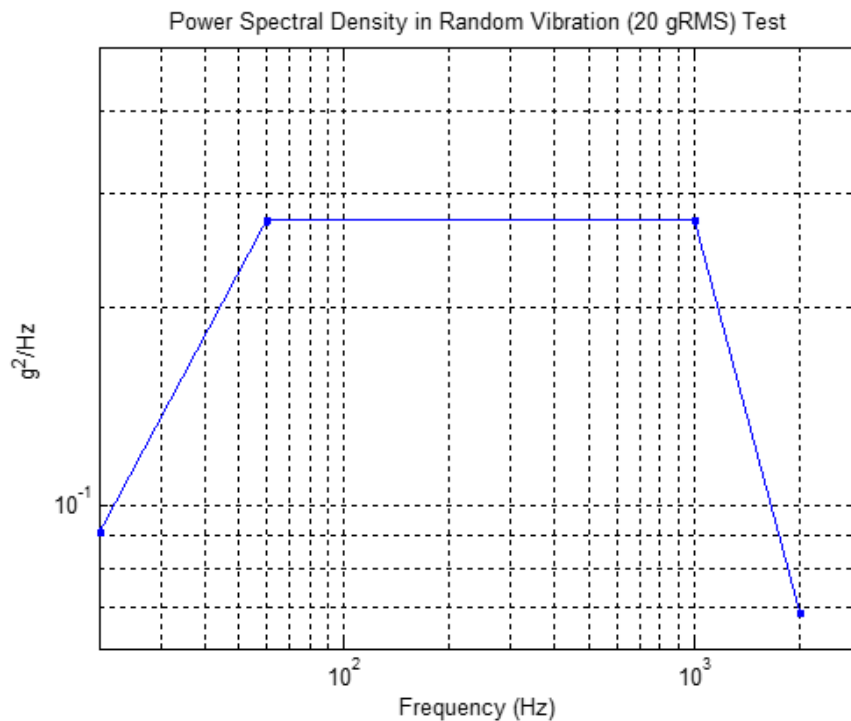
Figure 3.16 PSD under random vibration test environment

Table 3.5 Frequency offset in a random vibration environment

Oscillator	Specification in Datasheet	Frequency Offset Results	Etc.
TCXO	-	10 ppb	Relative to No vibration status
MEMS Oscillator	-	0	No change observed
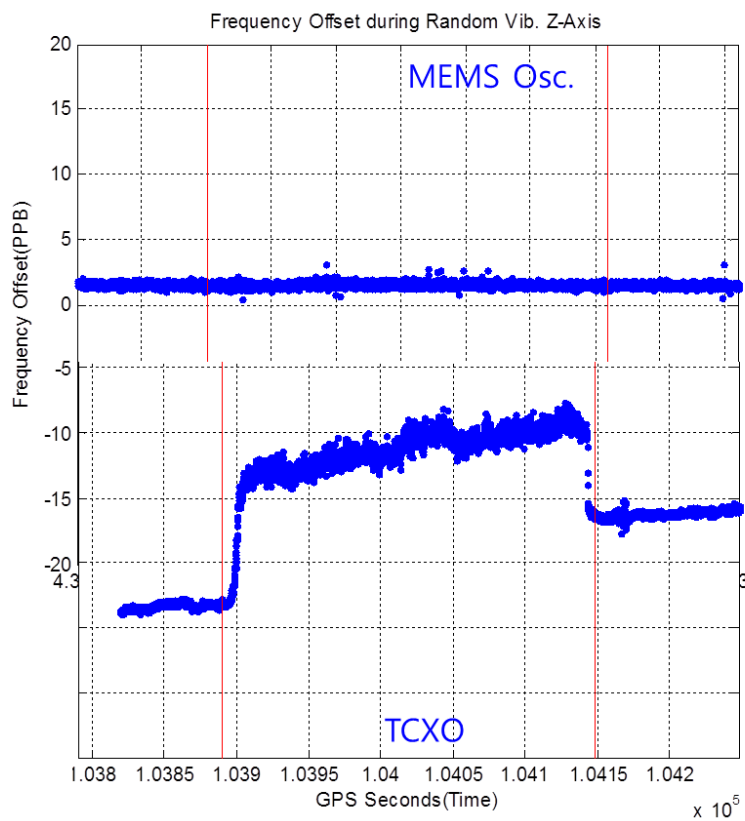
Figure 3.17 Frequency offset comparison in a random vibration environment

When 20 gRMS of random vibration was applied for four minutes, the TCXO showed a frequency change of 10 ppb, whereas the MEMS oscillator was not affected by vibration at all. This supports existing research findings, which indicated that MEMS oscillators are more robust to physical loads or stresses such as vibrations than the TCXO. The reason why frequency changes of TCXO occur throughout the entire test period, including the vibration period, is not related to the applied vibration but because the output frequency of the oscillator slowly varies.

In the sinusoidal vibration test conducted according to the specifications shown in Table 3.1 and Figure 3.18, variations in the output frequency of the TCXO and MEMS oscillator during the vibration period, as denoted by the red lines, are investigated. The frequency variations of each oscillator are shown in Table 3.6, and Figure 3.19 illustrates the estimated frequency variations during the sinusoidal vibration interval. The sinusoidal vibration specifications guaranteed by the manufacturers are as follows: 20 g @ 10 ~ 2000 Hz for the TCXO and 70 g @ 20 ~ 2000 Hz for the MEMS oscillator. As mentioned earlier, because the frequency offsets of the oscillators are obtained from the results of a navigation calculation in the GNSS receiver, the frequency offsets can change differently from an actual situation when satellite signals at a lower elevation are received. Therefore, the frequency offset during the vibration tests should be considered as a result of the sum of the velocity errors calculated in the GNSS receiver and the actual frequency change of the oscillator.
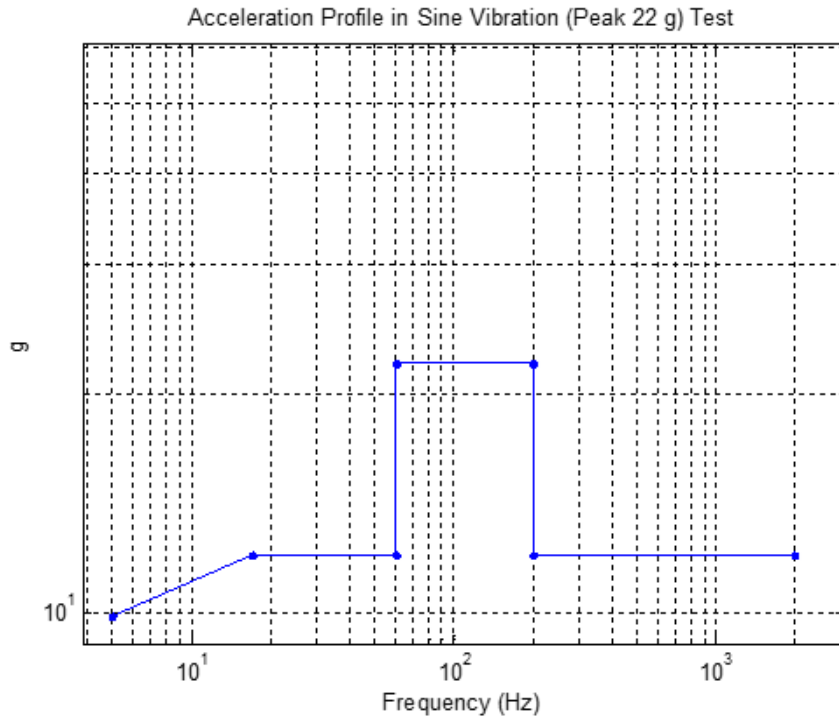
Figure 3.18 Acceleration under sinusoidal vibration test environment

Table 3.6 Frequency offset in a sinusoidal vibration environment

Oscillator	Specification in Datasheet	Frequency Offset Results	Etc.
TCXO	20g@10~2000 Hz	12 ppb	Relative to No vibration status
MEMS Oscillator	70g@20~2000 Hz	8 ppb	No change observed

The interval with 22 g sinusoidal vibration is shown with green arrows in Figure 3.19. The TCXO shows a slight frequency offset with the vibration interval of 22 g, and the frequency change at the level of 12 ppb was noted before the
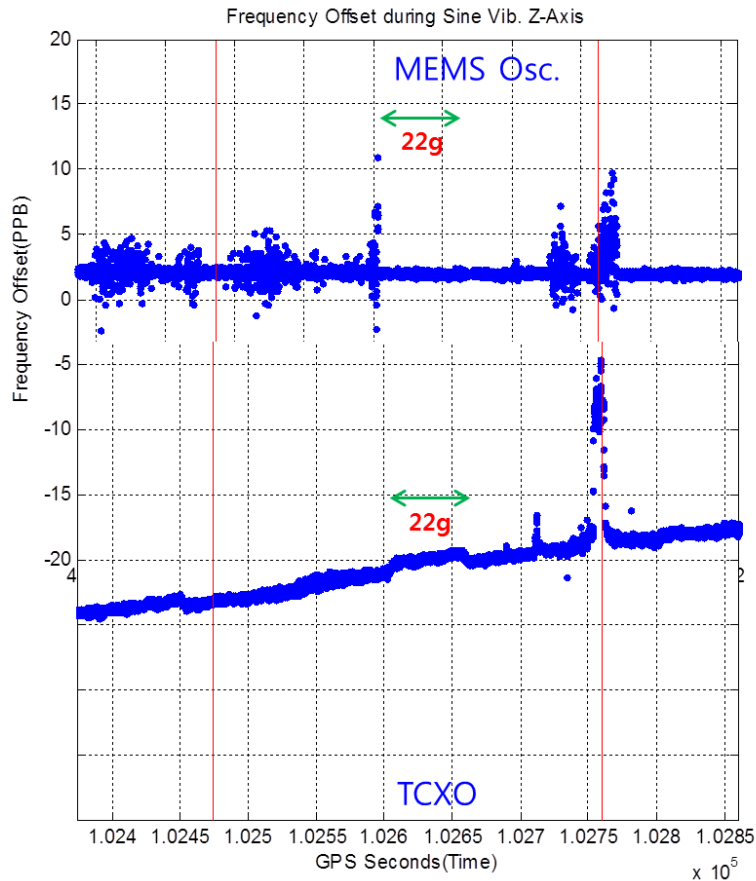
Figure 3.19 Frequency offset comparison in a sinusoidal vibration environment

vibration ended. The MEMS oscillator also shows a slight frequency offset before the vibration starts, confirming the effect of the velocity errors calculated in the GNSS receiver, and a frequency change at the level of 8 ppb arises before the endpoint of vibration and the start point of the vibration of 22g. The frequency offset of 8 ppb of the MEMS oscillator during the 22 g vibration interval is influenced by an outage of the GPS PRN22 satellite signal, with the actual frequency output remaining unchanged.

At the end of the vibration, denoted by the red line, it was found that both

oscillators exhibit significant frequency offsets, as shown in Figure 3.19, due to the amplification of the vibration caused by the significant transmissibility near the resonant frequency of the GNSS receiver. In Figure 3.20, the green line is the sinusoidal vibration reference value, the red line is the ± 6 dB of the green line, and the blue line is the acceleration measured from an accelerometer attached to the surface of the GNSS receiver. At the end of the vibration period, two peaks at an acceleration level of 100 g were measured, and the frequency offsets in Figure 3.19 greatly increased at the same time. 1600 Hz and 1900 Hz are expected to be the corresponding resonant frequencies of the jig, which holds the GNSS receiver, and of the GNSS receiver. At these frequencies, the sinusoidal vibration of 12 g was amplified to 100 g, i.e., by approximately eight times. In the sinusoidal vibration test, the output frequencies of both oscillators changed, and the amount of the frequency change of the MEMS oscillator is lower than that of the TCXO by 4 ppb, confirming its robustness in an environment with vibration.
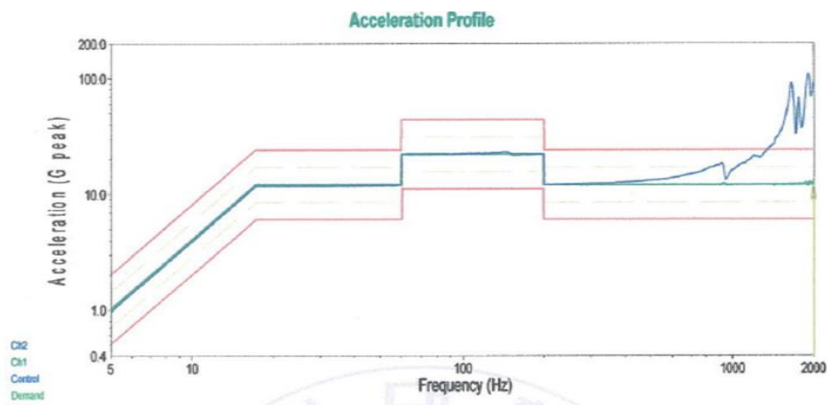
Figure 3.20 Accelerations of the jig and GNSS receiver surface in a sinusoidal vibration environment

3.4   Frequency Stability in Pyrotechnic Shock Test

The type of pyrotechnic shocks that can occur when the stage and fairing separation can cause cracks in oscillators, any ceramic materials, and the epoxy and soldering parts given that these are very high impacts which occur within a very short period of time compared to a normal shock. A pyrotechnic shock test is essential for the components of a launch vehicle or a satellites, as pyrotechnic shocks can cause malfunctions and failures [3,46]. The cut-off frequency and maximum acceleration values of the SRS (shock response spectrum) from the test specifications are tailored, as shown in Table 3.1. In an actual pyrotechnic shock test, three impacts on each axis are applied to verify the performance, but in the test here, five TCXO samples were subjected to one impact, and MEMS oscillator sample was subjected to three impacts, and the actual frequency offsets were measured by a frequency counter. A time series graph and SRS of the acceleration at the time of impact are shown in Figure 3.21, where the black line in the middle is the pyrotechnic shock reference value, and the red dashed line is the ± 6 dB value of the black line. As shown in the time-series graph, very high acceleration occurs within a very short time interval of 1 ms. When the GNSS receiver is exposed to such an impact, the tracking signals can be lost due to the rapid frequency change of the oscillator.
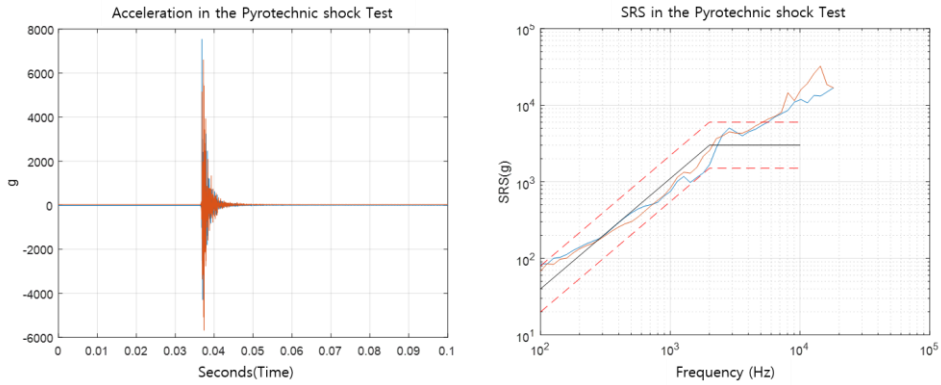
Figure 3.21 Acceleration and SRS in the pyrotechnic shock test

The frequency offsets measured in the pyrotechnic shock test are summarized in Table 3.7, and Figure 3.22 shows the frequency offsets at the time of impact. The frequency offsets of the TCXO and the MEMS oscillator are shown in Figures 3.23 and 3.24, respectively, and the impact moments are at 150 seconds.

In the pyrotechnic shock test, the MEMS oscillator shows very little frequency offset during the three impacts, whereas the frequencies of the output of the five TCXO samples appear to stabilize after showing a large frequency offset, but without fully recovering the previous frequency output. The output frequency changes permanently because the oscillator exceeds its elastic limit due to the applied pyrotechnic shock [26]. The TCXO output frequency varies from 0.90 Hz to 2.05 Hz after the impact depending on the sample, and the output frequency of the MEMS oscillator varies from 0.06 Hz to 0.20 Hz. The MEMS oscillator exhibits a small frequency offset, and it appears that the frequency output is only affected at the moment of the shock. The test results suggest that the GNSS receiver equipped with a MEMS oscillator can perform without signal loss of lock during pyrotechnic shocks, whereas when the GNSS receiver uses the TCXO, the

71

navigation performance should be determined in an actual pyrotechnic shock test.

Table 3.7 Frequency offsets of each oscillator measured in the pyrotechnic shock test

TCXO Sample	Δf (Hz)	Δf (ppb)	MEMS Oscillator	Δf (Hz)	Δf (ppb)
1	1.92	192	1st	0.06	6
2	2.05	205	2nd	0.20	20
3	1.20	120	3rd	0.09	9
4	0.90	90	-	-	-
5	1.83	183	-	-	-
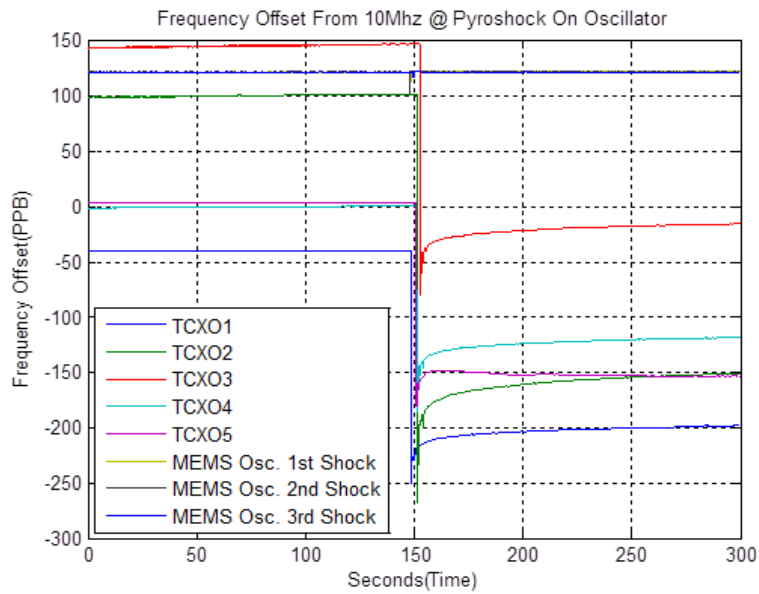
Figure 3.22 Frequency offsets under the pyrotechnic shock test
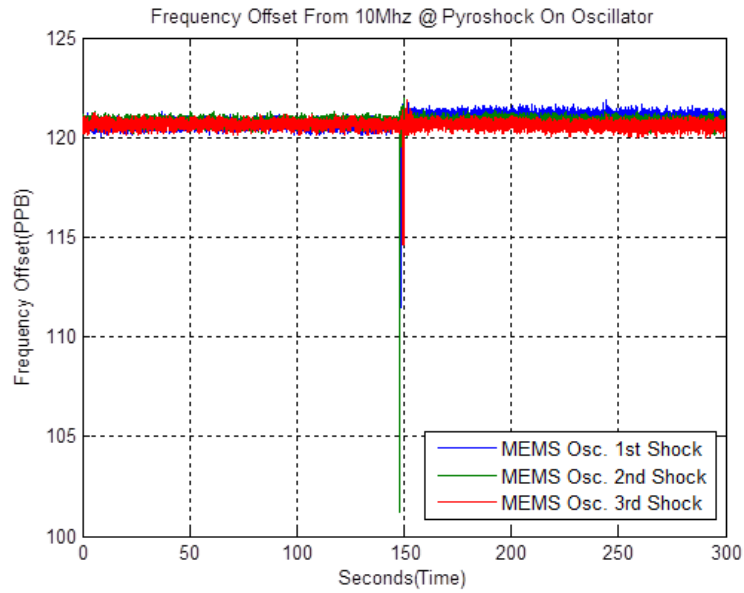
Figure 3.23 MEMS oscillator frequency output in the pyrotechnic shock test
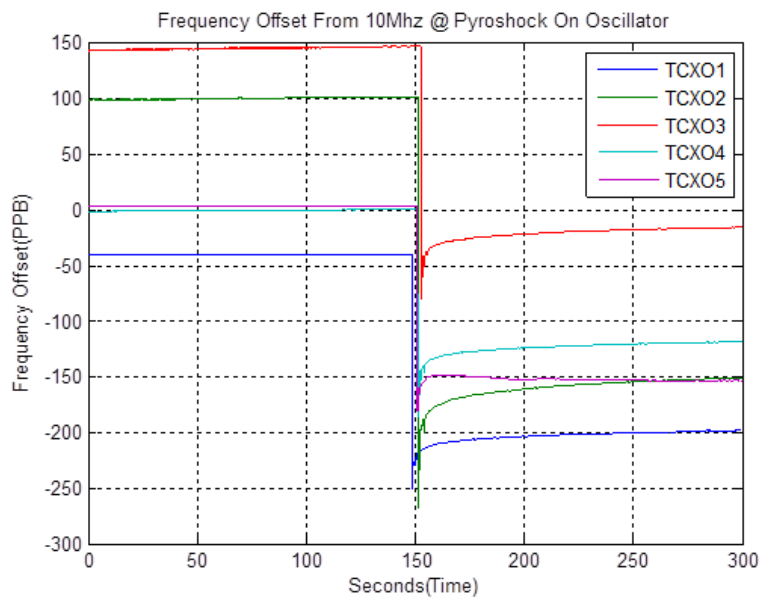
Figure 3.24 TCXO frequency output in the pyrotechnic shock test

73

Chapter 4

Simulation with GNSS Receiver under Reference Frequency Change

This chapter describes the results of the GNSS receiver performance test when the frequency output of TCXO is arbitrary changed abruptly using signal generator. The GNSS receiver loses signal tracking and fails to calculate navigation solutions during the pyrotechnic shock test and it is found that the rapid change in frequency output of TCXO causes the problem in signal tracking. In addition, instead of applying the pyrotechnic shock to unit directly, the signal generator is utilized to change reference frequency by a certain value. The relation of the amount of frequency change in reference frequency and loss of signal lock can be identified in this test, and this values are compared to theoretical values.

4.1 Tracking Loop of GNSS Receiver

The GNSS receiver for KSLV-II uses 2nd-order FLL(Frequency Lock Loop) with 6 Hz bandwidth for tracking signals, while the pre-integration time is 2 ms for GPS and GLONASS and 4 ms for Galileo signals, respectively. The 2nd FLL tracking loop consists of integrator, discriminator and loop filter. In the tracking loop, these three features determine the important characteristics of the carrier tracking loop such as thermal noise error and dynamic stress threshold. Because the discriminator of the FLL tracking loop generates frequency error estimates, it is robust to dynamic environment. However, to improve the accuracy of the measurements, pre-integration time must be increased, loop filter bandwidth reduced, and PLL is recommended. Therefore, a trade-off between these characteristics is required to design receiver that fits the dynamic requirements.

In the discriminator of tracking loop, the theoretical pull-in range is determined by the pre-integration time mentioned above and is affected by the bandwidth of the tracking loop and the C/N0. If the frequency of the tracking signal is outside of the pull-in range due to an external impact or noise, GNSS receiver loses track of the satellite signal.

The theoretical pull-in range for KSLV-II GNSS receiver is 500 Hz (±250 Hz) for GPS and GLONASS signal and 250 Hz (±125 Hz) for Galileo signal. Given that half of this theoretical pull-in range is linear region of traceable frequency range (250 Hz (±125 Hz) for GPS signal), this value corresponds to ±0.8 Hz of reference frequency with 10 MHz output. Therefore, when the frequency output of reference oscillator changes within ±0.8 Hz, signal tracking is done normally, but

in an environment where the output frequency of reference oscillator varies beyond this range, the signal tracking may be lost, or a false frequency lock may occur. The false frequency lock can occur at a frequency outside the actual pull-in frequency range in Figure 4.1. The linear region and the slope of the discriminator curve change with C/N0, and this effect has a material impact on the tracking performance of the frequency lock loop.
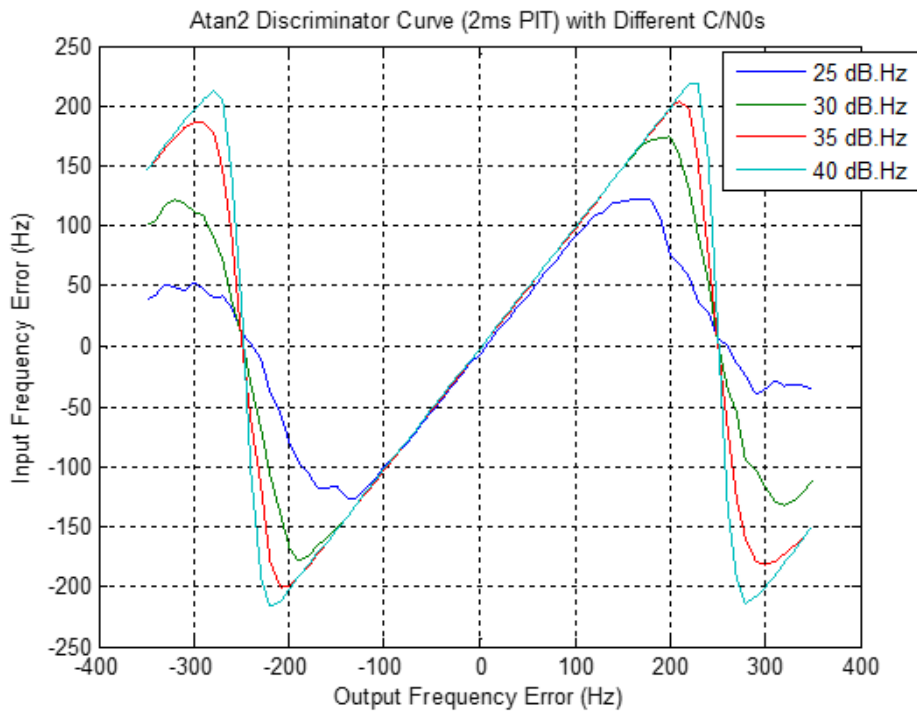
Figure 4.1 Atan2 discriminator curve

In this study, a simplified tracking loop is generated as shown in Figure 4.2 to analyze how changes in reference frequency output affect the tracking loop. Since the tracking loop cannot distinguish the difference between the dynamic stress experienced by the actual situation and the change in the reference frequency output, the tracking loop recognized that the actual signal undergoes a dynamic environment such as acceleration or jerk when the reference frequency output changes.
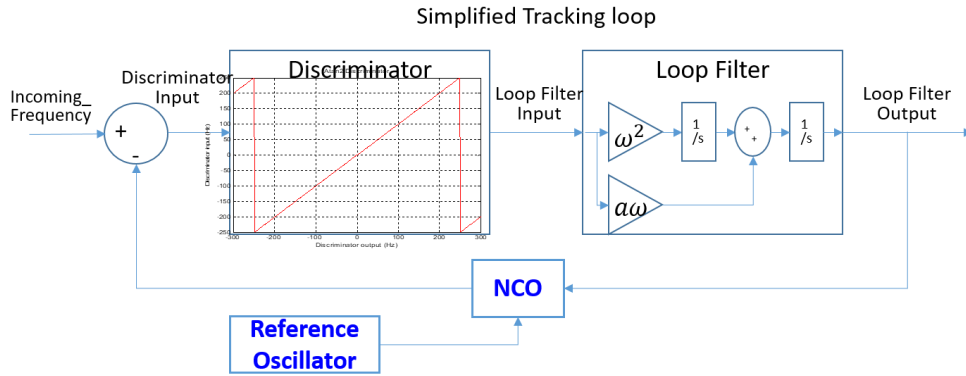
Figure 4.2 Simplified tracking loop

The frequency error of a typical tracking loop is largely divided into thermal noise and dynamic stress error. The tracking threshold is defined by a 3 sigma error should be less than one quarter of the FLL discriminator pull-in frequency and is expressed by the following [19].

$$3\sigma_{FLL} = 3\sigma_{FLL,t} + f_e \leq \frac{0.25}{T} \ (Hz) \qquad (4.1)$$

If the noise and dynamic characteristics due to the reference oscillator are low, only the $\sigma_{FLL,t}$ component should be considered, but f_e should also be

77

considered if the output of the reference oscillator itself changes due to external stress. FLL tracking loop error due to thermal noise is as follows.

$$\sigma_{FLL,t} = \frac{1}{2\pi T} \sqrt{\frac{4FB_n}{CN_0} \left(1 + \frac{1}{TCN_0}\right)} \ (Hz) \qquad (4.2)$$

FLL tracking loop error by acceleration is as follows.

$$f_e = \frac{f_0}{c} aT \ (Hz) \qquad (4.3)$$

Where T : $PIT\ (2ms)$

B_n : $Bandwidth\ (6Hz)$

CN_0 : $Signal\ Power\ (dB.Hz)$

F : $1\ for\ high\ CN_0$

$2\ near\ the\ threshold$

a : $Relative\ LOS\ Acceleration$

c : $Speed\ of\ Light$

f_0 : $1.57542 * 10^9\ (Hz)$

The FLL discriminator threshold of expression Eqn.(4.1) is divided by case 1 and case 2 and organized in Table 4.1. Case 1 is when loop filter is 6 Hz and PIT is 2 ms, and case 2 is when loop filter is 6 Hz and PIT is 1 ms. For case 2, which has a PIT of 1 ms, the thermal noise exceeds the tracking threshold when the C/N0 is less than 25. Increasing the PIT to 2 ms reduces the thermal noise component and enables signal tracking at the same C/N0 environment. This reduced error from the

thermal noise allows signal tracking to be maintained even if the dynamic induced error grows larger.

Table 4.1 Discriminator threshold

Case	C/N0 in dB.Hz	Thermal Noise in Hz	Acceleration in g	Dynamic Stress in Hz	3*Thermal+Dynamic stress in Hz	Tracking Error Threshold in Hz
1	15	402	10	1.0	1207	125
1	20	95	100	10.3	295	125
1	25	35	100	10.3	115	125
1	30	15	100	10.3	55	125
1	35	7	100	10.3	31	125
2	15	1119	10	0.5	3357	250
2	20	258	100	5.1	779	250
2	25	89	100	5.1	272	250
2	30	35	100	5.1	110	250
2	35	16	100	5.1	53	250

Under the same PIT and C/N0 conditions, the thermal noise is the same, so the threshold can be represented only by the error of the frequency change or dynamic characteristics. The Table 4.2 summarizes the tracking threshold for case where C/N0 is 30 dB.Hz and PIT is 2 ms. If C/N0 is 30 dB.Hz with GPS L1 signal, it starts to exceed the tracking threshold when the reference frequency change of 10 MHz is 0.6 Hz, and if it changes more than 0.8 Hz, it can be seen that the tracking threshold is unconditionally exceeded regardless of C/N0 value. In pyrotechnic shock environment, the frequency output of TCXO changed from 0.9 Hz to 2.0 Hz,

which can be converted to 917 g to 3059 g. These values cannot be seen in real-world acceleration environments and are estimated by the very short time impact due to pyrotechnic shock.

Table 4.2 Tracking threshold due to changes in reference frequency

Changes in reference frequency in Hz	C/N0 in dB.Hz	Thermal Noise in Hz	Dynamic Stress in Hz	3*Thermal + Dynamic Stress in Hz	Tracking Error Threshold in Hz
0.1	30	15	15.7	60.7	125
0.2	30	15	31.5	76.5	125
0.3	30	15	47.3	92.3	125
0.4	30	15	63.0	108	125
0.5	30	15	78.8	123.8	125
0.6	30	15	94.5	139.5	125
0.7	30	15	110.2	155.2	125
0.8	30	15	126.0	171	125
1	30	15	157.5	202.5	125
2	30	15	315.1	360.1	125

The frequency error output from the discriminator in tracking loop is fed into loop filter and integrator and the frequency estimates is compared with incoming signal frequency. The tracking loop filter must determine the appropriate order and bandwidth according to the dynamic characteristics of the GNSS receiver, which in high dynamic conditions, the bandwidth should be widened and the order has to be

increased to minimized errors.
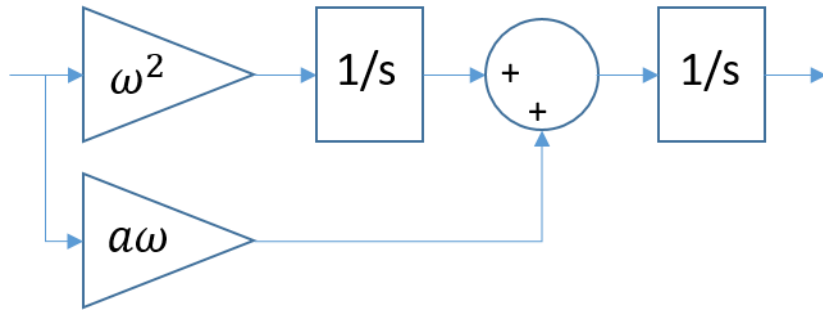
Figure 4.3 2nd order FLL loop filter and integrator

Figure 4.3 illustrates the block diagram of the 2nd FLL loop filter with coefficients of $a = 1.414$, $B_n = 0.53w$ and $w = 11.32$ with a bandwidth of 6 Hz [19]. The loop filter filters the frequency error output from the discriminator and generates frequency of the NCO using the filter output and the reference oscillator output. The loop filter input and output are shown in Figure 4.4 when the bandwidth is 2, 6, 10 and 12 Hz. Although frequency estimates converges quickly as bandwidth of loop filters increases, it can also be seen that overshooting increases. Larger bandwidth and small PIT are required for the receiver in high dynamics, the thermal noise component may become significant, which cause difficulty in signal tracking. Thus, if the frequency estimate changes rapidly within one PIT period, such as pyrotechnic shock, the discriminator loses its signal tracking or can track the false frequency signal. Note that in a PIT of 2 ms, the doppler shift of 300 Hz in the GPS L1 signal is approximately 2915 g of acceleration in terms of receiver dynamics.
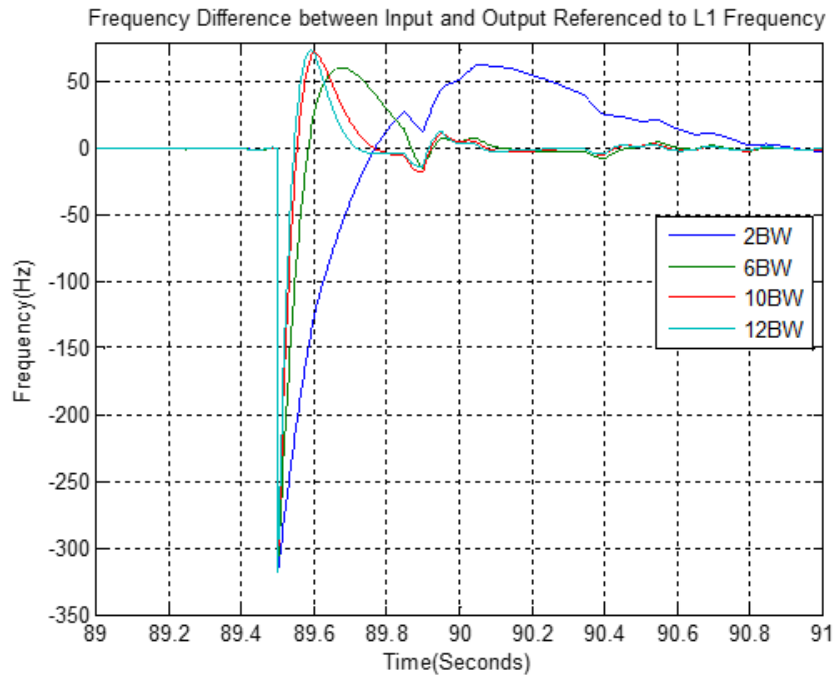
Figure 4.4 Frequency difference between filter input and output with different BW

Meanwhile, the discriminator obtains the frequency error continuously after signal acquisition, the tracking can be lost or be wrong when the frequency change occurs above pull-in frequency range. The frequency estimates are shown in Figure 4.5, Figure 4.6 and Figure 4.7 when the reference frequency output varies by 2.0 Hz, 1.6 Hz and 0.2 Hz, respectively. There are frequency errors of 500 Hz in Figure 4.5 and Figure 4.6. However, if the estimated frequency errors are more than 500 Hz, the signal powers of adjacent peaks are compared to stop signal tracking as shown in Figure 4.8. A new frequency estimate is obtained from re-acquency process. If there is a 0.2 Hz change in the referency frequency, the accurate frequency is estimated.

As previously confirmed in chap. 3.4, TCXO showed a frequency output change of 2.0 Hz and MEMS oscillator showed a frequency output change of 0.2 Hz. Therefore, according to the analysis of tracking loop, TCXO is expected to fail in signal tracking, and MEMS oscillator is not.
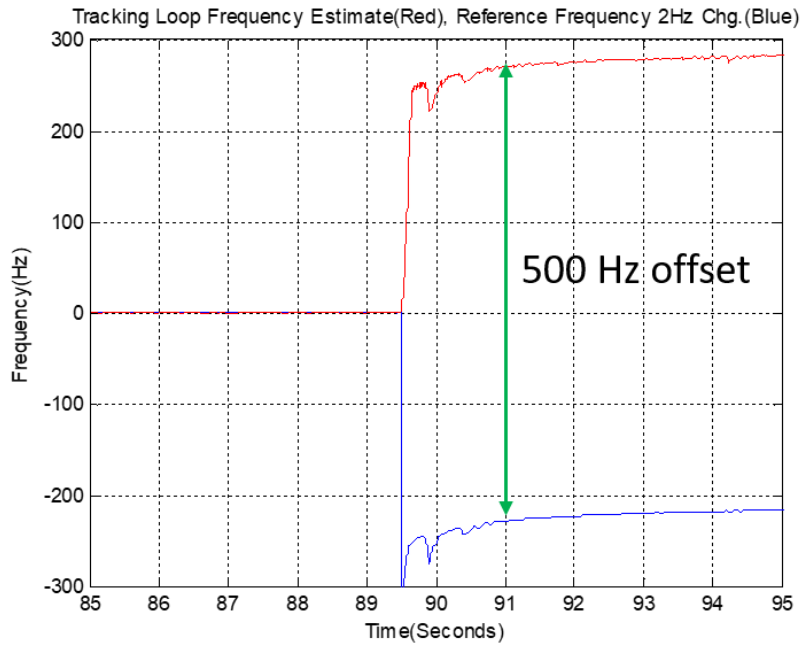
Figure 4.5 Frequency estimate under 2.0 Hz reference frequency change
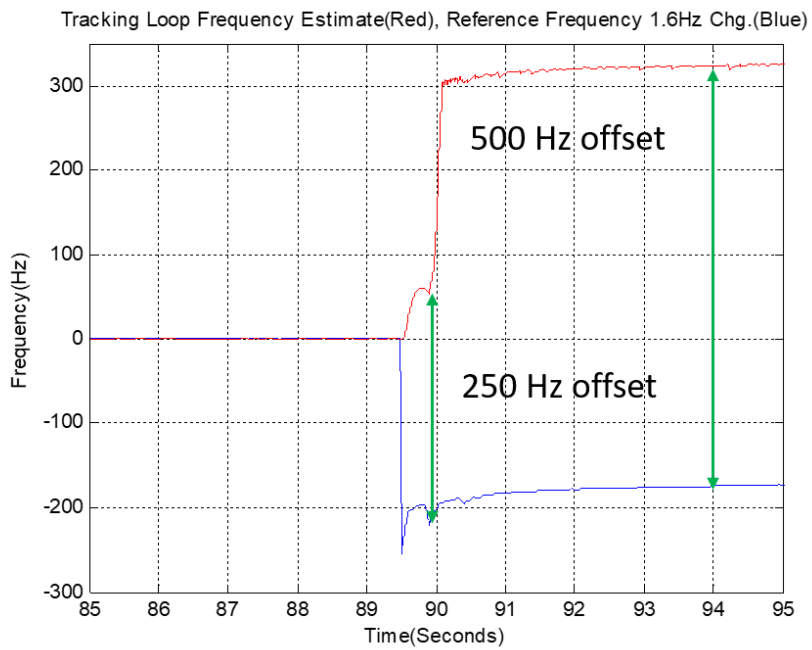
Figure 4.6 Frequency estimate under 1.6 Hz reference frequency change
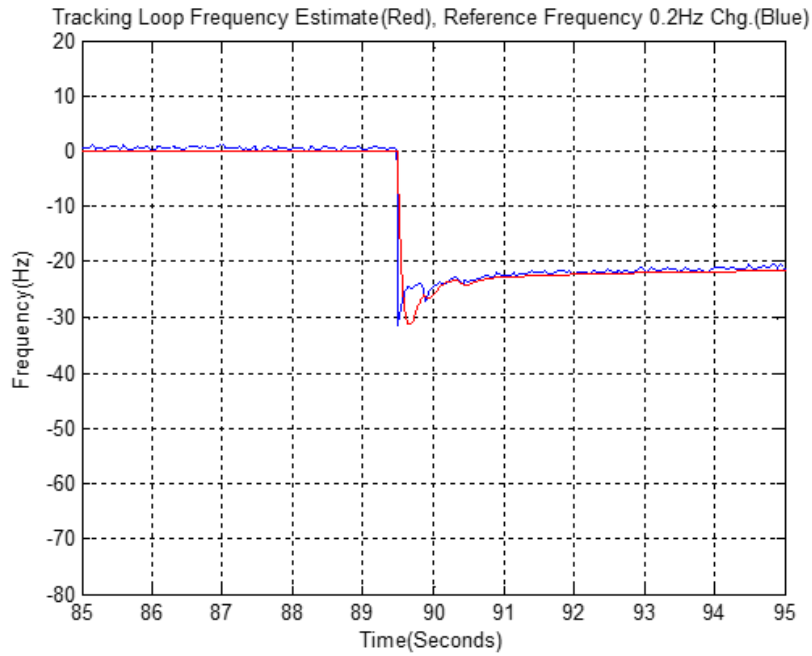
Figure 4.7 Frequency estimate under 0.2 Hz reference frequency change
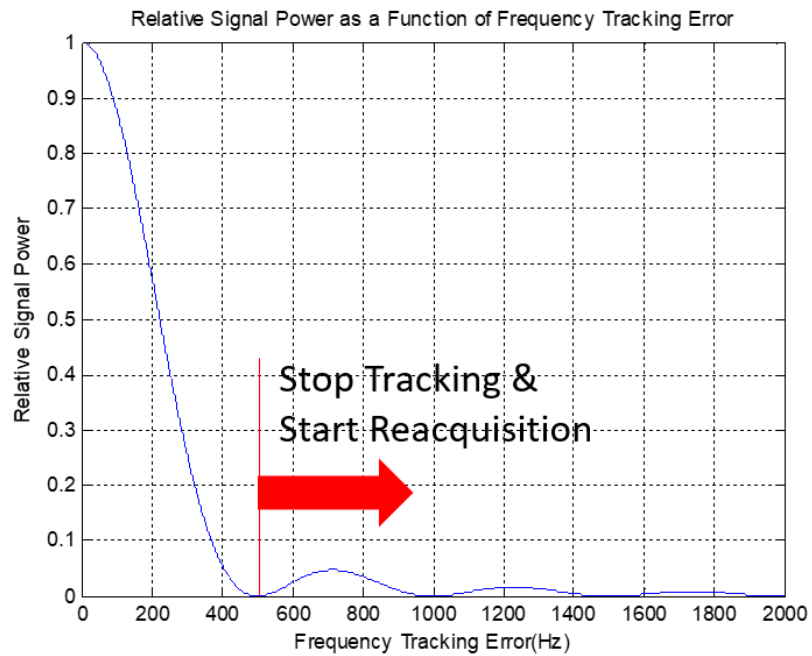
Figure 4.8 Relative signal power as a function of frequency error

4.2 GNSS Receiver Operation under the Change of Reference Frequency

In the pyrotechnic shock test conducted during the KSLV-II GNSS receiver development, the frequency output of TCXO changed by more than 0.8 Hz after the impact. This makes the GNSS receiver lose track of the signal, and the navigation solution cannot be obtained temporarily. When the GNSS receiver loses track of the signal temporally, the GNSS receiver can recover its navigation status shortly with signal reacquisition. But when a false frequency lock occurs during physical stress interval, the pseudorange rate can be incorrectly obtained, which is reflected in the velocity errors.

Although the frequency output change of TCXO in vibration test or in acceleration test does not affect the tracking status in frequency tracking loop, it is found that even TCXOs designed to be robust against physical stress also have difficulty in tracking navigation signals under pyrotechnic shock test.

As shown in Table 3.7, the frequency change of TCXO samples ranges from 0.9 Hz to 2.0 Hz under pyrotechnic shock test, and the GNSS receiver with these TCXOs is expected to lose signal tracking under the same shock condition. To identify more quantitatively the effect of frequency output change in reference frequency for GNSS receiver to track signals, the planned and fixed amount of reference frequency change is required, which cannot be realized using pyrotechnic shock test equipment.

A signal generator with 10 MHz output is fed into the GNSS receiver, just like a TCXO, the frequency of the signal generator is changed to certain values. During this operation, the effect on the GNSS receiver tracking status is investigated. The

change in the reference frequency varied by 0.1 Hz from 0.0 to 1.0 Hz and by 1.0 Hz from 1.0 to 10.0 Hz. The test configuration is shown in Figures 4.9, 4.10, and Table 4.3 shows the theoretical calculated pull-in frequency range for each GNSS signal. The reference frequency entered into the GNSS receiver was changed as shown in the second column of Table 4.4 ~ Table 4.7, and the status and test results of the GNSS receiver were shown accordingly. The GNSS receiver lost signal tracking of GPS and GLONASS signals from 0.6 Hz to 0.8 Hz of reference frequency change and Galileo signals from 0.3 Hz to 0.4 Hz of reference frequency change. All signal tracking is lost when the reference frequency change reaches 0.8 Hz, and the navigation status is resumed through signal reacquisition. This is consistent with the theoretical analysis of the tracking loop previously discussed, and since C/N0 is different for each satellite signal being tracked, the timing of missing the signal is slightly different. The reacquisition starts when the GPS or GLONASS signal is missed and navigation is restarted.

Table 4.3 Pull-in frequency range according to GNSS signals

	Pull-In Frequency Range Linear Region (Hz)	Frequency shift by TCXO (Hz)	Remark
GPS/GLONASS L1 for 2ms PIT*	250 Hz (±125 Hz)	1.6 Hz (±0.8 Hz)	50 % of theoretical value
Galileo E1 for 4ms PIT*	125 Hz (±62.5 Hz)	0.8 Hz (±0.4 Hz)	50 % of theoretical value
GPS L5 for 2ms PIT*	250 Hz (±125 Hz)	1.6 Hz (±0.8 Hz)	50 % of theoretical value
Galileo E5 for 4ms PIT*	125 Hz (±62.5 Hz)	0.8 Hz (±0.4 Hz)	50 % of theoretical value
L1, E1 for 1ms PIT*	500 Hz (±250 Hz)	3.2 Hz (±1.6 Hz)	Tracking loop to prevent false frequency lock

*PIT : Pre-Integration Time

Figure 4.9 Test configuration
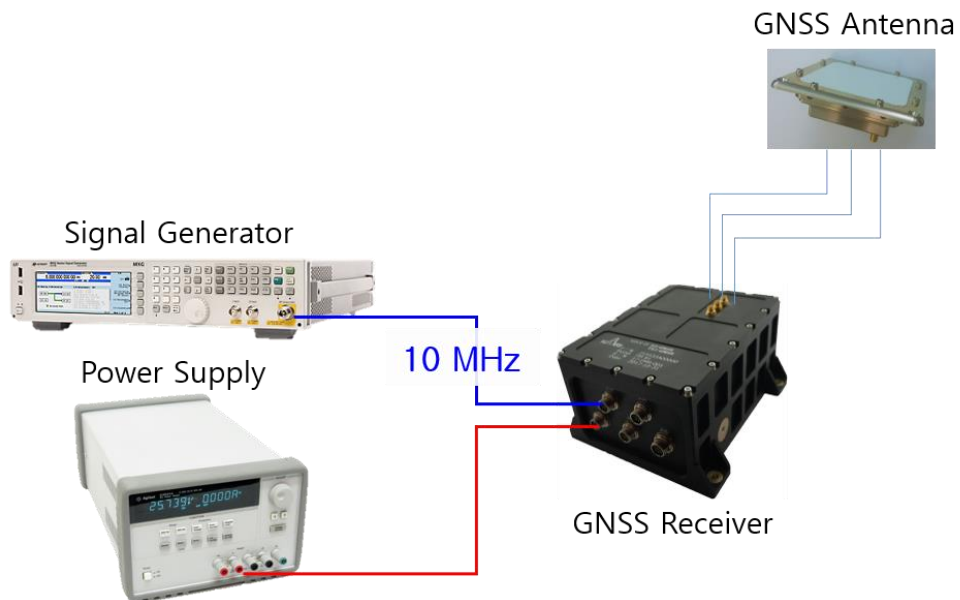
Figure 4.10 Test configuration for GNSS receiver
under the reference frequency change

Table 4.4 Test #1 results (1/2)

Test No.	Input Frequency (MHz)	Tracking / Navigation Status	Δf (Hz)	GPS Sec
1-1	10.0000000→10.0000001	Normal / Normal	0.1	284748
1-2	10.0000001→10.0000003	Normal / Normal	0.2	284808
1-3	10.0000003→10.0000006	Normal / Normal	0.3	284868
1-4	10.0000006→10.0000010	Galileo Signal Lock Loss / Normal	0.4	284928
1-5	10.0000010→10.0000015	Galileo Signal Lock Loss / Normal	0.5	284988
1-6	10.0000015→10.0000021	GPS, Galileo Signal Lock Loss / Normal	0.6	285048
1-7	10.0000021→10.0000028	GPS, Galileo Signal Lock Loss / Normal	0.7	285108
1-8	10.0000028→10.0000036	GPS,GLONASS,Galileo Signal Lock Loss / Velocity Error Increase	0.8	285168
1-9	10.0000036→10.0000045	GPS,GLONASS,Galileo Signal Lock Loss / Velocity Error Increase	0.9	285228
1-10	10.0000045→10.0000055	GPS,GLONASS,Galileo Signal Lock Loss / 0.1 sec. No Fix	1	285288

Table 4.5 Test #1 results (2/2)

Test No.	Input Frequency (MHz)	Tracking / Navigation Status	Δf (Hz)	GPS Sec
1-11	10.000000→10.000002	GPS,GLONASS,Galileo Signal Lock Loss / 0.1 sec. No Fix	2	285468
1-12	10.000002→10.000005	GPS,GLONASS,Galileo Signal Lock Loss / 0.1 sec. No Fix	3	285528
1-13	10.000005→10.000009	GPS,GLONASS,Galileo Signal Lock Loss / 2.2 sec. No Fix	4	285588
1-14	10.000009→10.000014	GPS,GLONASS,Galileo Signal Lock Loss / 2.0 sec. No Fix	5	285708
1-15	10.000014→10.000020	GPS,GLONASS,Galileo Signal Lock Loss / 1.8 sec. No Fix	6	285768
1-16	10.000020→10.000027	GPS,GLONASS,Galileo Signal Lock Loss / 2.0 sec. No Fix	7	285828
1-17	10.000027→10.000035	GPS,GLONASS,Galileo Signal Lock Loss / 2.2 sec. No Fix	8	285888
1-18	10.000035→10.000044	GPS,GLONASS,Galileo Signal Lock Loss / 2.0 sec. No Fix	9	285948
1-19	10.000044→10.000054	GPS,GLONASS,Galileo Signal Lock Loss / 2.0 sec. No Fix	10	286008

Table 4.6 Test #2 results (1/2)

Test No.	Input Frequency (MHz)	Tracking / Navigation Status	Δf (Hz)	GPS Sec
2-1	10.0000000←10.0000001	Normal / Normal	-0.1	287410
2-2	10.0000001←10.0000003	Normal / Normal	-0.2	287388
2-3	10.0000003←10.0000006	Normal / Normal	-0.3	287328
2-4	10.0000006←10.0000010	Galileo Signal Lock Loss / Normal	-0.4	287268
2-5	10.0000010←10.0000015	Galileo Signal Lock Loss / Normal	-0.5	287208
2-6	10.0000015←10.0000021	Galileo Signal Lock Loss / Normal	-0.6	287148
2-7	10.0000021←10.0000028	GLONASS, Galileo Signal Lock Loss / Normal	-0.7	287088
2-8	10.0000028←10.0000036	GPS,GLONASS,Galileo Signal Lock Loss / Normal	-0.8	287028
2-9	10.0000036←10.0000045	GPS,GLONASS,Galileo Signal Lock Loss / Normal	-0.9	286968
2-10	10.0000045←10.0000055	GPS,GLONASS,Galileo Signal Lock Loss / 0.1 sec. No Fix	-1	286908

Table 4.7 Test #2 results (2/2)

Test No.	Input Frequency (MHz)	Tracking / Navigation Status	Δf (Hz)	GPS Sec
2-11	10.000000←10.000002	GPS,GLONASS,Galileo Signal Lock Loss / 2.0 sec. No Fix	-2	286728
2-12	10.000002←10.000005	GPS,GLONASS,Galileo Signal Lock Loss / 1.8 sec. No Fix	-3	286668
2-13	10.000005←10.000009	GPS,GLONASS,Galileo Signal Lock Loss / 1.8 sec. No Fix	-4	286608
2-14	10.000009←10.000014	GPS,GLONASS,Galileo Signal Lock Loss / 1.9 sec. No Fix	-5	286548
2-15	10.000014←10.000020	GPS,GLONASS,Galileo Signal Lock Loss / 1.9 sec. No Fix	-6	286488
2-16	10.000020←10.000027	GPS,GLONASS,Galileo Signal Lock Loss / 2.1 sec. No Fix	-7	286428
2-17	10.000027←10.000035	GPS,GLONASS,Galileo Signal Lock Loss / 1.8 sec. No Fix	-8	286368
2-18	10.000035←10.000044	GPS,GLONASS,Galileo Signal Lock Loss / 2.1 sec. No Fix	-9	286308
2-19	10.000044←10.000054	GPS,GLONASS,Galileo Signal Lock Loss / 3.8 sec. No Fix	-10	286248

As mentioned earlier, C/N0 is the factor that affects navigation signal tracking performance according to the change in oscillator frequency frequency when the integration time of the tracking loop is the same. For each signal, C/N0 at the time of the first loss its tracking, and C/N0 of signals that were maintaining their tracking are compared in Table 4.6 and Table 4.7.

Test #1 results show that the satellite signal of PRN26 with the lowest C/N0 missed its signal track at 0.6 Hz of reference frequency change, the GLONASS signal lost its signal for the first time at 0.8 Hz of reference frequency change, and the Galileo signal at 0.4 Hz of reference frequency change, respectively. For GLONASS signals and Galileo signals, signal tracking began to be lost at the frequency change corresponding to the integral period, but for GPS signals, signal tracking was lost at the reference frequency change of 0.6 Hz, which is lower than 0.8 Hz. This is due to the low C/N0 of PRN 26. Test #2 results show that the satellite signal of PRN91 with the lowest C/N0 missed its signal track at -0.7 Hz of reference frequency change, the GPS signal lost its signal for the first time at -0.8 Hz of reference frequency change, and the Galileo signal at -0.4 Hz of reference frequency change, respectively. For GPS signals and Galileo signals, signal tracking began to be lost at the frequency change corresponding to the integral period, but for GLONASS signals, signal tracking was lost at the reference frequency change of -0.7 Hz, which is lower than 0.8 Hz. This is due to the low C/N0 of PRN 91.

Based on the results of the tests, a signal with lower C/N0 lost its signal tracking in a smaller reference frequency change environment compared to other signals. And even if a signal with higher C/N0, the signal tracking is lost at a 1 Hz or higher level of the reference frequency change due to the restriction of the

integration cycle. Meanwhile, no false frequency lock occurred in this test, so there were no position or speed errors. However, temporal speed errors at the time of changing the reference frequency rarely occur due to discontinuous changes in the reference frequency between integral times of the frequency tracking loop.

Table 4.8 Tracking status of each GNSS signal
under reference frequency change of test #1

Constellation	GPS L1 (0.6 Hz)		GLONASS L1 (0.8Hz)		Galileo E1 (0.4 Hz)	
	PRN	C/N0	PRN	C/N0	PRN	C/N0
The first lost GNSS signal	26	35.4	87	46.4	123	50.3
			94	49.2	144	43.1
Other signals	10	44.7	81	52.1	122	50.2
	12	47.4	84	44.3	125	46.2
	14	48.6	88	54.9	128	47.9
	18	39.9	89	53.2		
	22	41.7	91	39.5		
	25	49.2	93	40.3		
	29	44.4				
	31	51.9				
	32	53.6				

Table 4.9 Tracking status of each GNSS signal
under reference frequency change of test #2

Constellation	GPS L1 (-0.8 Hz)		GLONASS L1 (-0.7Hz)		Galileo E1 (-0.4 Hz)	
	PRN	C/N0	PRN	C/N0	PRN	C/N0
The first lost GNSS signal	25	44.7	91	37.0	122	50.1
	32	49.4				
Other signals	3	42.6	81	50.8	123	49.6
	10	40.7	84	50.6	125	41.4
	12	46.1	87	45.0	128	49.3
	14	47.0	88	54.5	144	42.6
	16	40.1	89	54.7	150	42.5
	22	42.9	90	40.4		
	26	43.6	92	45.7		
	29	45.2	94	48.7		
	31	48.7				

4.3   False Frequency Lock

For GPS signals with pre-integration time of 2 ms, a false frequency lock can occur at every 250 Hz away from the original frequency, which corresponds 1.6 Hz (250 Hz / 1.575 GHz * 10 MHz) based on the output frequency of TCXO. Five TCXOs' output frequencies are measured during the pyrotechnic shock test as shown in Table 3.7, three showed frequency changes over 1.6 Hz, and if this TCXO is used in the GNSS receiver, the false frequency lock will occur.

The false frequency lock is inherently caused by the pre-integration time of the discriminator, a shorter integration time can be utilized to detect and compensate the frequency offset over 1.6 Hz. With the addition of 1 ms pre-integration time discriminator, the pull-in frequency range can be doubled, meaning that the frequency change up to ± 500 Hz (± 3.2 Hz change in 10 MHz reference frequency) can be tracked without false frequency lock. But this also is likely to have a false frequency lock at every 500 Hz.

However, if there is a frequency change over 500 Hz or more, the signal can hardly be tracked because the correlation result value is lower than the peak value by 3 dB or more. In this case, each signal should be re-acquired. The pre-integration time can be designed up to 20 ms, and the smaller the pre-integration time, the larger the pull-in frequency range, but it is difficult to track weak signals or track signals under a severe multi-path environment.

Even if a false frequency lock occurs on all channels temporarily, the velocity can be obtained correctly because the clock drift absorbs range rate measurements by the same amount.

The fix modes and velocities of the GNSS receiver under pyrotechnic shock test are shown in Figure 4.11 and Figure 4.12. The velocity errors do not appear immediately after the pyroshock impact, but the range rate estimates from the doppler measurement for each satellite signal show that they are affected by the frequency change of the reference oscillator. Immediately after pyroshock impact, the range rate measurements of all tracking signals are false-locked and no velocity errors are shown at the moment. The range rate and C/N0 of PRN 13, PRN 15 and PRN 18 are shown in Figure 4.14 ~ Figure 4.19. After 40 seconds of pyrotechnic shock, range rate of the PRN13 is acquired correctly, resulting in velocity errors while other tracking signals remain false-locked. At 284280s, a normal navigation status is recovered after lock loss and signal re-acquisition process. As shown in Figure 4.15, Figure 4.17 and Figure 4.19, C/N0s of tracking signals decrease in the false-locked interval and C/N0s gradually decrease over time. When each false-locked signal has been re-acquired for all tracking satellites, the accurate velocities are calculated after 284310s. After re-acquisition, a bias of 50 m/s occurred in all tracking signals, the equivalent value as the false-lock at the 250 Hz as previously analyzed.
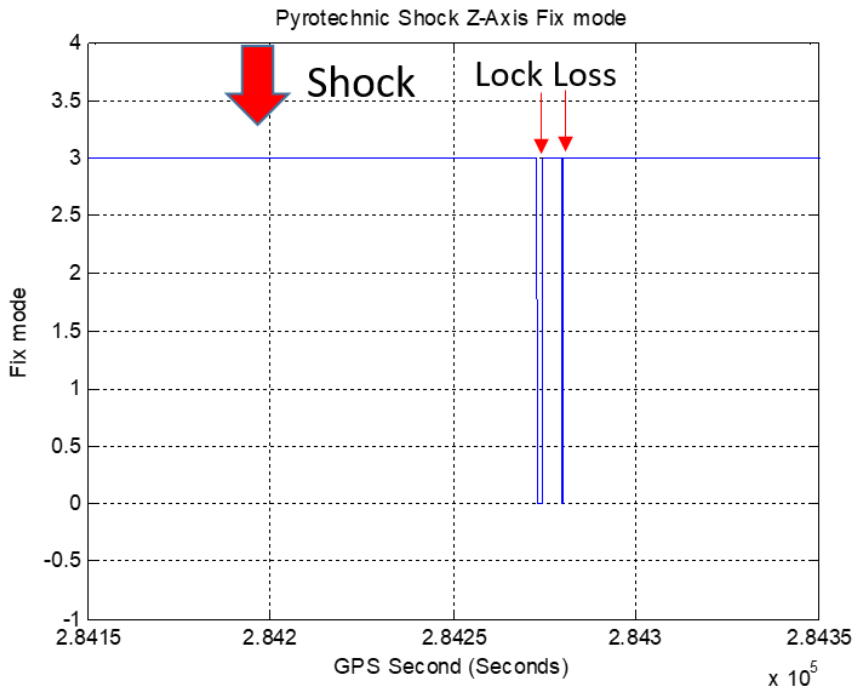
Figure 4.11 Fix mode under pyrotechnic shock test
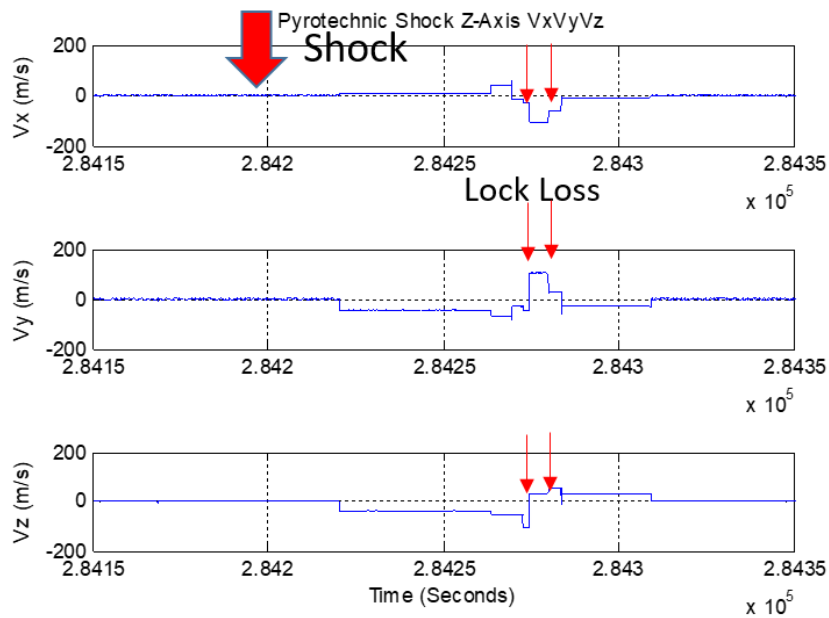
Figure 4.12 Velocities under pyrotechnic shock test
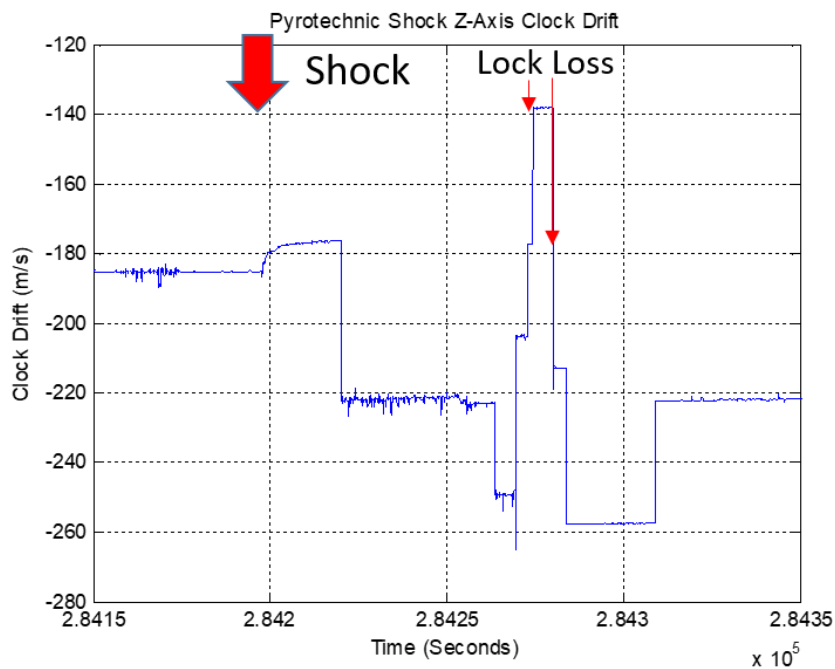
Figure 4.13 Clock drift under pyrotechnic shock test
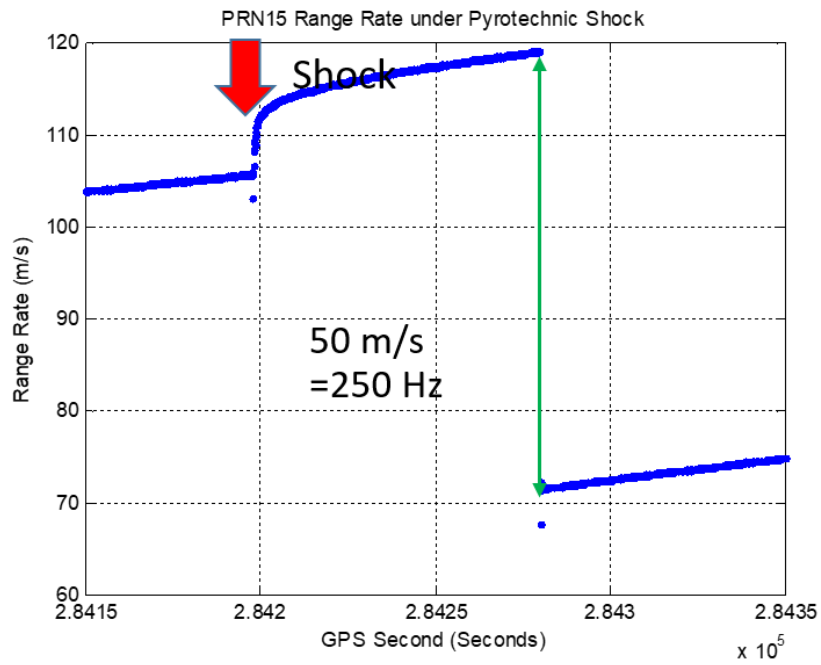
Figure 4.14 PRN15 range rate under pyrotechnic shock test
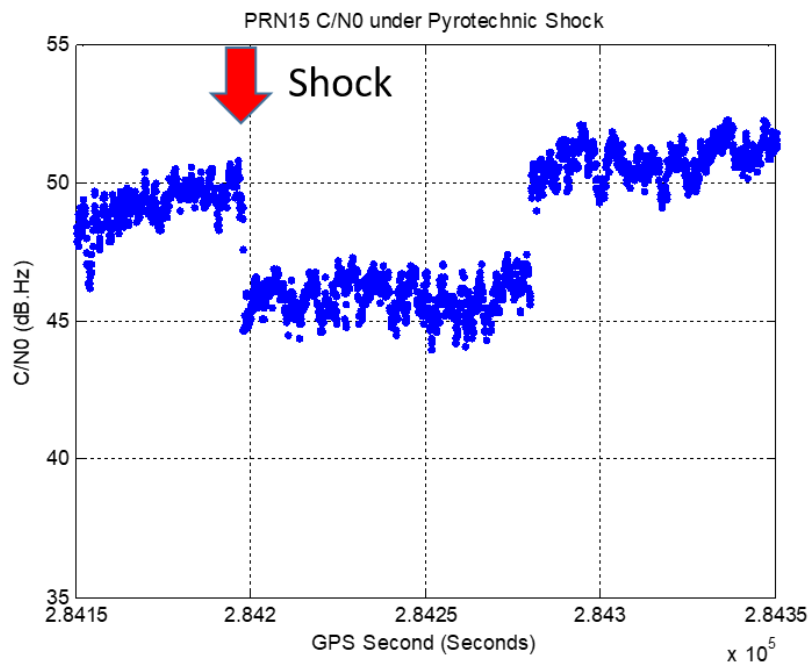
Figure 4.15 PRN15 C/N0 under pyrotechnic shock test

100
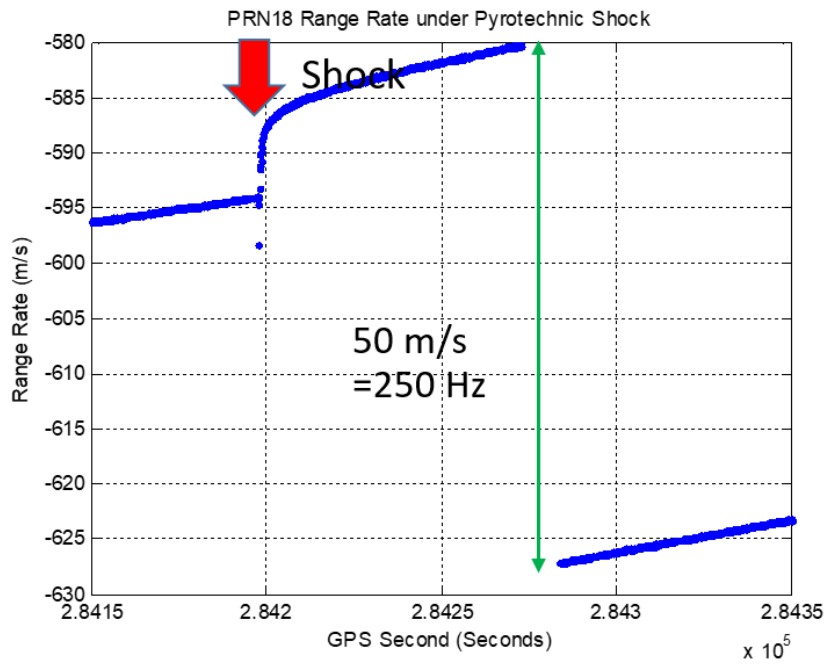
Figure 4.16 PRN18 range rate under pyrotechnic shock test
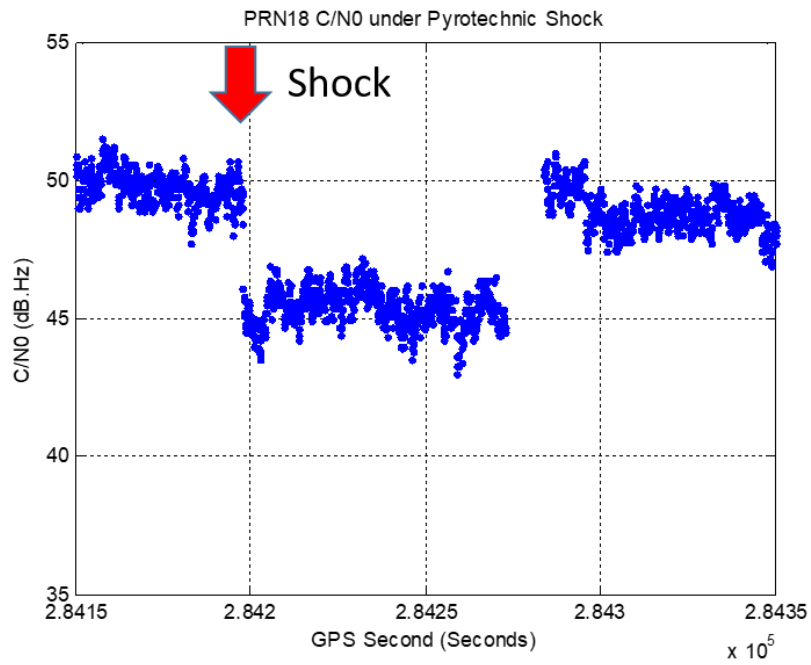
Figure 4.17 PRN18 C/N0 under pyrotechnic shock test

101
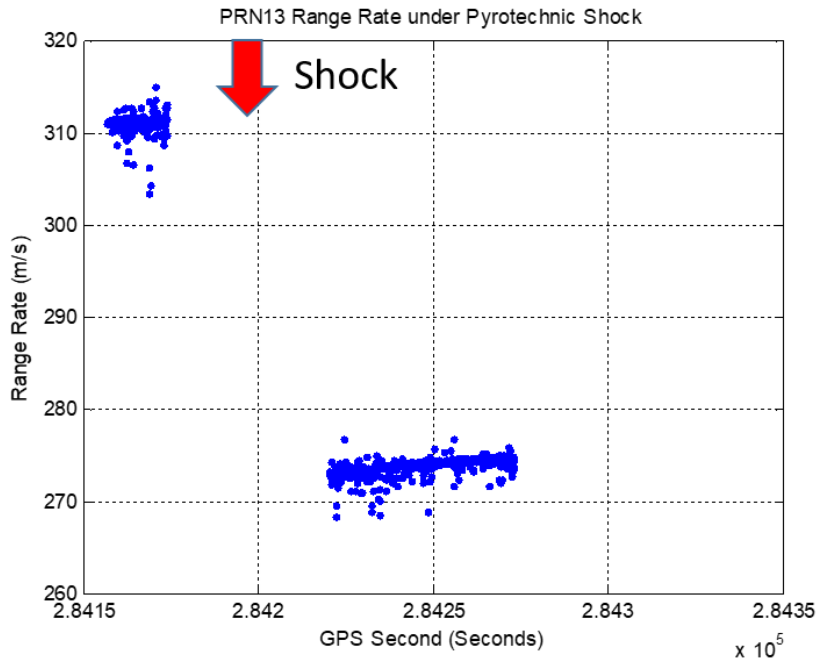
Figure 4.18 PRN13 range rate under pyrotechnic shock test
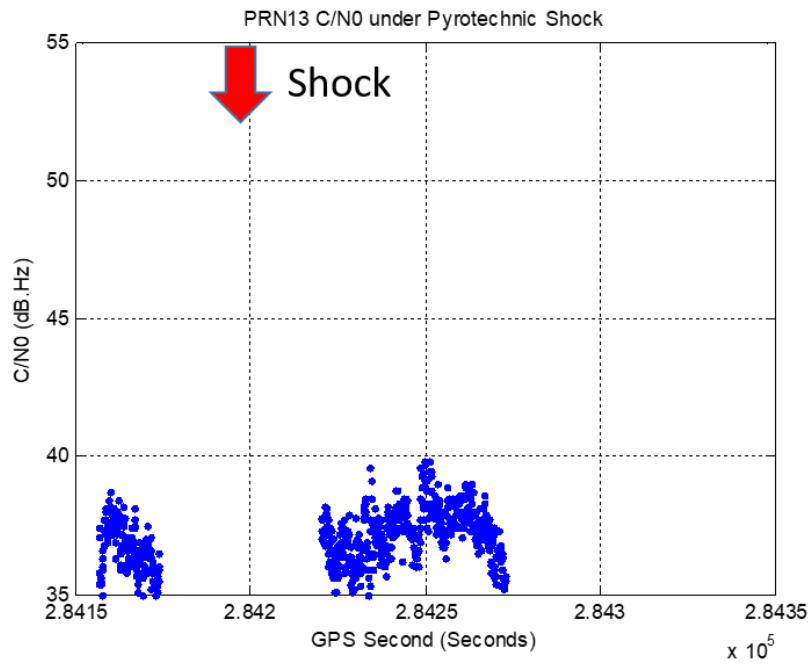
Figure 4.19 PRN13 C/N0 under pyrotechnic shock test

102

Chapter 5

Environmental Test Results of GNSS Receiver

In Chapter 3, the test results for oscillators under temperature, vibration, and pyrotechnic shock types of stress are examined to determine how the frequency output of each oscillator varies, and in this chapter, the navigation performance of a GNSS receiver equipped with each type of oscillator is presented under identical environmental stress conditions. Because the tracking performance of a GNSS receiver depends on the output frequency of the oscillator, the GNSS receiver with the MEMS oscillator is expected to be more robust in a harsh environment compared to a GNSS receiver with a TCXO. Moreover, it is necessary to assess the navigation performance under a normal condition through extensive performance tests. The GNSS receiver with the TCXO for KSLV-II is shown in Figure 5.1(a), and the pyrotechnic shock, temperature, and vibration tests of the GNSS receiver are described in Figures 5.1(b), 5.1(c), 5.1(d), respectively. The existing GNSS receiver with the TCXO is replaced with a GNSS receiver with a MEMS oscillator for the environmental test here, and the possibility of using the MEMS oscillator as a replacement is examined through a comparison of the navigation performance.

(a) GNSS receiver for KSLV-II	(b) Pyrotechnic shock test
(c) Temperature test	(d) Vibration test
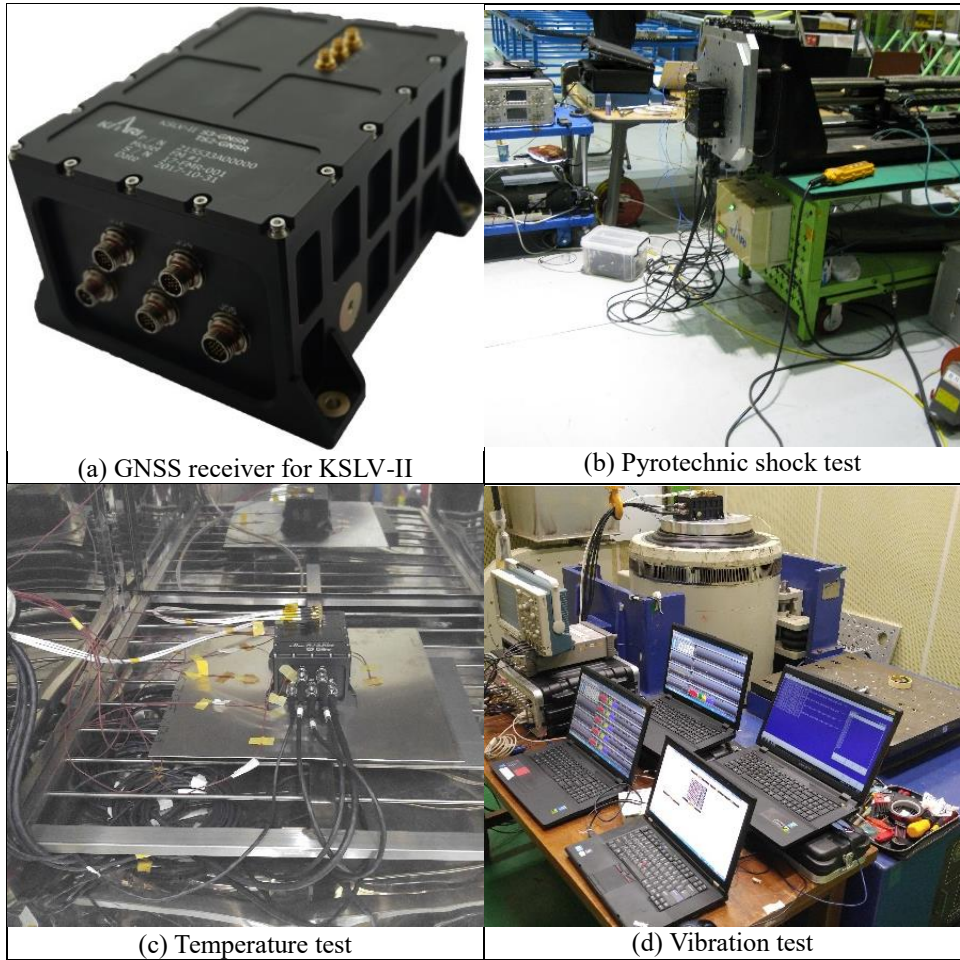
Figure 5.1 Environmental tests of GNSS receiver

5.1 Navigation Performance during the Temperature Test

In accordance with the test specifications shown in Table 3.1, temperature tests of the GNSS receivers are conducted, as shown in Figure 5.1(c). The position and velocity errors of the GNSS receiver in high temperature and low temperature tests are shown in Figures 5.2 and Figure 5.3, respectively, and the results are summarized in Table 5.1. As the temperature changes, the frequency outputs of the TCXO and MEMS oscillator vary, but the performance of the GNSS receiver is not affected, as given in Table 5.1. It is confirmed that the navigation accuracy of the GNSS receiver with the MEMS oscillator does not differ significantly from that of the GNSS receiver with the TCXO in high and low temperature environments. The wide range of velocity errors of both GNSS receivers stems from the use of GNSS signals at low elevations.

Table 5.1 Navigation performance comparison in the temperature test

		GNSS Receiver with TCXO	GNSS Receiver with MEMS Oscillator
PositionError (m, RMS)	High Temp.	10.97	11.17
	Low Temp.	10.04	10.40
VelocityError (m/s, RMS)	High Temp.	0.17	0.17
	Low Temp.	0.18	0.17

| (a) Calculated position with TCXO GNSS receiver | (b) Calculated velocity with TCXO GNSS receiver |
| (c) Calculated position with MEMS Osc. GNSS receiver | (d) Calculated velocity with MEMS Osc. GNSS receiver |
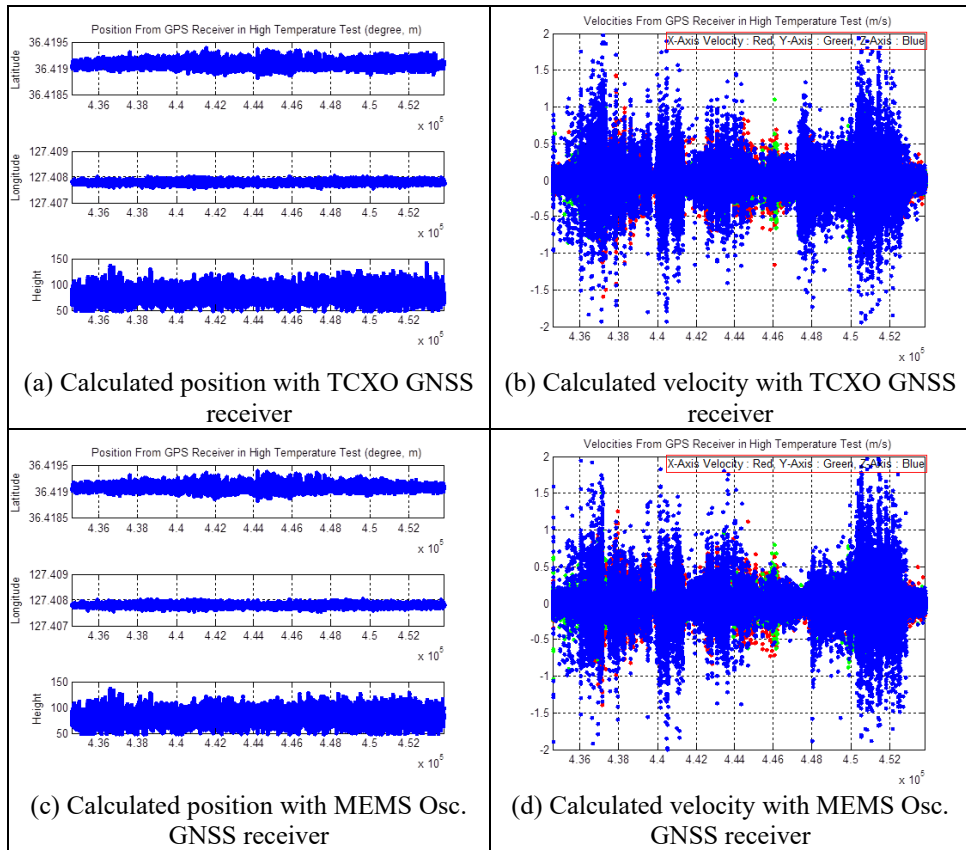
Figure 5.2 Navigation performance of a GNSS receiver in the high temperature test

(a) Calculated position with TCXO GNSS receiver

(b) Calculated velocity with TCXO GNSS receiver

(c) Calculated position with MEMS Osc. GNSS receiver

(d) Calculated velocity with MEMS Osc. GNSS receiver
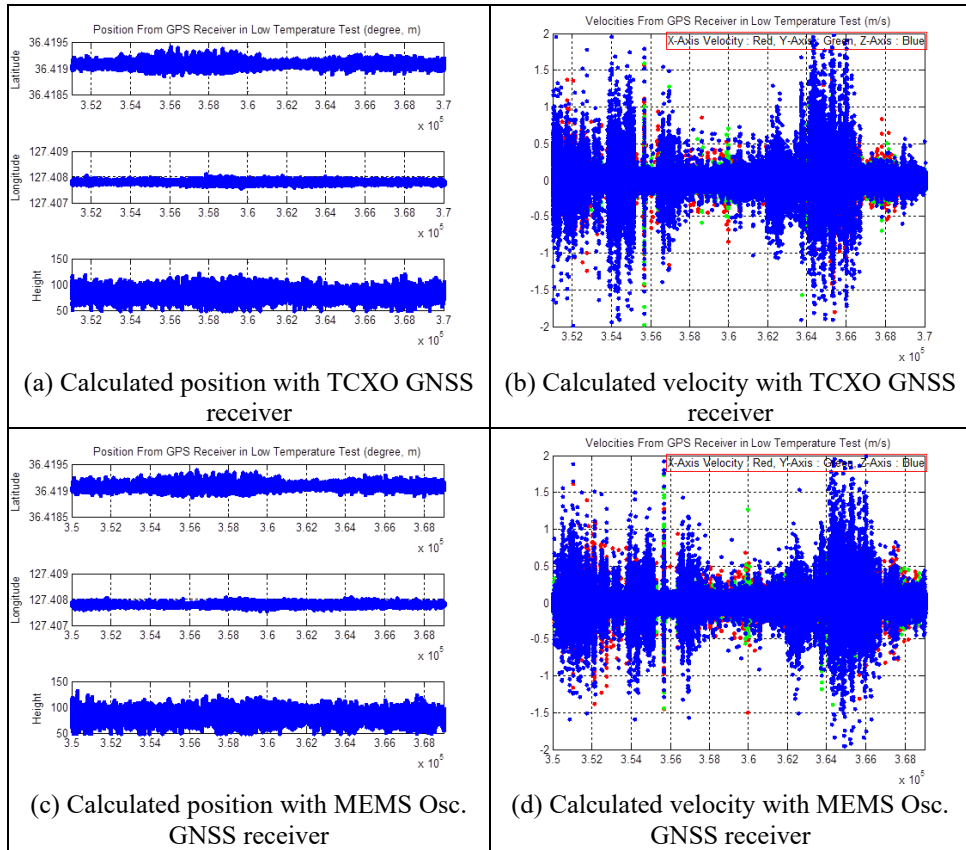
Figure 5.3 Navigation performance of a GNSS receiver in the low temperature test

107

5.2   Navigation Performance during the Vibration Test

In accordance with the test specifications in Table 3.1, vibration tests of GNSS receivers are conducted, as shown in Figure 5.1(d). The position and velocity errors of the GNSS receiver during random and sinusoidal vibration tests are shown in Figures 5.4 and 5.5, respectively. Red lines indicate the beginning and end of the vibration, and the results are summarized in Table 5.2. The frequency outputs of the TCXO and MEMS oscillator vary, as in chapter 3, due to vibration stress, but the performance of the GNSS receiver is not affected because the navigation errors are not large. It is also confirmed that the navigation accuracy of the GNSS receiver with the MEMS oscillator does not differ from that of the GNSS receiver with the TCXO under vibration conditions. However, the cause of the large velocity error by the GNSS receiver with the MEMS oscillator during sinusoidal vibration is not vibration, but because one GNSS signal at a low elevation is repeatedly used and dropped.

Table 5.2 Navigation performance comparison in the vibration test

		GNSS Receiver with TCXO	GNSS Receiver with MEMS Oscillator
PositionError (m, RMS)	Sinusoidal	4.68	7.12
	Random	8.73	9.87
VelocityError (m/s, RMS)	Sinusoidal	0.09	0.19
	Random	0.08	0.10

(a) Calculated position with TCXO GNSS receiver

(b) Calculated velocity with TCXO GNSS receiver

(c) Calculated position with MEMS Osc. GNSS receiver

(d) Calculated velocity with MEMS Osc. GNSS receiver
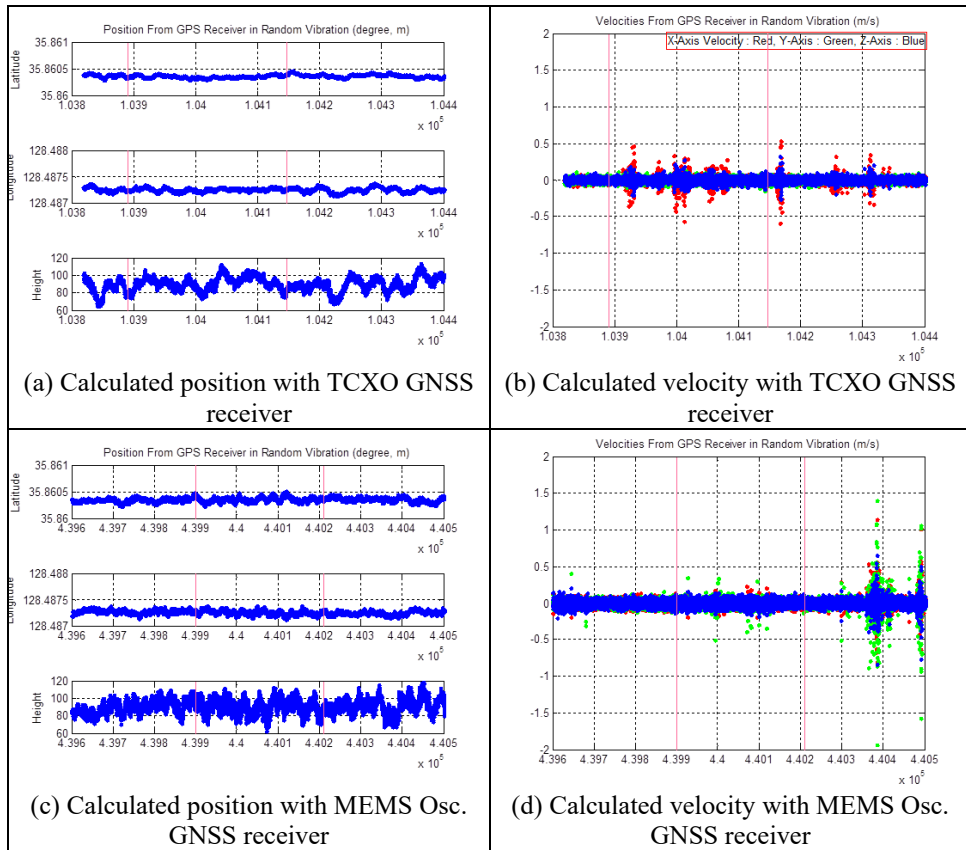
Figure 5.4 Navigation performance of GNSS receiver in the random vibration test

(a) Calculated position with TCXO GNSS receiver

(b) Calculated velocity with TCXO GNSS receiver

(c) Calculated position with MEMS Osc. GNSS receiver

(d) Calculated velocity with MEMS Osc. GNSS receiver
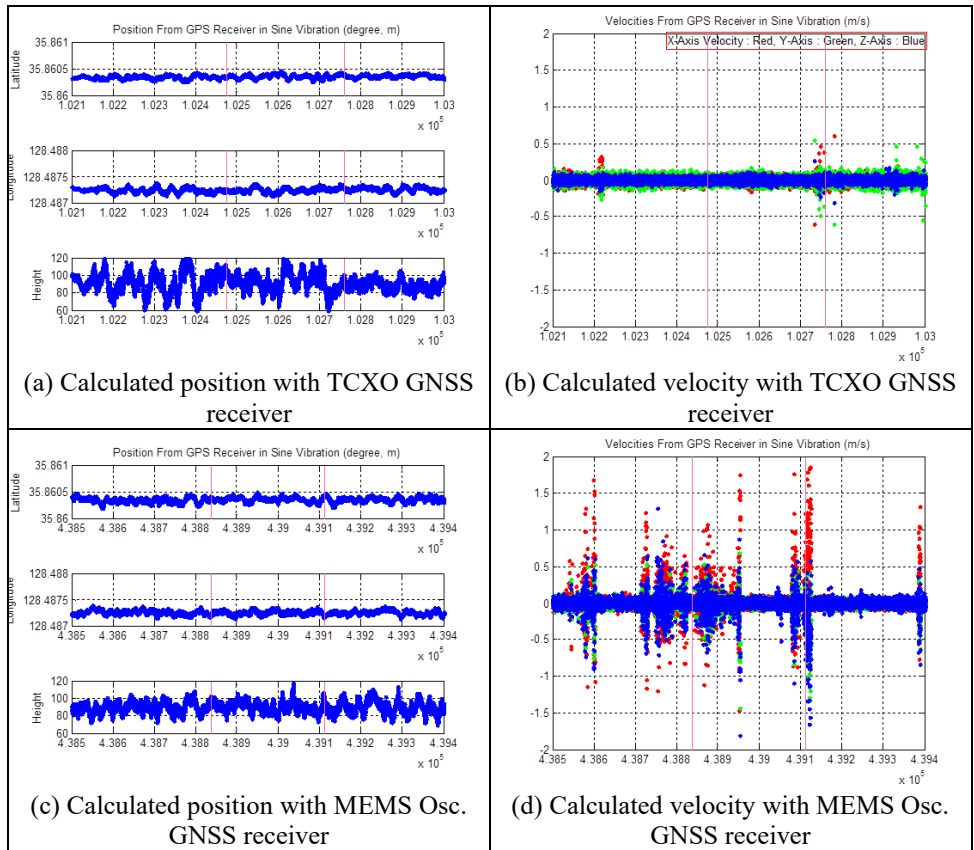
Figure 5.5 Navigation performance of GNSS receiver in the sinusoidal vibration test

5.3 Navigation Performance during the Pyrotechnic Shock Test

In accordance with the test specifications in Table 3.1, pyrotechnic shock tests of GNSS receivers are conducted, as shown in Figure 5.1(b). The position and velocity errors of the GNSS receivers in the pyrotechnic shock tests are shown in Figure 5.6. Red lines denote the moments of impacts, and the results are summarized in Table 5.3. The navigation solution of the GNSS receiver with the TCXO was temporarily interrupted at the time of impact (119180 s), with the receiver considered to have failed to track the navigation signal due to a significant change in the frequency output of the oscillator. The frequency offset of the TCXO at this moment occurs in the form shown in Figure 5.7, and the GNSS receiver resumed navigation again after 2.5 s.

Although not shown here, there are certain cases when a false frequency lock occurs, and the velocity error may persist while performing navigation with the TCXO. On the other hand, for the GNSS receiver equipped with the MEMS oscillator, the obtained navigation solution was not affected by the three pyrotechnic shocks. This is consistent with the results showing that the frequency output of the MEMS oscillator changed only slightly in the previous pyrotechnic shock test.

The position and velocity error of the GNSS receiver with the TCXO is smaller than those of the GNSS receiver with the MEMS oscillator, as shown in Table 5.3, most likely due to the fact that an RF input signal is supplied to by the GNSS simulator during the pyrotechnic shock test for the TCXO, while a live signal is used in the pyrotechnic shock test of the MEMS oscillator. The signal

generated by the GNSS simulator contains no errors except its thermal noise, but the actual signals propagated from GNSS satellites contain errors such as multipath, ionospheric, and tropospheric delays.

The clock drift output from the GNSS receiver with the TCXO is shown in Figure 5.7(a) and Figure 5.7(b), and the corresponding C/N0 ratios are presented in Figure 5.7(c). It can be seen that the C/N0 ratio is not calculated directly after the shock impact because the GNSS receiver loses signal tracking. The clock drift decreased by 0.34 PPM and navigation was performed again 2.5s after the pyrotechnic shock impact. If satellite signals are physically blocked or obscured, the C/N0 ratios of all received signals do not drop simultaneously. But if the reference frequency of the oscillator changes significantly due to some form of external stress, the C/N0 ratios of all tracking signals can drop altogether, as shown in Figure 5.7(c).

Table 5.3 Navigation performance comparison in the pyrotechnic shock test

		GNSS Receiver with TCXO	GNSS Receiver with MEMS Oscillator
Position (m, RMS)	Error	3.34	4.41
	Status	No Fix After Impact	Normal Operation
Velocity (m/s, RMS)	Error	0.07	0.11
	Status	No Fix After Impact	Normal Operation

(a) Calculated position with TCXO GNSS receiver

(b) Calculated velocity with TCXO GNSS receiver

(c) Calculated position with MEMS Osc. GNSS receiver

(d) Calculated velocity with MEMS Osc. GNSS receiver
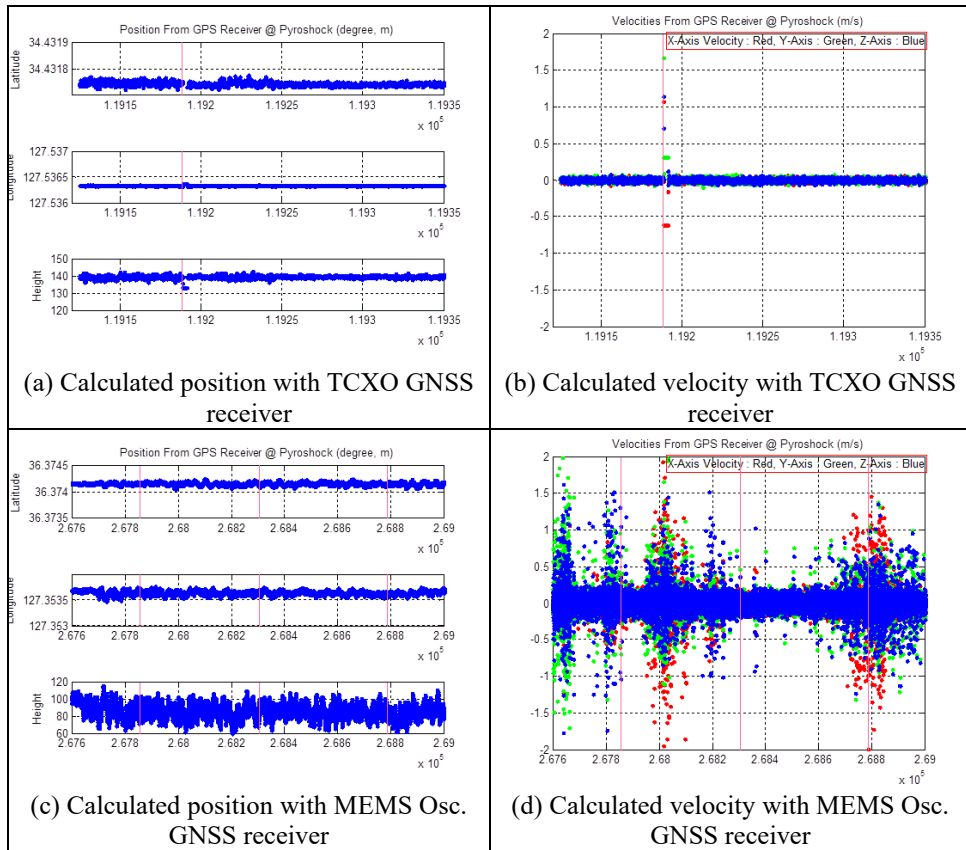
Figure 5.6 Navigation performance of a GNSS receiver in the pyrotechnic shock test

(a) Clock drift of the GNSS receiver with TCXO at the moment of pyrotechnic shock impact

*Blue vertical line is the impact point

(b) Enlargement of (a)

(c) C/N0 change
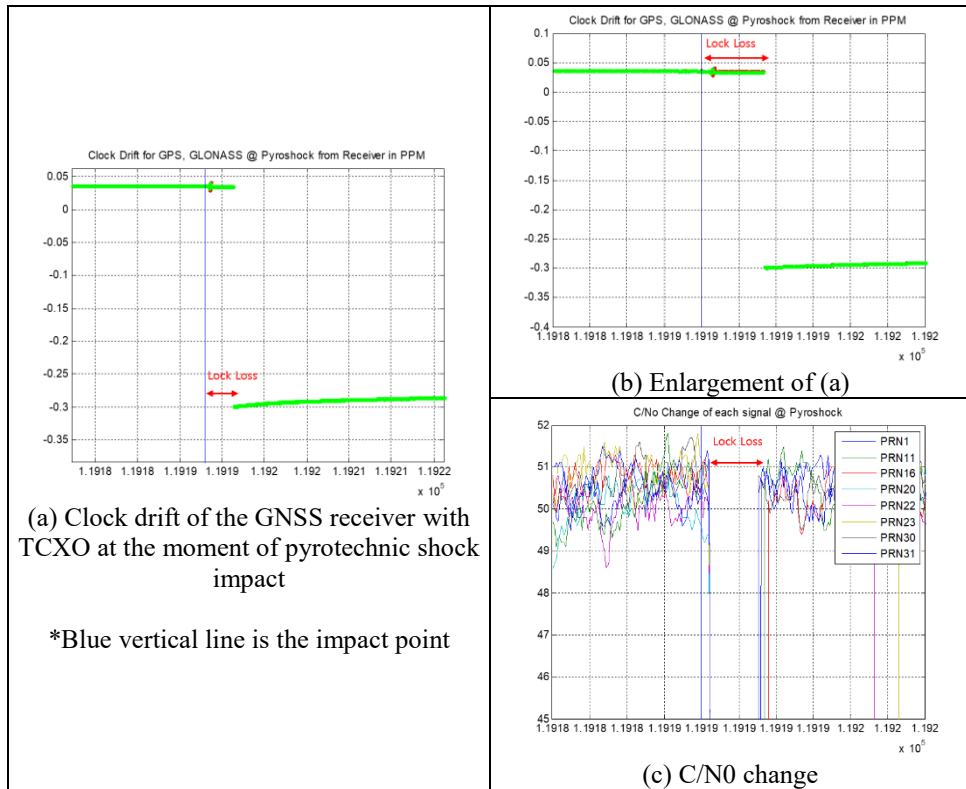
Figure 5.7 Clock drift and C/N0 of a GNSS receiver with TCXO in the pyrotechnic shock test

Chapter 6

Conclusion

In this study, the performance of a MEMS oscillator is analyzed under temperature, vibration, and pyrotechnic shock environmental conditions of the types that can be experienced by space launch vehicles, and the applicability of the MEMS oscillator in a GNSS receiver system is examined based on test results, with a comparison to the existing GNSS receiver with the TCXO. The GNSS receiver with the conventional TCXO showed good performance under the temperature and vibration conditions, but failed to calculate the navigation solution due to an abrupt change in the reference frequency at the time of an impact in a pyrotechnic shock condition. However, the GNSS receiver with the MEMS oscillator was able to calculate the navigation solution at the time of impact without any errors. The navigation performance of the GNSS receiver with the MEMS oscillator does not differ from that of the existing GNSS receiver with the TCXO under the temperature and vibration environmental conditions, implying that replacing the TCXO with a MEMS oscillator as a reference frequency source in GNSS receivers can be a practical solution to the loss of lock induced by pyrotechnic shock. After a burn-in test and an electromagnetic test have been carried out, it is expected that the MEMS oscillator will be able to replace the TCXO.

In this study, the effect of frequency changes in reference frequency output on GNSS receivers are analyzed when pyrotechnic shock is applied. At this point, the output of the reference frequency changes rapidly, resulting in a lock loss or velocity error, which can be attenuated by location change or by using shock absorber. When the shock absorber is applied, high-frequency shocks such as pyrotechnic shocks can be attenuated, but further analysis on relatively low-frequency vibration is required, which could be future work. And the tracking loop design other than existing tracking loop which is directly affected by reference frequency output, can also be worth researching.

Bibliography

[1]   J. S. Leung, G. L. Fayii, T. A. Patrick and S. L. Osburn, "Space-Based Navigation for RLV's and ELVs," *Aerospace Report No. ATR-2006(5200)-1*, Feb., 2006.

[2]   T. Miyano, S. Matsumoto, Y. Suzuki, T. Mugitani and N. Kohtake, "GPS Range Safety for The H-IIA Launch Vehicle," *Proc. of the Institute of Navigation GPS 2001*, pp. 2327-2333, 2001.

[3]   Y.S. Shin, B.M. Kwon, K.S. Ma, "The Design of the GNSS Antenna Preventing LNA Saturation by S-band Signal," in *Proc. of KSAS 2018 Fall Conference*, Nov. 2018.

[4]   B. Braun, M. Markgraf and O. Montenbruck, "Performance Analysis of IMU-Augmented GNSS Tracking Systems for Space Launch Vehicles," *CEAS Space J.* Vol.8, pp. 117-133, 2016.

[5]   J. Simpson, "GNSS Solutions: Spaceborne GNSS Receivers," *InsideGNSS*, Vol. 4, No. 6, pp. 18-21, Nov., 2009.

[6]   O. Montenbruck and G. Holt, "Spaceborne GPS Receiver Performance Testing," *DLR/GSOC*, TN 02-04, Issue 1.2, May 9, 2002.

[7]   "MIL-STD-810G: Environmental Engineering Considerations and Laboratory Tests,"

[8]   "IEC 60068-2: Electronic Equipment & Product Standards,"

[9]   "DEF STAN 00-35,"

[10]   Y.S. Shin, B.M. Kwon, K.S. Ma, "TCXO Behavior Under the Pyroshock Test," in *Proc. of KSAS 2016 Fall Conference*, Nov. 2016.

[11]   J. R. Vig, "Quartz Crystal Resonators and Oscillators," in *For Frequency Control and Timing Applications – A Tutorial*, 2004.

[12]   B. M. Aumayer and M. G. Petovello, "Feasibility Assessment of MEMS Oscillator for GNSS receivers," *GPS Solutions*, Vol. 20, Issue 3, pp. 385-398, July, 2016.

[13]   J. H. Kuypers, G. Zolfagharkhani, A. Gaidarzhy, R. Rebel, D. M. Chen, S. Stanley, D. LoCascio, K. J. Schoepf, M. Crowley and P. Mohanty, "High Performance MEMS Oscillators for Communications Applications," in *Proc. of the 4th International Symposium on Acoustic Wave Devices for Future Mobile Communication Systems*, 2010.

[14]   SiTime Corp., "Shock and Vibration Performance Comparison of MEMS and Quartz-based Oscillators," Application Note 10032, Available online at http://www.sitime.com/support2/documents/AN10032-Shock-Vibration-Comparison-MEMS-and-Quartz-Oscillators.pdf.

[15]   SiTime Corp., "Resilience and Reliability of Silicon MEMS Oscillators," Application Note 10045, Available online at http://www.sitime.com /support2/documents/AN10045-Resilience and Reliability of Silicon MEMS Oscillators.pdf.

118

[16]   B. Kim, R. H. Olsson III, K. Smart and K. E. Wojciechowski, "MEMS Resonators with Extremely Low Vibration and Shock Sensitivity," *Proc. IEEE Sensors*, pp. 606-609, Oct. 2011.

[17]   H. Lee, A. Partridge and F. Assaderaghi, "Low jitter and Temperature Stable MEMS Oscillators", in *Proc. of IEEE International Frequency Control Symposium*, pp. 1-5, May, 2012.

[18]   Available online at https://www5.epsondevice.com/en/products/tcxo/

[19]   E.D. Kaplan and C. J. Hegarty, "Understanding GPS: Principles and Applications," Artech House, pp. 192-194, 2006.

[20]   A. V. Kosykh, I. V. Khomenko and A. N Lepetaev, "Dual-mode Quartz Resonators Suitable for TCXO and OCXO," in *Proc. of 24th European* Frequency *and Time Forum*, pp. 1-8, 2010.

[21]   RAKON, "E7386 Specification Sheet, Pluto Low Acceleration Sensitivity TCXO," 2016.

[22]   Available online at http://txccrystal.com/tcxo.html

[23]   Available online at https://www.iqdfrequencyproducts.com/products/search/?type=tcxos

[24]   Available online at https://www.vectron.com/products/tcxo/tcxo_ archive.htm

[25]   P. Nampoothiri, "Shock, Rattle and Roll – Vibration Management in VHF Oscillators,"   MtronPTI,   Available   online   at http://www.mtronpti.com/sites/default/files/Shock%20rattle%20and%20roll.pdf

[26]   J. B. Donovan and M. M. Driscoll, "Vibration-Induced Phase Noise in Signal Generation Hardware," in *Frequency Control Symposium joint with the 22nd European Frequency and Time Forum*, pp. 14-15, 2009.

[27]   J. R. Vig, "The Effects of Acceleration on Precision Frequency Sources," *Proc. 1992 IEEE Frequency Control Symposium*, IEEE Cat. No. 92CH3083-3, 1992.

[28]   C. T. C. Nguyen, "MEMS Technology for Timing and Frequency Control," *IEEE Trans. on Ultrasonics, Ferroelectrics, and Frequency Control*, Vol. 54, No. 2, pp. 251-270, Feb., 2007.

[29]   M. H. Perrott, J. C. Salvia, F. S. Lee, A. Partridge, S. Mukherjee, C. Arft, J. Kim, N. Arumugam, P. Gupta, S. Tabatabaei, S. Pamarti, H. Lee and F. Assaderaghi, "A Temperature-to-Digital Converter for a MEMS-Based Programmable Oscillator with < ±0.5-ppm Frequency Stability and < 1-ps Integrated Jitter," *IEEE Journal of Solid-State Circuits*, Vol. 48, No. 1, pp. 276-291, Jan., 2013.

[30]   M. S. Islam, S. Mandal, G. Xereas and V. P. Chodavarapu, "A Dual-Ring Breath-Mode MEMS-Based 10.00 MHz GPS-Disciplined Reference Oscillator," in *2020 Joint Conference of the IEEE International Frequency Control Symposium and International Symposium on Applications of Ferroelectrics (IFCS-ISAF)*, pp. 1-5, 2020.

[31]   G. Mussi, M. Carrara, G. Langfelder and G. Gattere, "Polysilicon MEMS Resonator for 28-MHz Oscillators," in *2019 Joint Conference of the IEEE*

International Frequency Control Symposium and European Frequency and Time Forum (EFTF/IFC), pp. 1-3, 2019.

[32]   P. Lall, A. S. Abrol, L. Simpson and J. Glover, "A Study on Damage Progression in MEMS Based Silicon Oscillators Subjected to High-g Harsh Environments," in *2016 15th IEEE Intersociety Conference on Thermal and Thermomechanical Phenomena in Electronic Systems (ITherm)*, pp. 546-559, 2016.

[33]   H. Kwon, L. C. Ortiz, G. D. Vukasin, Y. Chen, D. D. Shin and T. W. Kenny, "An Oven-Controlled MEMS Oscillator (OCMO) With Sub 10mw, ± 1.5 PPB Stability Over Temperature," in *2019 20th International Conference on Solid-State Sensors, Actuators and Microsystems & Eurosensors XXXIII (TRANSDUCERS & EUROSENSORS XXXIII)*, pp. 2072-2075, 2019.

[34]   W. Hsu, "Reliability of Silicon Resonator Oscillators," in *2006 IEEE International Frequency Control Symposium and Exposition*, pp. 389-392, 2006.

[35]   "Shock and Vibration Performance Comparison of MEMS and Quartz-based Oscillators," Available online at https://ilsiamerica.com/shock-and-vibration-performance-comparison-of-mems-and-quartz-based-oscillators

[36]   D. K. Agrawal and A. A. Seshia, "An Analytical Formulation for Phase Noise in MEMS Oscillators," *IEEE Trans. on Ultrasonics, Ferroelectrics, and Frequency Control*, Vol. 61, No. 12, pp. 1938-1952, Dec., 2014.

[37]   G. I. Taylor, "The Coalescence of Closely Spaced Drops When They Are at

Different Electric Potentials," *Proc. R. Soc*. Vol.306, pp 423-34, 1968.

[38]   H. C. Nathanson, W. E. Newell, R. A. Wickstrom and J. R. Davis, "The Resonant Gate Transistor," *IEEE Trans. Electron Devices*, Vol.14, pp 117-33, 1967.

[39]   H. A. Tilmans and R. Legtenberg, "Electrostatically Driven Vacuum-Encapsulated Polysilicon Resonators: part I. Design and Fabrication," *Sensors Actuators*, Vol.45, pp. 57-66, 1994.

[40]   S. Pamidighantam, R. Puers, K. Baert and H. A. C. Tilmans, "Pull-in Voltage Analysis of Electrostatically Actuated Beam Structures with Fixed–fixed and Fixed-free End Conditions," *J. Micromech. Microeng*. Vol.12, pp. 458-64, 2002.

[41]   W. M. Zhang and G. Meng, "Nonlinear Dynamical System of Micro-cantilever under Combined Parametric and Forcing Excitations in MEMS," *Sensor Actuator A-Phy*. Vol. 119, pp. 291-299, 2005.

[42]   R. Gao, X. Wang, M. Wang, M. Yu and M. Xie, "Nonlinear Dynamics of Lateral Micro-Resonator including Viscous Air Damping," *Chinese J. Mech. Eng*. Vol. 20, pp. 75-78, 2007.

[43]   J. M. Pryjemski, "Improvement in System Performance using A Crystal Oscillator Compensated for Acceleration Sensitivity," in *Proc. 32nd Annu. Symp. Freq. Contr.*, pp. 426-430, 1978.

[44]   A. A. Zainuddin, J. Karim, A. N. Nordin, S.Pandian and S. Khan, "Design and Simulation of 20MHz Oscillator using CMOS-MEMS Beam

Resonators," *Proc. RSM*, pp 45-49, 2013.

[45]   F. Nabki, K. Allidina and F. Ahmad, "A High Gain-bandwidth Product Transimpedance Amplifier for MEMS-based Oscillator,". *Proc. European Solid-State Circuit Conf.(ESSCIRC)*, p. 454, 2009.

[46]   "Pyroshock Test Criteria," NASA-STD-7003A.

[47]   J. R. Vig, "Quartz Crystal Resonator and Oscillators," US Army Communications-Electronics Research, Development & Engineering Center, Jan., 2004.

[48]   "Fundamentals of Quartz Oscillators", AN 200-2, Hewlett-Packard Co.

[49]   A. Ballato, "Resonators Compensated for Acceleration Fields," in *Proc. 33rd Annu. Symp. Freq. Contr.*, pp. 322-336, 1979.

[50]   R. L. Filler, "The Acceleration Sensitivity of Quartz Crystal Oscillators: A review," *IEEE Trans. Ultrason., Ferroelec., Freq. Contr*. Vol. 35, pp.297-305, 1988.

[51]   F. L. Walls and J. R. Vig, "Acceleration Insensitive Oscillator," U. S. Pat. No. 4,575,690, 1986.

[52]   J. M. Pryjemski. "Improvement in System Performance using A Crystal Oscillator Compensated for Acceleration Sensitivity," in *Proc. 32nd Annu. Symp. Freq. Contr*., pp. 426-430, 1978.

[53]   V. J. Rosati and R. L. Filler, "Reduction in the Effects of Vibration on SC-cut Quartz Oscillators," in *Proc. 35th Annu. Symp. Freq. Contr*., pp. 117-121, 1981.

[54]   Y. S. Zhou and H. F. Tiersten, "On the Influence of A Fabrication Imperfection on the Normal Acceleration Sensitivity of Contoured Quartz Resonators with Rectangular Supports," in *Proc. 44th Annu. Symp. Freq. Contr.*, pp. 452-453, 1990.

[55]   M. H. Watts, E. P. EerNisse, R. W. Ward. and R. B. Wiggins, "Technique for Measuring the Acceleration Sensitivity of SC-Cut Quartz Resonators," in *Proc. 42nd Annu. Symp. Freq. Contr.*, pp. 442-446, 1988.

[56]   R. Besson, "A New Piezoelectric Resonator Design," in *Proc. 30th Annu. Symp. Freq. Contr.*, pp. 78-83, 1976.

[57]   A. F. B. Wood and A. Seed, "Activity Dips in AT-cut crystals," in *Proc. 21st Annu. Symp. Freq. Contr.*, pp. 420-435, 1967.

[58]   J. Birch and D. A. Weston, "Frequency/Temperature, Activity/Temperature Anomalies in High Frequency Quartz Crystal Units," in *Proc. 30th Annu. Symp. Freq. Contr.*, pp. 32-39, 1978

[59]   J. E. Deeter and H. Inoue, "Temperature Dependence of the Ginga Clock Rate," *ISAS Res. Note 430*, Jan. 1990.

[60]   J. A. Kusters, "The SC-Cut Crystal-An Overview," in *Proc. IEEE Ultrason. Symp.*, pp. 402-409, 1981.

[61]   W. Thomson, "Theory of Vibration with Applications," Second Edition, Prentice-Hall, New Jersey, 1981.

[62]   A. Chu, "Zero Shift of Piezoelectric Accelerometers in Pyroshock Measurements," in *57th Shock and Vibration Symposium*, 1986.

[63] A. Piersol, "Pyroshock Data Acquisition and Analysis for U/RGM-109D Payload Cover Ejection Tests NWC TP 6927," Naval Weapons Center, China Lake, CA, 1988.

[64] H. Luhrs, "Designing Electronics for Pyrotechnic Shock," Pyrotechnic Shock Workshop, Shock and Vibration Bulletin 57, Shock and Vibration Information Center, Naval Research Laboratory, Washington D.C., 1987.

[65] A. Piersol, "Recommendations for the Acquisition and Analysis of Pyroshock Data," Sound and Vibration; April 1992.

[66] W. Kacena, M. McGrath and A. Rader, "Aerospace Systems Pyrotechnic Shock Data," Vol. VI, NASA CR 116406, Goddard Space Flight Center, 1970.

[67] C. Harris, "Shock and Vibration Handbook, Fourth Edition," MCGraw-Hill, New York, 1996.

[68] "Handling Environment Assessment & Simulation Test Procedure Using Test Tailoring," Institute of Hard Disk Drive Equipment and Materials Association (IDEMA), San Jose, California, 1998.

[69] H. Gaberson and R. Chalmers, "Modal Velocity as a Criterion of Shock Severity," Shock and Vibration Bulletin 40, Part 2, 1969.

[70] "Environmental Test Methods and Engineering Guidelines," Military Standard MIL-STD-810E, U.S. Department of Defense, 1989.

국문초록

본 학위논문에서는 온도보상 수정발진기와 멤스 발진기에 대한 환경시험 및 성능시험 결과를 제시한다. 또한 각각을 탑재한 위성항법수신기에 대한 검증시험을 통해 위성항법수신기에 널리 사용되고 있는 온도보상 수정발진기를 물리적인 충격에 강인한 멤스 발진기로 대체하고자 한다.

온도보상 수정발진기는 압전성질을 지닌 쿼츠를 이용하여 안정적이고 정확한 주파수를 출력하는 부품으로 위상잡음과 손실이 작아 기준주파수로 적합하다. 온도보상 수정발진기는 이미 정밀시계와 시각장치에 많이 이용되고 있으며, 위성항법수신기에도 널리 사용되고 있다. 단순한 수정진동자는 주변 온도에 민감하게 반응하지만 온도보상 수정발진기는 주변 온도를 측정하는 보상회로가 삽입되어 높은 온도 안정성을 보인다.

멤스 발진기는 멤스 기술과 반도체 생산기술에서 파생된 제조기술을 바탕으로 온도보상 수정발진기와 비교해서 크기와 무게를 크게 줄였다. 크기가 작아짐에 따라 물리적인 충격과 진동에 강하나 출시 초기에는 높은 위상잡음과 온도변화에 의해 주파수 안정성이 낮아 제한적인 용도에만 사용되어 왔다. 최근 반도체 제작기술의 발달로 멤스 발진기도 온도보상 수정발진기 수준의 잡음 성능을 보이며, 시스템과의 일체화가 더욱 쉬워 응용분야가 넓어지고 있다.

우주발사체의 전자탑재물은 엔진 점화 혹은 페어링 분리와 같은 이벤트가 있을 때마다 강한 진동, 가속도 및 충격을 겪는다. 따라서 전자탑재물 제작시 온도, 진동, 가속도 및 충격과 같은 환경시험을 수행하는데 온도보상 수정발진기를 탑재한 위성항법수신기가 파이로 충격시험시 항법신호를

126

놓치는 문제가 발생하였다. 이 현상은 위성항법수신기에 탑재된 온도보상 수정발진기의 출력주파수가 충격에 의해 급격히 변하였기 때문이며 이를 위해서 여러 종류의 온도보상 수정발진기를 시험해보았으나 해결이 어려웠다.

멤스 발진기의 위성항법수신기 적용가능성을 확인하기 위해 먼저 파이로 충격환경 하에서 기존 수신기 추적루프에 대한 분석을 제시한다. 그리고 멤스 발진기에 대해 기존에 수행했던 온도, 진동 및 파이로 충격시험을 수행하고 온도보상 수정발진기와 주파수 출력을 비교하였다. 물리적인 환경인 진동과 파이로 충격 이외에 온도에 대해서도 멤스 발진기는 온도보상 수정발진기에 비해 좋은 주파수 안정성을 보였다. 멤스 발진기 자체의 환경시험 이후 위성항법수신기에 탑재하여 동일한 환경에서의 동작 성능을 확인하였고, 온도보상 수정발진기가 탑재된 기존의 위성항법수신기와 비교하여 성능차이가 없었으며 파이로 충격시험에서는 항법신호를 놓치지 않고 연속적인 항법을 수행하였다.

앞서 수행된 시험을 바탕으로 멤스 발진기를 위성항법수신기에 탑재하는데 문제가 없음이 확인되어 온도보상 수정발진기를 대체할 수 있을 것으로 판단된다.

주요어: 위성항법수신기, 우주발사체, 온도보상 수정발진기, 멤스 발진기, 환경시험, 파이로 충격

학번: 2012-30922